Evaluating Wettability and Imbibition Oil Recovery of the Core Plugs and Crushed Rock Samples from the Duvernay Formation

by

Momotaj Begum

A thesis submitted in partial fulfillment of the requirements for the degree of

Master of Science

in

PETROLEUM ENGINEERING

Department of Civil and Environmental Engineering
University of Alberta

© Momotaj Begum, 2017

ABSTRACT

Unconventional sources have become the leading sources of hydrocarbons in North America. These unconventional resources with low porosity and ultra-low permeability can produce hydrocarbon at profitable rates from the hydraulically fractured horizontal well. However, rock-fluid properties need to be characterized to obtain an efficient hydrocarbon recovery. Therefore, a detailed understanding of rock properties especially wettability is crucial as it has an effect on both waterflooding and enhanced oil recovery (EOR) techniques.

The primary objective of this research is to determine the wettability characteristics of shale by conducting contact angle and imbibition experiments. We investigate the functional dependence of wettability on the mineralogy, petrophysical properties, and the geochemical properties that are associated with source rock. Moreover, we present the potential driving factor of imbibition by using the spontaneous imbibition and co-current imbibition data of shale samples. We also characterize the mechanisms controlling oil recovery from shales by soaking process.

In this study, we evaluate the wettability of organic shale samples drilled in the Duvernay Formation, which is a source rock located in the Western Canadian Sedimentary Basin (WCSB). We characterize the shale samples by measuring pressure-decay permeability, effective porosity, initial oil and water saturation, mineralogy, total organic carbon (TOC) content. We also conduct thin section analysis and Scanning Electron Microscope (SEM) and energy-dispersive X-ray spectroscopy (EDS) analyses on shale samples to characterize the location, type, and size of pores. We use reservoir oil and brine to conduct air-liquid contact angle and air-liquid spontaneous imbibition tests for wettability measurements of both intact core plugs and crushed shale packs

(CSP) prepared from drilling cuttings. We also conduct co-current imbibition to calculate the capillary pressure ratio. After evaluation of wettability, we conduct soaking experiments. First, we measure liquid-liquid contact angles of soaking fluids and reservoir oil equilibrated on the surface of the oil saturated core plugs. Then, we conduct the soaking test by immersing the oil-saturated plugs and CSP samples in soaking fluids with different compositions and physical properties and record oil volume produced due to spontaneous imbibition of the soaking fluids. The soaking fluids are characterized by measuring surface tension, interfacial tension (IFT), viscosity, and pH. We analyze the results of soaking tests performed on core plugs and CSPs and investigating the controlling parameters affecting capillary pressure and imbibition oil recovery factor (RF).

The results of wettability measurements demonstrate that the Duvernay samples have a stronger wetting affinity to oil compared to brine. The positive correlations of TOC content with both effective porosity and pressure-decay permeability suggest that the majority of connected pores are present within the organic matter which can also be supported by the SEM/EDS analysis. Organic porosity may explain the strong oil-wetness of the shale samples. The results of liquid-liquid contact angle tests show that the soaking fluid with lower IFT shows a stronger wetting affinity towards the shale samples. Similarly, the results of soaking tests conducted on the core plugs and CSPs show that oil RF is higher for the soaking fluids with lower IFT, which may be due to wettability alteration towards less oil-wet conditions. In addition, comparing the results of air-brine imbibition with those of the soaking tests indicates that adding the non-ionic surfactant to the soaking fluid may alter the wettability of organic pores towards less oil-wet conditions, leading to the displacement of oil from hydrophobic organic pores. The results also show that the presence of water film in shale samples may increase their wetting affinity towards the soaking fluids, leading to higher oil RF in the samples with higher initial water saturation.

To Almighty ALLAH

&

My Beloved Family

ACKNOWLEDGEMENTS

I would like to express the inmost appreciation to my supervisor Dr. Hassan Dehghanpour for his continuous support and guidance in this research and throughout my MSc program. Without his encouragement and persistence, this thesis would have been incomplete.

I owe to my parents Md. Mahibul Islam and Mrs. Iffat Ara Islam for their countless sacrifices and moral support for me. They have always been there for me with their love and patience to achieve my goal. My cordial thanks to my husband, Md Samrat Alam for listening and encouraging me (sometimes by preparing dinner) along the tough way. I must thank all of my friends and family members for their kind prayers and well wishes for me throughout the journey.

My special gratitude to all lab mates for sharing tea with me and providing expertise and direct involvement in this research. I am also appreciative to Engineering Technologist Todd Kinnee for his constant assistance when there were technical difficulties in my experiments.

I want to acknowledge Athabasca Oil Corporation for supporting this project by providing funding, samples and required data. We also thank Calfrac Well Services for providing the chemical components of fracturing fluids. I am also immensely grateful to Natural Sciences and Engineering Research Council of Canada (NSERC) and Natural Resources Canada (NRCan) for providing the financial support.

TABLE OF CONTENTS

LIST OF TABLES

LIST OF FIGURES

NOMENCLATURE

A= Surface area, L^2

BV= Bulk volume, L^3

D=Pore diameter, L

g= Gravity acceleration, LT^{-2}

IFT=Liquid-liquid interfacial tension, MT^{-2}

N_B=Bond number

N_{ca}=Capillary number

P_c=Capillary pressure, $ML^{-1}T^{-2}$

PV= Pore volume, L^3

σ =Surface tension, MT^{-2}

TOC=Total organic carbon, M/M%

t_D=Dimensionless time, dimensionless

V_o=Produced oil volume in soaking test, L^3

V_b=Imbibed brine volume in air-brine imbibition test, L^3

γ_{ss}= interfacial tension between solid surface and soaking fluid

γ_{sk}= interfacial tension between solid surface and kerosene

μ=Fluid viscosity, $ML^{-1}T^{-1}$

θ=Contact angle, Degree

ρ=Density, ML^{-3}

Chapter 1

Introduction

1.1 Overview

Unconventional oil and gas resources (shale gas, shale oil etc.) is becoming the largest contributor of hydrocarbon in North America (Stark et al., 2008; Wang et al., 2014; Akrabadi et al., 2015). Due to the concern that conventional resources will not meet the growing requirement for fuel worldwide, unconventional resources are considered as a viable and economically important source of energy in the future (Law and Curtis, 2002; Stark et al., 2008). Moreover, organic-rich shales are also considered as potential hydrocarbon resources across the world (Gonzalez et al., 2013). However, besides the organic richness, these resources have three main characteristics: low porosity, ultra-permeability, and non-ductile nature (Jarvie 2014), which make the production of hydrocarbons from unconventional resources challenging. In order to confront these challenges, increase the commercial production of hydrocarbons, and enhance our understanding of unconventional resources, rigorous research is needed.

Unconventional oil and gas resources with ultra-low porosity and permeability can produce hydrocarbons at economic rates by drilling hydraulically-fractured horizontal wells. However, efficient hydrocarbon recovery from such reservoirs needs deep understanding of the characteristics of rock/fluid properties, such as relative permeability, capillary pressure, and wettability.

Hydraulic fracturing is one of the most popular ways to extract hydrocarbons from unconventional sources. This technique was introduced in 1947 to stimulate the oil and gas production (Clark,

1949) and has been applied to more than 2 million wells worldwide (Montgomery and Smith, 2010). This process is mainly based on the results of rock-fluids interaction. Hydraulic fracturing effectively increases the drainage area by exposing a massive surface area within the reservoir while maintaining contact with fracturing fluids. In the context of production engineering, fracturing increases the productivity index of a production well by increasing the flow rate of hydrocarbons from an unconventional reservoir. Thus, it is of utmost importance to understand the phenomena related to rock-fluid interaction, including adsorption of water, imbibition, clay swelling, and wettability.

Since the early age of petroleum industry, understanding the wettability of rock has been an important subject in improving oil recovery. It mainly defines the preference of rock to get covered by a certain phase in the presence of another immiscible phase (Dake 1977; Abdullah et al., 2007). It determines the distribution of oil, water, and gas in the pore system, and describes the capillary force to hold reservoir fluids of different phases (Morrow, 1990). The distribution of different fluid phases in the pores affect rock/fluid properties, including capillary pressure, water flood behavior, relative permeability and electrical characteristics of rock (Anderson, 1986-1987). Wettability of tight rocks can be measured by various techniques such as Nuclear Magnetic Relaxation (NMR) (Brown and Fatt, 1956), USBM wettability index (Donaldson et al., 1969), contact angle measurement (Johnson and Dettre, 1969) and spontaneous imbibition tests (Bobek et al., 1958) using plugs. The simplest technique for determining the wettability of a reservoir rock sample is by measuring the equilibrium contact angle. However, recent experiments show that this technique may not give representative results (Dehghanpour et al., 2012) for low permeability rocks that are rich in clay and/or organic materials. Spontaneous imbibition has been used as a reliable technique

to quantify the wettability of reservoir rocks such as sandstones and carbonates (Morrow et al. 2001; Zhou et al., 2002; Takahashi et al., 2010). This technique is specifically attractive for tight rocks since a forced displacement in such low permeability rocks requires a significant pressure drop. However, measurement, interpretation, and modeling of even spontaneous imbibition in hydrocarbon-bearing tight rocks are challenging, since their extremely fine pores have a complex structure (Clarkson et al., 2013). Although the organic component of the rock may be hydrophobic, the inorganic component can be hydrophilic in the presence of clay minerals. Clay minerals can adsorb a considerable amount of water, which is controlled by clay chemistry and water salinity (Chenevert 1970; Hensen and Smith 2002). For example, organic shale can be a mixture of hydrophilic and hydrophobic materials. Swelling of reactive clay minerals in shales results in wellbore instability, which has been well studied in drilling engineering (Hensen and Smith 2002). However, the role of this adsorption force on brine intake and wettability of organic shales is poorly understood.

On the other hand, the effects of TOC and kerogen maturity in oil uptake of organic-rich tight rocks need to be further studied. Previous studies provided a lot of evidence for rock properties that affect the wettability of tight rocks. The surface texture of rock, pore morphology, the chemical composition, and the physicochemical properties of brine and crude oil were studied to understand the wettability of organic shale (Drummond and Israelachvili, 2004; Buckley, 2001). Several previous studies demonstrated that wettability depends on the type of source rock and thermal maturity of kerogen (Elijah et al., 2011; Peng, S et al., 2015). In a microscopic study by *Hu* et al. (2014), it was found that highly mature kerogen is hydrocarbon wetting whereas immature kerogen displays hydrophilic behaviour. Moreover, *Boult* et al. (1997) also found that organic rich shale

becomes oil wet through the kerogen maturity. The abundance of organic pore, organic pore volume, and the pore sizes also depends on the thermal maturity of rock that may affect the wettability. Thus, the organic porosity evolves with its maturity (Curtis et al., 2011; Kitty L. Milliken, 2013; Cao, Q. and Zhou, W. 2015). Duvernay samples with different maturities were also examined, and it was found that organic pore morphology varies with the maturity level of kerogen (Munsun, 2015). The amount of organic pore volume that stores hydrocarbons (Curtis et al., 2011) may also affect the oil imbibition and, in turn, affect wettability (Akkutlu et al., 2011.; Xiaong et al., 2012).

In order to improve the EOR technique, it is important also to investigate the wettability and the interfacial phenomena. Evaluation of shale wettability in shale reservoirs is significant for 1) enhancing fracturing fluid load recovery after fracturing operations (Cheng, 2012; Ghanbari and Dehghanpour, 2016), 2) investigating water blockage in shale matrix followed by fast production rate decline (Bertoncello et al., 2014), and 3) selecting the type of fracturing fluid (water-based or oil-based) and additives such as surfactants (Montgomery, 2013; Gupta, 2009). The completion of shale formations is performed by using large volumes of water, as well as by the addition of chemicals like surfactants, friction reducers, biocides, clay stabilizers, and scale inhibitors along with various proppants (Roychaudhuri et al., 2013). Among several known methods for EOR, surfactants are widely used (Standnes and Austad, 2000; Chen et al., 2001). Application of surfactants may lead to changing of rock wettability by reducing the interfacial tension, thus the capillary pressure, and improve flowback of the fracturing fluid (Penny. G. et al., 2012; Jose E. Parra et al. 2016). The wettability of rocks may be altered to favorable conditions by addition of appropriate surfactants to the fracturing or treatment fluids (Standnes and Austad, 2000). Different parameters such as brine salinity, surfactant concentration, structure of surfactant and formation

of the microemulsion can change the wettability of the rock (Yarveicy and Haghtalab, 2017; Yassin et al. 2015). Wang et al. (2011) investigated the effect of different parameters on surfactant EOR in Bakken shale formation, and it was found that for a particular type of surfactant, oil recovery can be improved by optimizing the surfactant concentration, brine salinity, and divalent cation content. Another surfactant EOR study was conducted by Neog and Schechter (2016) on intermediate-wet Wolfcamp shale formation. They investigated the possibility of wettability alteration by surfactants. Jones et al. (2016) used weak emulsifying surfactants to solubilize oil and reduce IFT between oil and water. The resulting emulsion could increase oil mobility and flow through the small pore throat of Wolfcamp shale oil formation.

1.2 Statement of the Problem

Unconventional resources are characterized by low porosity (<15%) and ultra-low permeability (<0.1D; micro-Darcy for tight sandstone reservoirs and nano-Darcy for shale source rock) (Jarvie, 2014; Arogundade et al., 2012). However, it is impossible to get the hydrocarbon production in a commercial flow from shale formation without any fracturing. Hydraulic fracturing operation creates complex fracture networks by pumping fluid into the rock matrix, which interacts with the rock, to unlock the oil and gas from the reservoir (Britt, 1985). Due to water retention (Ghanbari et al., 2013), imbibition (Mahadevan et al., 2009; Dehghanpour et al., 2012, 2013), and other contributing factors, a very low amount of the injected water can be recovered. Clay swelling is another occurrence when the fracturing fluid interacts with shale due to the abundance of clay minerals, which may absorb water.

Moreover, the characteristics of shale source rock are variable due to the presence of organic content with different maturity levels. Several studies show the role of kerogen maturity on rock

wettability. Thus, it is challenging to measure the wettability of shale considering the thermal maturity of its organic contents. Additionally, the evolution of wettability is also important in selecting the suitable type of fracturing fluid. A suitable fracturing fluid for a certain reservoir can improve the flowback of fracturing fluid with maximum hydrocarbon production.

Also, it is very important to study the fluid and rock characteristics with its petrophysical and geochemical properties. In order to achieve efficient petroleum recovery, the evolution of the geochemical process of shale needs to be explained along with an understanding of wettability.

1.3 Objectives of the Research

My M.Sc thesis is intended to determine the fluid and rock characteristics with its petrophysical and geochemical properties of Ireton and Duvernay formations, and also investigate the influence of evolution of geochemical process on wettability. The main objectives of this study are summarized below:

1. Investigating the sample properties in a micro-scale using SEM-EDS, and thin section analysis.
2. Characterizing the wettability of Duvernay sample and examining the effect of heating on wettability performance.
3. Determining the functional dependence of wettability on the mineralogy, petrophysical properties, and source rock attributed geochemical properties of the rocks.
4. Investigate the potential driving factor of imbibition of Duvernay samples.
5. Characterizing the mechanisms controlling oil recovery from shales by soaking process.

1.4 Thesis Structure

The chapters are designed sequentially to obtain the above objectives of this study. They are briefly discussed below:

Chapter 1- Introduction: This chapter briefly explains the technical challenges of extracting hydrocarbons from unconventional resources. Previous literature regarding rock fluid-interactions are reviewed to learn the related difficulties, and acquired knowledge was used to structure the objectives of this study, and address the research gaps.

Chapter 2- Background and petrophysical properties of Ireton and Duvernay Formations: The origin and geological background of Ireton and Duvernay Formation are explained. The samples' mineralogy, porosity, permeability, TOC content, and the maturity of organic content were also analyzed and depicted in this chapter.

Chapter 3- Thin section and SEM-EDS analysis: In this chapter, a microscopic study was conducted to investigate the texture, mineralogy, and most importantly the pore morphology of the rock samples.

Chapter 4- Investigating the wettability of Ireton and Duvernay Formations and the functional dependence of Duvernay wettability on its rock properties: The wettability of organic shale samples from the results of air-liquid contact angle and spontaneous imbibition experiments on the core plugs were characterized. SEM/EDS analyses were used to explain the results of wettability measurements. Finally, the dependence of rock wettability on petrophysical and geochemical properties was investigated.

Chapter 5- Co-current Spontaneous Imbibition Data for Calculation of Oil/Water Capillary Pressure Ratio: Modeling the 1D imbibition data using Handy model and Young-Laplace equations to investigate the potential driving factor of imbibition of Duvernay samples.

Chapter 6- Rock-Fluid Interactions in the Duvernay Formation: Soaking Fluid Evaluation: Soaking test results are explained in this chapter. Soaking fluids were compared concerning oil recovery factor (RF), and the results explained by analyzing liquid-liquid contact angles, and IFT of soaking fluids. Finally, the mechanisms controlling oil recovery from shales by imbibition process were characterized.

Chapter 7- Mechanism of oil recovery from crushed shale packs: Soaking tests of packed samples are explained in investigating the controlling factor of oil recovery by challenging the effect of initial oil saturation.

Chapter 8- Conclusions: The main finding of this study is summarized in this chapter.

Chapter 2

Background and Petrophysical Properties of Ireton and Duvernay Formations

2.1 Overview and Background

In this chapter, the detailed background of Ireton and Duvernay shale samples is discussed. First, the location of Ireton and Duvernay formation and their origin with a brief description of the geology of these formations is presented. Then the petrophysical properties, mineralogy, and the results of rock-eval pyrolysis to characterize the Duvernay shale samples are discussed.

2.1.1 Location

The prospective area of Duvernay Formation is divided into Kaybob, Edson, and Willesden Green regions which are located in the north-western part of Alberta (Figure 1(a). For this study, ten twin core plugs from a single well drilled in Kaybob region were selected. The depth of twin core plugs ranges from 2780.41 to 2804.41 meters. We have samples from both Ireton and Duvernay Formations. Ireton is the shale formation that overlies on Duvernay Formation.

2.1.2 Origin and Geology

The stratigraphic column (Figure 1 (b)) shows that the Duvernay Formation is sandwiched by two shale formation. Ireton is the overlying formation, and Majeau Lake is the underlying formation of Duvernay. All these three formations deposited at the Frasnian age under the Woodbend Group

as shown in Figure 1 (b) (Switzer et al., 1994). A detail about the origin and geology of Duvernay and Ireton Formations are described below.

Duvernay Formation: The Duvernay Formation was deposited during the maximum transgressive stage of the Woodbend Group (Stoakes, 1980). Transgressive and high stand sea levels in conjunction with high rates of primary productivity provided favourable conditions for the preservation of high amounts of organic matter creating a world class source rock and now reservoir (Fothergill et al., 2014). The Duvernay Formation is characterized by three lithofacies: 1- siliceous organic-rich mudstones, 2- argillaceous mudstones, and 3- non-reservoir carbonates (Dunn and Humenjuk, 2014). Among nine pairs of Duvernay twin plugs, eight plugs are from siliceous organic-rich mudstones, and one pair is from non-reservoir carbonate layer.

Ireton Formation: Ireton formation was deposited at the early regression stage, just after Duvernay formation. The regression stage represents the shelf development period in basin filling procedure (Creaney et al., 1994). Ireton formation was the initial formation when the cyclic basin filling shales and carbonates started to form (Fothergill et al., 2014). According to Switzer et al. (1994), Ireton formation is a calcareous mudstone and does not contain enough TOC to have a potential source of hydrocarbon.

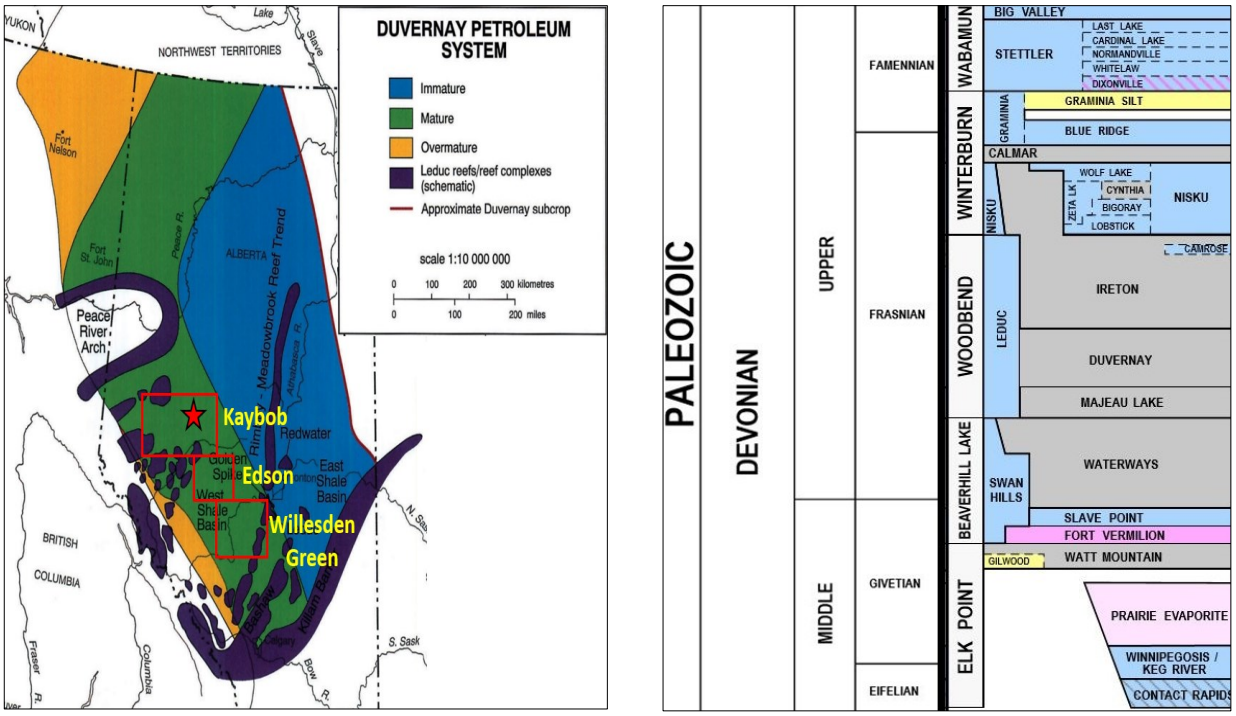

(a) **(b)**

Figure 1: (a) Location of Duvernay Formation (Revised from Creaney et al., 1994) (b) Stratigraphic column of east central plain of Alberta. Duvernay Formation is under Woodbend Group of upper Devonian period and belongs to Frasnian age (Revised from Alberta Table of Formations, 2015).

2.2 Sample Properties

2.2.1 Gamma Ray Log

Figure 2 shows the core log gamma ray (GR) and its spectrometry including potassium (wt %), thorium (ppm), and uranium (ppm) concentrations along the cored interval for Ireton and upper Duvernay Formations. The blue points are corresponding data to the Ireton core samples and the red points are corresponding data to the Duvernay core samples used in this study. The high value of GR is attributed to the presence of clay minerals and organic matter in shale samples. Table 1 shows that the GR value of the given pair of Ireton sample is 119.44 API. It includes potassium, thorium and uranium spectra emitting from minerals. Gamma ray emission from potassium is

2.08%, thorium 1.15 ppm, and uranium is 2.62 ppm. Duvernay GR ranges from 69 to 150 API. A wide range of GR value in Duvernay is attributed to different mineral concentration in the rock and consequently, different lithology in the formation. Gamma ray emission from potassium ranges from 0.79 to 2.9 %, thorium 3.02 to 12 ppm, and uranium 0.29 to 9.23 ppm. Among all the Duvernay sample - AOK 6 is showing comparatively minimum GR value of 80.67 API, possibly attributed to the low concentration of potassium (0.79%).

Table 1: Extracted gamma ray core log data for core samples of Ireton and Duvernay

Sample ID	GR (API)	Potassium (%)	Thorium (ppm)	Uranium (ppm)
AOK1	119.44	2.08	1.15	2.62
AOK2	115.95	1.09	9.07	2.84
AOK3	132.51	2.07	5.46	9.23
AOK4	123.09	1.97	12.00	5.53
AOK5	118.69	1.84	9.23	1.72
AOK6	80.67	0.79	4.08	6.62
AOK7	105.43	1.43	5.39	5.83
AOK8	150.70	1.62	3.56	6.42
AOK9	130.26	2.90	11.06	0.29
AOK10	135.43	1.67	3.02	8.84

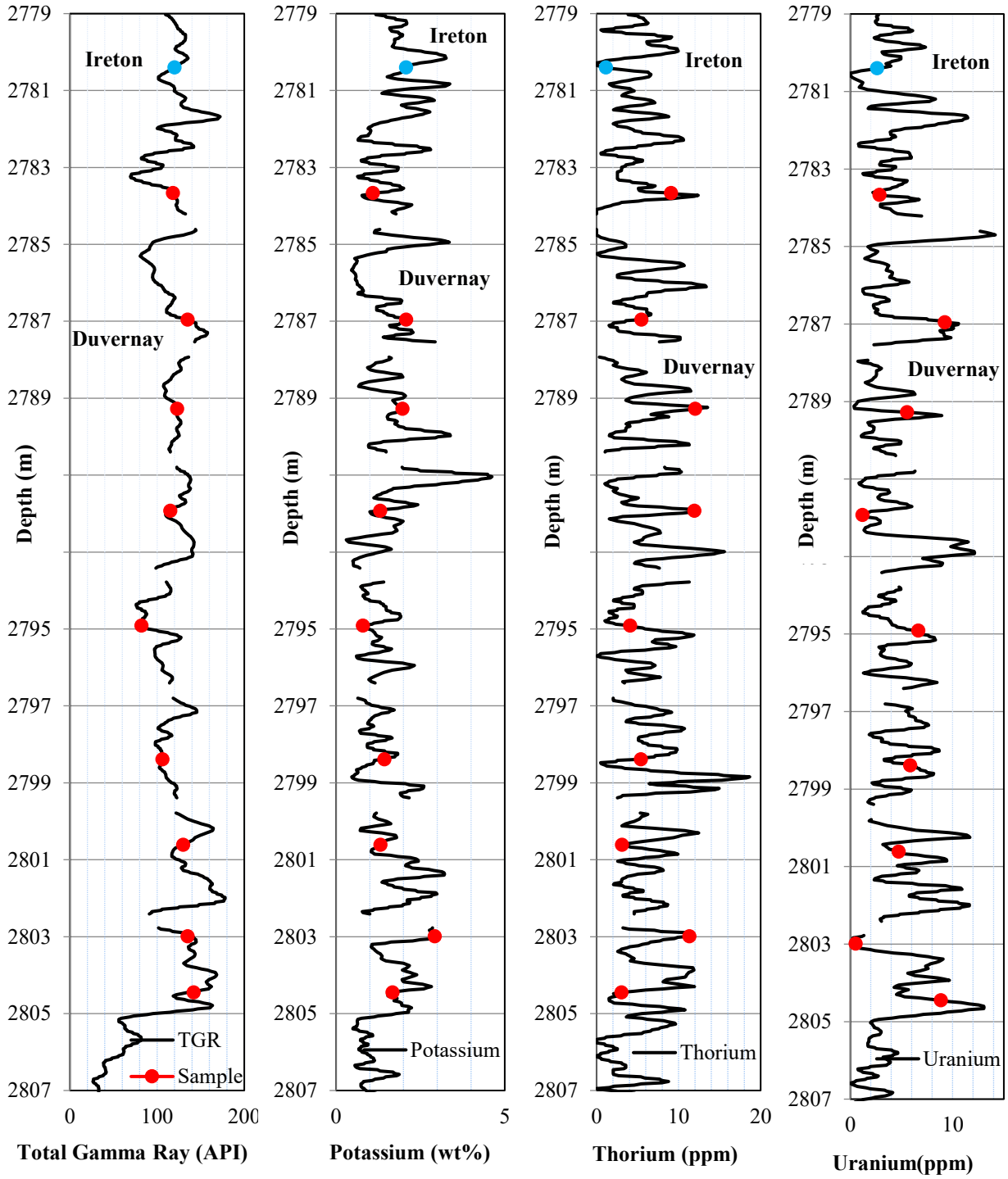

Figure 2: Core log gamma ray (API) and its spectrometry including potassium (wt%), thorium (ppm), and uranium (ppm) concentrations. 10 twin core plugs were selected from one well drilled in Kaybob region.

2.2.2 XRD Analysis (Mineralogy)

Table 2 lists the predicted mineralogy of core samples based on a robust core tied model developed from offsetting X-ray diffraction (XRD) data points. According to Table 2, quartz and calcite are the dominant non-clay minerals, and Illite/smectite and illite/mica are the dominant clay minerals. Ireton sample (AOK1) has 41wt% of non-clay and 59wt% of total clay content which the maximum wt% among all samples. AOK1 also contains high chlorite content (11wt %). Among the clay minerals, the kaolinite has the maximum expandability, followed by smectite and illite. The amount of kaolinite and smectite is almost zero in all samples. However, the illite content is considerable, especially in AOK1.

Table 2: Predicted mineralogy (wt%) of Ireton and Duvernay core samples.

Sample ID	Depth (m)	Quartz	K-feldspar	Plagioclase	Calcite	Ankerite/ Fedolomite	Dolomite	Pyrite	Total non-clay	Illite/ Smectite	Illite/ Mica	Chlorite	Total clay
AOK1	2780.41	22	4	1	5	2	3	4	41	10	38	11	59
AOK2	2783.66	63	1	3	12	5	1	2	87	5	7	1	13
AOK3	2786.94	51	6	1	15	3	2	3	82	6	11	1	18
AOK4	2789.27	47	1	4	15	3	2	3	75	6	18	1	25
AOK5	2791.85	40	7	6	12	2	1	3	71	11	16	2	29
AOK6	2794.91	52	1	4	13	3	2	3	78	9	12	1	22
AOK7	2798.36	64	2	3	9	2	2	2	84	3	12	1	16
AOK8	2800.60	54	2	3	10	3	1	3	76	11	12	1	24
AOK9	2802.94	54	4	4	9	2	2	3	76	11	11	2	24
AOK10	2804.44	37	3	1	16	0	2	3	62	11	24	3	38

2.2.3 Tight Rock Analysis (TRA) Data (Porosity and Permeability determination)

Interpreted petrophysical values based on a robust core tied petrophysical model developed from 26 offsetting TRA points are presented in Table 3. Core samples are named AOK1 to AOK10 as depth increases from 2780.41m (AOK1) to 2804.44m (AOK10). The effective porosity is measured by Boyle's law helium porosimetry method on offset crushed grains near the original core plugs. The predicted effective porosity ranges from 2.33% (AOK1) to 3.93% (AOK8) of bulk volume (BV). We also used offset crushed grains and measured absolute permeability by the pressure-decay method. The predicted pressure-decay permeability ranges from 63.04 nD (AOK1) to 141.51 nD (AOK7). The measurements of effective porosity and pressure-decay permeability on intact core plugs may be affected by artifacts such as induced features and may lead to erroneous results. The crushing of shales enhances the accessibility to pore space and reduces the effects of experimental artifacts on effective porosity and pressure-decay permeability. Table 3 also lists the predicted initial gas, water and oil saturations of core samples measured by retort method on offset crushed grains. To measure the water saturation, crushed grains are heated up to 250^{o}F, and the extracted vapor is condensed by cooling. The accumulated condensed liquid is comprised of water and oil. The temperatures are further increased to 600^{o}F to extract the rest of oil remained in crushed grains. The water content condensed between 250 ^{o}F to 600^{o}F is considered as clay-bound water (Handwerger et al., 2012) which is not taken into account for the calculation of water saturation listed in Table 3. AOK1 (Ireton) has the maximum water saturation of 54.61% P.V compared to other Duvernay samples. The effect of high water saturation of Ireton sample on the results of imbibition experiments is discussed in the following sections. The water saturation is in the form of sub-irreducible and ranges from 2.89% (AOK2) to 38.04% (AOK10) of pore volume (PV). It should be noted that we received the core plugs four months after saturation measurements

by a commercial lab. Despite preserving the core plugs in cellophane coatings, it is expected that a portion of water and oil saturations were evaporated after four months. Therefore, the actual water and oil saturations at the start of experiments are lower than those listed in Table 3.

Table 3: Predicted petrophysical properties based on offset TRA measurements

Sample ID	Depth (meter)	Effective porosity (%BV)	Pressure-decay permeability (nD)	Gas saturation (%PV)	Water saturation (%PV)	Oil saturation (%PV)
AOK1	2780.41	2.33	63.08	21.41	76.41	2.18
AOK2	2783.66	2.83	98.27	56.70	2.89	40.41
AOK3	2786.94	3.24	112.35	56.43	2.90	40.67
AOK4	2789.27	2.97	102.85	54.76	3.23	42.01
AOK5	2791.85	3.08	105.72	46.85	5.60	47.55
AOK6	2794.91	3.32	115.69	59.84	5.74	34.42
AOK7	2798.36	3.62	127.68	66.93	4.13	28.94
AOK8	2800.60	3.93	141.51	60.08	7.48	32.44
AOK9	2802.94	3.33	115.75	57.41	11.21	31.38
AOK10	2804.44	3.33	85.22	33.94	38.04	28.03

2.2.4 Rock Eval pyrolysis

The results of measured rock-eval pyrolysis on offset samples listed in Table 4 are used to determine kerogen type, kerogen maturity, and TOC content. Table 4 presents TOC content, S_1, S_2, S_3, T_{max}, hydrogen index, oxygen index (OI), and production index (PI). S_1 shows the amount of free hydrocarbon present in the rock, S_2 presents the amount of carbon after thermal cracking of kerogen in pyrolysis process, and S_3 is the amount of CO_2 after the thermal cracking of kerogen. T_{max} shows the maximum temperature needed to release the maximum amount of hydrocarbon by

kerogen cracking. Hydrogen index, oxygen index (OI), and production index (PI) are calculated using S_1, S_2, S_3, and TOC content as follows (Tissot and Welte, 1984),

$$HI = (S_2 / TOC) \times 100 \text{ (mg HC/g TOC)} \quad (1)$$

$$OI = (S_3 / TOC) \times 100 \text{ (mg } CO_2\text{/g TOC)} \quad (2)$$

$$PI = S_1 / (S_1 + S_2) \quad (3)$$

The crossplot of HI vs. OI describes the type of kerogen. According to the Van Krevelen diagram (Krevelen, 1950) presented in Figure 3 (a), kerogen type of Duvernay samples is Type II that shows the potential of kerogen to produce a mix of oil and wet gas (Raquejo et al., 1992). The crossplot of PI vs. T_{max} Figure 3(b) can be interpreted to identify the maturity of kerogen. As shown in Table 4, PI ranges from 0.34 to 0.56 with T_{max} in the range of 440 to 458 ^{o}C. T_{max} within the 435 to 455 ^{o}C interval represents type (II) of kerogen maturity (Baskin, 1997). Type (II) of kerogen usually come up with oil generation potential and consequently, most of the Duvernay shale samples lies in the oil zone as shown in Figure 3 (b).

Table 4: The results of measured rock-eval pyrolysis test on offset samples.

Sample ID	Depth (m)	TOC (wt%)	S_1 (mg/g)	S_2 (mg/g)	S_3 (mg/g)	T_{max} (°C)	HI	OI	PI
AOK1	2780.41	0.94	1.28	0.99	0.35	440	105.00	37	0.56
AOK2	2783.66	2.75	2.03	2.60	0.14	452	155.69	8.38	0.44
AOK3	2786.94	3.13	2.42	3.43	0.19	451	147.84	8.19	0.41
AOK4	2789.27	2.90	2.78	4.94	0.23	455	154.86	7.21	0.36
AOK5	2791.85	3.01	2.73	5.02	0.22	455	140.22	6.15	0.35
AOK6	2794.91	3.21	2.38	4.57	0.19	458	150.33	6.25	0.34
AOK7	2798.36	3.49	3.16	5.26	0.15	456	167.52	4.78	0.38
AOK8	2800.60	3.80	3.30	4.47	0.20	456	156.84	7.02	0.37
AOK9	2802.94	3.25	2.55	4.93	0.19	458	157.01	6.05	0.34
AOK10	2804.44	4.12	3.32	6.34	0.14	456	154.25	3.19	0.34

TOC content is the total amount of organic carbon present in the rock sample and explains the quality of the source rock in terms of hydrocarbon potential (Baskin, 1997) (Table 5). As shown in Table 4, Ireton contains 0.94wt% of TOC that represents “fair” petroleum potentiality of the sample. Duvernay TOC content ranges from 2.75 to 4.12 wt% and classifies the samples as “very good” source rock in terms of hydrocarbon potential (Baskin, 1997).

Table 5: Classification of source rock quality by TOC content.

Petroleum Potential	TOC (wt %)
Poor	0-0.5
Fair	0.5-1
Good	1-2
Very Good	2-4
Excellent	>4

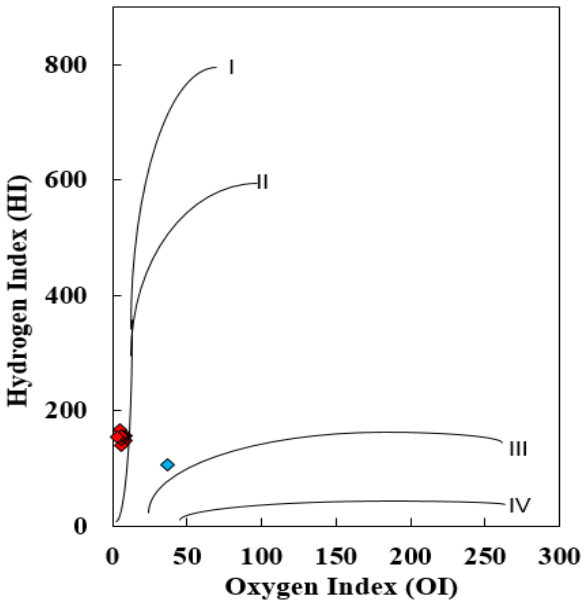

(a)

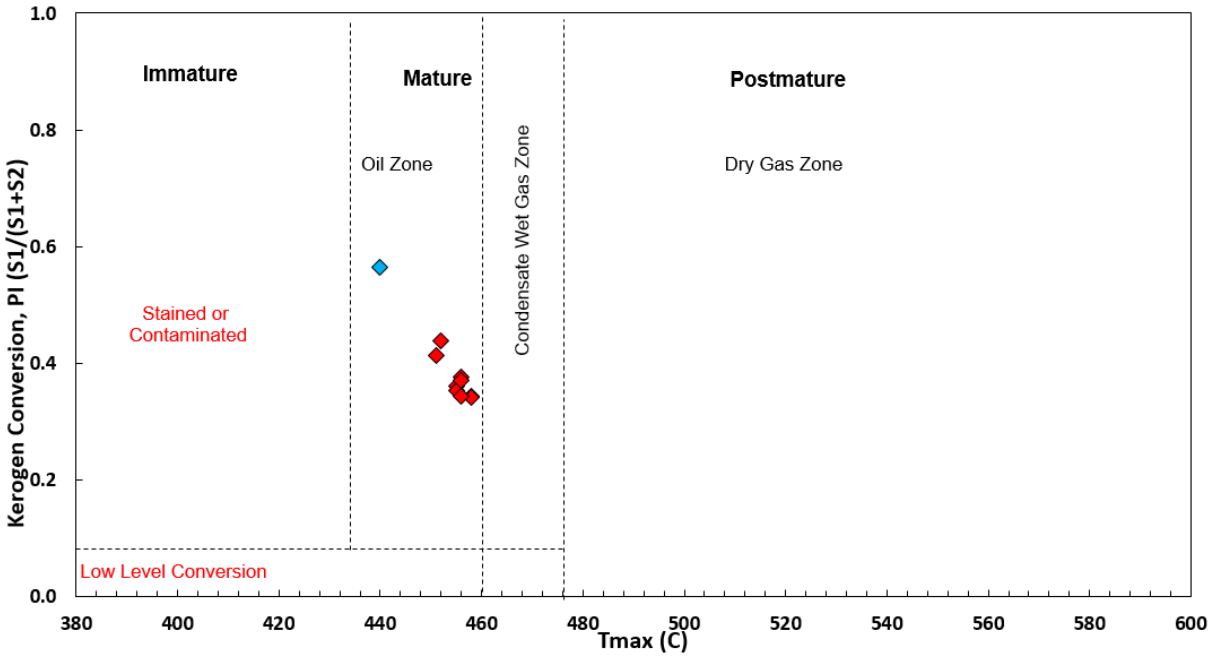

(b)

Figure 3: The crossplots of (a) hydrogen index vs. oxygen index (OI), and (b) production index (PI) vs. Tmax. Kerogen type of Duvernay core samples is Type II. In terms of kerogen maturity level, the samples are in oil-window.

Chapter 3

Thin Section and SEM-EDS Analysis

In this section, the thin section and the scanning electron microscopy with energy dispersive X-ray spectroscopy (SEM/EDS) analysis on the Duvernay sample is discussed. Thin section analysis is the most precise way to evaluate the texture, mineralogy, presence of bioclasts and pore system of the rock (Anovitz and Cole 2015). Besides identifying the individual minerals and clay structure, SEM images can also determine the petrofacies of the rock including pore types, pore sizes and a detail information about the presence of minerals around the pore system.

3.1 Sample Preparations and Methodology

3.1.1 Thin Section Analysis

Thin sections of Duvernay samples were prepared in the lab and analyzed them under the polarizing microscope. The rocks were sliced very thin and attached with a piece of glass in the presence of blue epoxy. Blue epoxy commonly is used to identify the pores present in the rock. We have used Nikon ECLIPSE 50i POL polarizing microscope to analyze the thin sections. The microscope was equipped with a digital camera, and an ELMO P10 Visual Presenter to capture images of the thin sections. Analyzing thin sections under polarizing microscope provide information about the percentage of dominating minerals, the presence of organic matter, inorganic pores, etc. Several pictures of different thin sections were captured and used them to analyze the properties of the corresponding rock sample. 20x, 40x, 60x and 100x magnifications were used to

get the detail of a particular area of the thin section. Due to the magnification limitations of the polarizing microscope, we could not identify any pores from the thin section of the rock sample.

3.1.2. Scanning Electron Microscope (SEM) Images

Cubic pieces were prepared using the end pieces of Duvernay core plugs. Cubic samples were polished and coated with carbon to get a smooth surface. Then, the samples were scanned, and high-resolution pictures were taken under electron microscope. These SEM images were used to interpret the presence of organic substances, organic and inorganic pores, pore structure, pore network. EDS elemental maps of a corresponding SEM image were also taken to determine the concentration of a specific element. Therefore, minerals with known compounds were identified by analyzing the elemental map and so as the organic substances with the presence of high concentration of carbon.

3.2 Results and discussion

3.2.1 Thin Section Analysis

Mineral Identification: Minerals were identified at x100 magnification using both plane polarized light (PPL) and cross polarized light (XPL). Figure 4(a) shows the field of view under plane polarized light and Figure 4(b) shows the field of view under cross polarized light at the same location of the thin section.

Under PPL, few minerals were identified by observing its color and the relief. Heavy minerals are always opaque and show black color because light cannot pass through the mineral under the polarizing microscope. Under the reflected light microscope, the golden yellow color assures that the thin sections mostly contain pyrite (P). No camera was attached to the reflected light

microscope; so, we were unable to provide any pictures of pyrite under the reflected light microscope. Carbonates (C) were identified because of its extremely high relief under PPL. Some feldspar (F) were also identified by its very low relief under PPL.

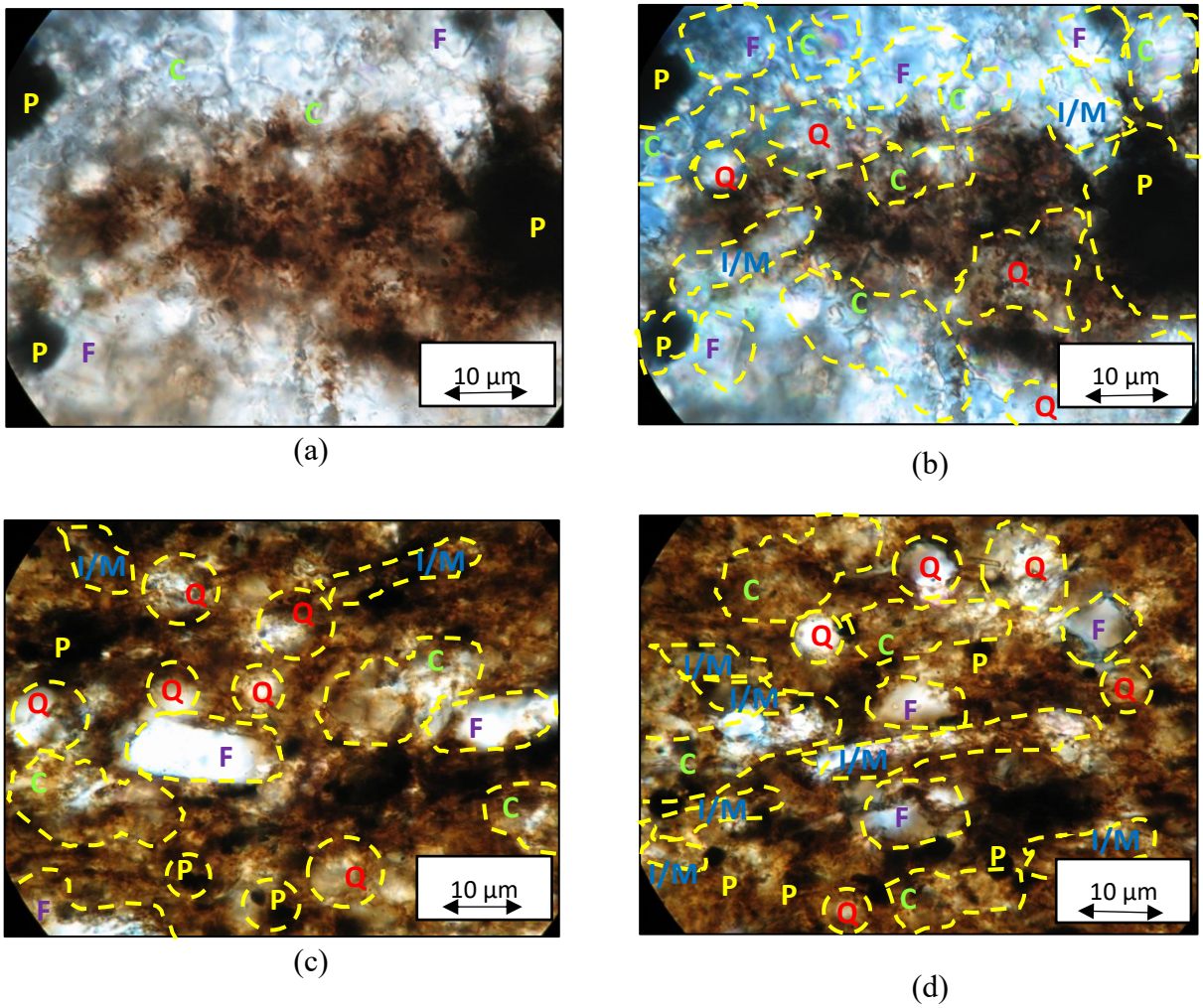

Figure 4: Thin sections of Duvernay rock samples; (a) mineral identification under PPL (sample AOK2) (b) mineral identification under XPL (sample AOK2) (c) mineral identification under PPL (sample AOK5) (d) mineral identification under PPL (sample AOK9). Quartz (Q), feldspar (F), carbonate (C), pyrite (P), illite (I) and mica (M) are the common minerals identified by thin sections.

Under cross polarized light (XPL), most of the minerals (quartz, Feldspar, carbonates, mica) can be identified (**Figure 4(b)**). Carbonates (C) show high order interference color with its pearly appearance. Comparatively low relief, sub-rounded grain structure, grayish interference color

confirms the presence of quartz (Q). Feldspar (F) also has low relief and gray interference color, however, the presence of cleavage can differentiate it from the quartz mineral. It was very challenging to identify the Illite/Mica from the thin sections. Elongated grains and bright second order interference color in XPL helped to identify some minerals under mica group. It was observed that most of the mica minerals are aligned along the lamination of the rock (Figure 4 (b) and 4(d)). Based on the above criteria, we identified minerals from few thin sections shown in Figure 4 (c) and 4(d) (AOK5 and AOK9 respectively).

Grain sizes and shapes: Duvernay is a dark colored clastic sedimentary rock. It consists of mineral grains and clay minerals those were transported to the site of deposition. The rock mainly contains clay to silt sized particles which range between 5 μm to 50 μm. Rounded quartz grains of <10 μm were mostly found in the rock. Detrital calcite grains vary from sub-rounded silt sized (60 μm) to rounded clay sized (5 μm) particles. Clusters of pyrite are very common in the Duvernay samples. Grains are usually <5 μm and rounded in shape.

Distinct layers: Figure 5(a) represents different layers present in Duvernay shale sample. Various sizes of mineral grains, the abundance of a certain mineral, the presence of organic substances, etc. are responsible for creating distinct layers at the time of deposition. The contact between two layers can be considered as a weak zone. It may not be noticeable at the subsurface condition under high pressure. However, fracture along the laminations were seen on the rock sample. In Figure 5(a) the line filled with the blue epoxy represents the fracture along the laminations. This type of fractures are very common in Duvernay rock samples. Some of them are wide enough that can be seen even by naked eyes. As an evident, Figure 5(b) shows that the heated samples after brine

imbibition leave traces of salts into the fractures. In Figure 4(c) and (d) we have seen the random distribution of pyrite mineral, but the Pyrite bands are not very common in Duvernay samples. Figure 5(c) shows the pyrite bands which was found only in the sample no AOK2. These pyrite bands were visible even in naked eyes (Figure 5(d)).

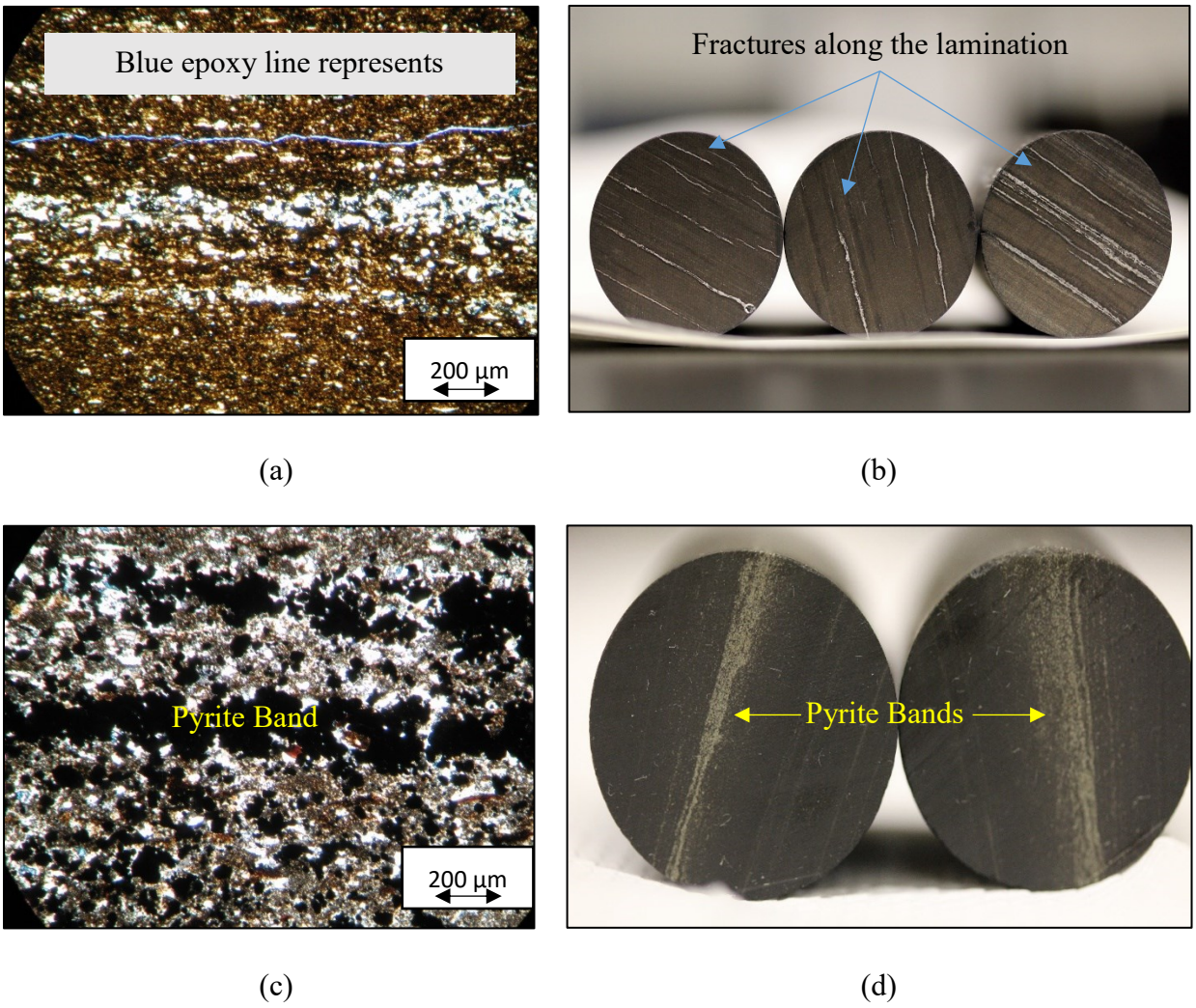

Figure 5: The presence of fractures and pyrite band in thin section analysis. (a) Different layers present in the rock sample with the presence of fracture along the laminations on thin sections (b) the presence of fracture along the laminations on core samples (after brine imbibition) (c) the pyrite band (black layer) on thin sections (sample AOK2) (d) the pyrite bands on core sample AOK2.

Presence of microfossils: Some microfossils were also found in the samples shown in Figure 6 (a) and (b). Microfossils were not very common for all samples, but some intact skeletal grains are mostly found on sample AOK5 and AOK9. The presence of skeletal grains suggests the quite water depositional environment (Nicholas, 2000) in an open marine transgressive stage. The grains are around 150 μm to 200 μm in size.

Presence of organic carbon: Dark black spot represents the presence of organic matter that sometimes conflicts with the presence of heavy minerals because, under the polarizing microscope organic matter and heavy minerals both are opaque and show dark spots. For example, the dark spots in Figure 6 (c) and (d) can be organic matter and/or pyrite. By using reflected light microscopy, it is possible to separate the organic matter and pyrites. We have distinguished the organic matters and the pyrites using reflected light microscopy (Figure 6 (c) and (d)).

Lens shaped organic matters were also found in the rock thin sections. Figure 6 (e) and (f) show the presence of organic lenses which were found more often in Duvernay shale (length 60 μm to 150 μm). Some scattered organic contents are also very common and are usually <10 μm (Figure 6 (c) and (d)). Amorphous organic matter along with the laminations was also found in the rock. Some layers were identified which contain comparatively more organic matter (Figure 6 (g) and (h)). These layers define the anoxic depositional environment which is the most suitable environment to preserve organic contents (Rezaee, R., 2015).

Duvernay formation is very compacted shale formation. No inorganic pores were identified by the thin section analysis. The organic pores are usually even smaller than the inorganic pores. Due to the limitation of magnification, we could not identify any inorganic or organic pores. To determine

the inorganic and organic pores, SEM-EDS analyses were carried out which is discussed in detail in the next section.

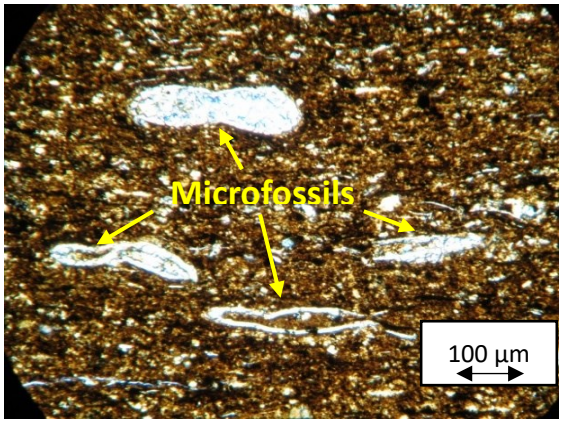

(a)

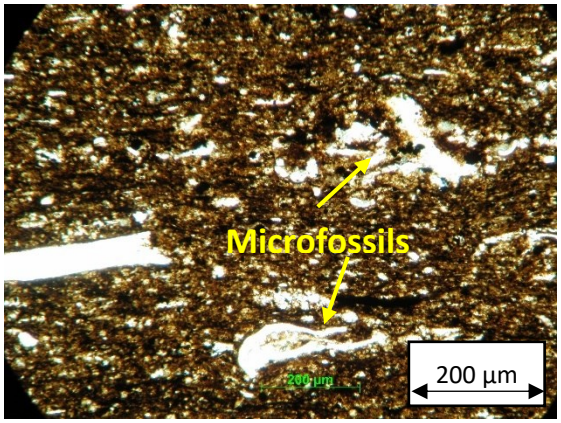

(b)

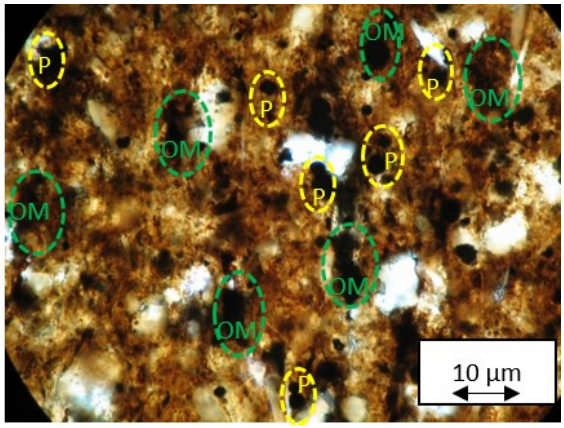

(c)

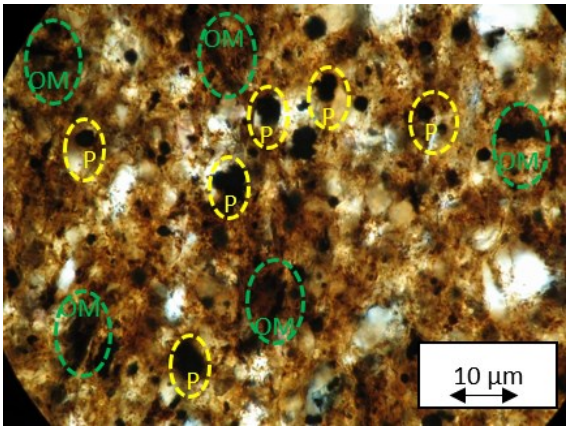

(d)

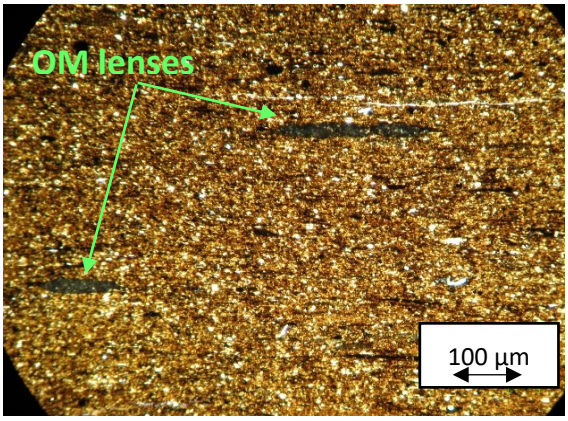

(e)

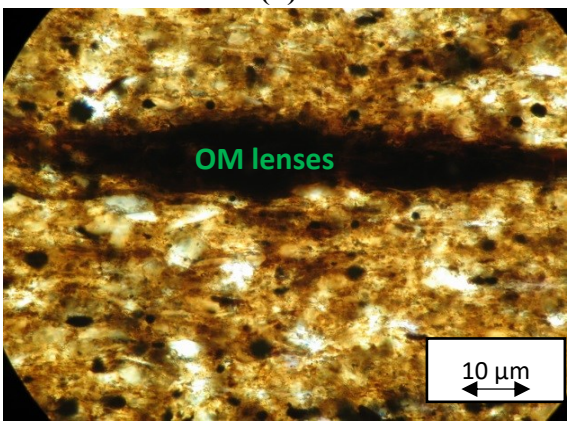

(f)

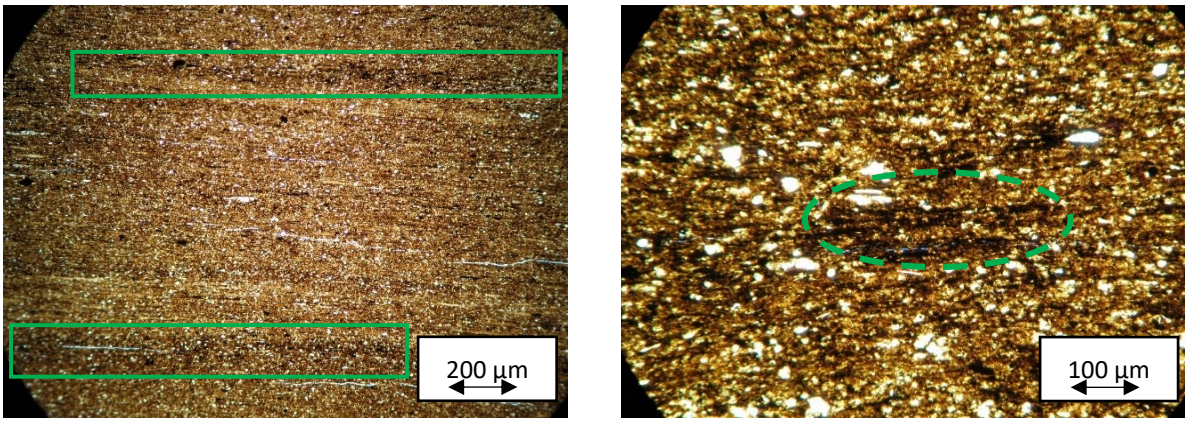

(g) (h)

Figure 6: Thin section Duvernay rock samples; (a) the presence of microfossils on sample AOK5; (b) the presence of microfossils on sample AOK9; (c) and (d) distinguishing between pyrite and organic contents; (e) and (f) the presence of organic lenses; (g) layers containing comparatively more organic matters and (h) organic matters along the laminations

3.2.2 Scanning Electron Microscope (SEM) Images

Mineral identification: SEM and EDS images are used to characterize the mineralogy, identify pore structure and pore network, the presence of organic substances, etc. At first, a position is selected to take SEM image, and then EDS images of the same positions are captured. Following Figure 7 shows the SEM image 7(a) with its corresponding EDS images 7(b) of sample AOK5. Here different colors in EDS images represent different chemical elements including sulfur, iron, calcium, magnesium, silicon, carbon, potassium, sodium, aluminum etc. Thicker color means the higher concentration of the corresponding element. We can identify a mineral by using the co-existence of several elements at the same location. For example, in Figure 7 (b), the blue map represents the concentration of sulfur (S), and green map represents the concentration of Iron (Fe). Thus, the coexistence of both sulfur and iron at the same position represents the presence of pyrite (FeS2). Similarly, other dominant minerals such as quartz (SiO2), feldspar (K,Ca,Na(AlSi3O8)) and carbonates (Ca (Mg,Fe)(CO3)2) can also be identified.

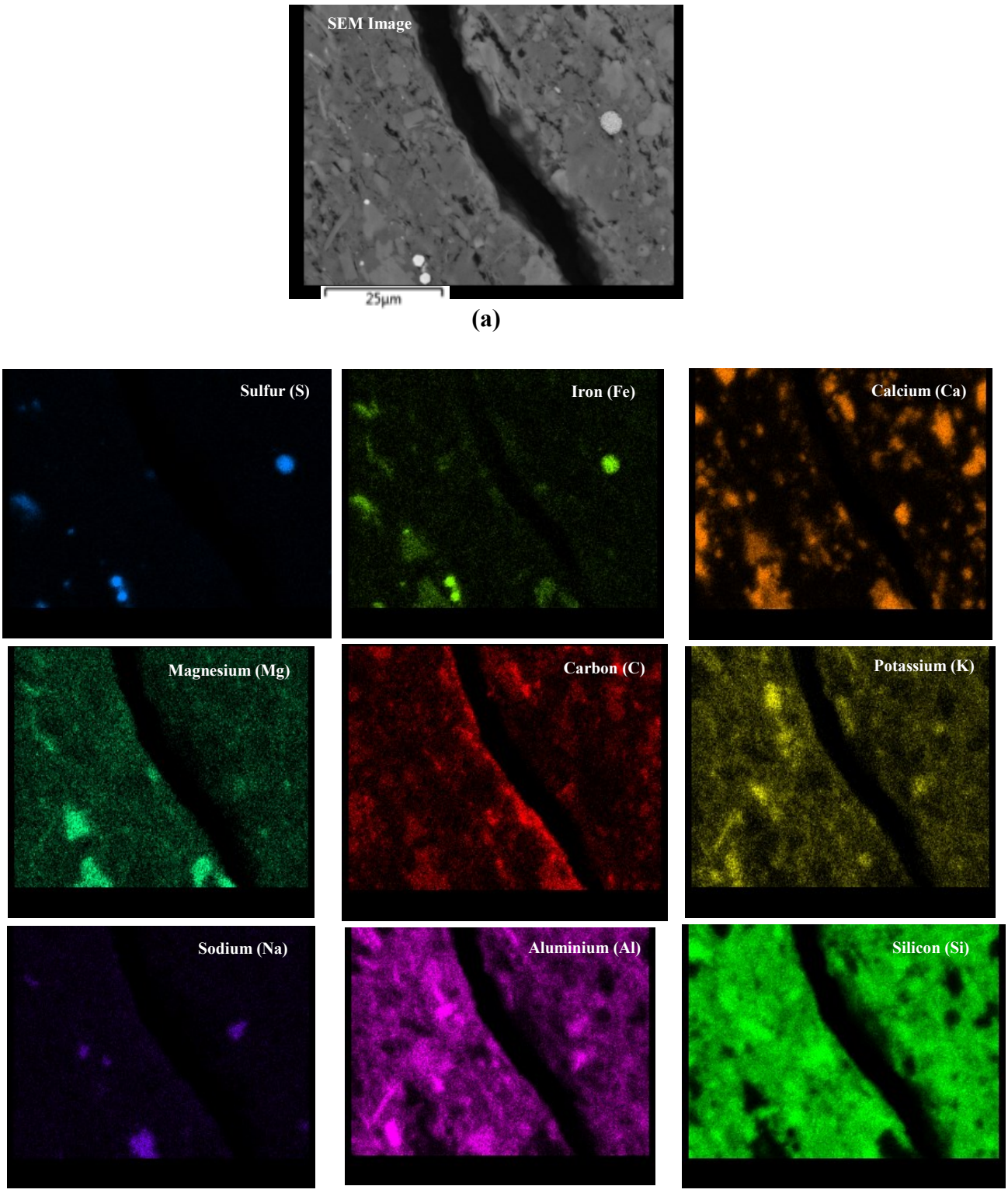

Figure 7: (a) SEM image and (b) EDS images of (a) representing different elements.

Presence of organic carbon: Organic matters (OM) in sedimentary rock are mainly carbon based compound. Some mineral grains were coated by organic carbon shown in Figure 8(a) (SEM image). OM coating was confirmed by the carbon map of EDS image (Figure 8(b)). Some scattered organic fragments (500 nm-800 nm) in between clay minerals were also found in the rock (Figure 8(c) and (d)). Amorphous OM were mostly found in the rock matrix. They were found in between mineral grains and usually align along the laminations. Most of the pores are hosted by these amorphous organic matters (Figure 8(e) and (f)). The presence of a certain amount of organic carbon determines the quality of the rock as a source of potential hydrocarbon. In another word, the total amount of organic carbon (TOC) describes whether the rock is good or bad as a hydrocarbon potential. The quality of the rock in terms of hydrocarbon potential was also described in chapter 2.

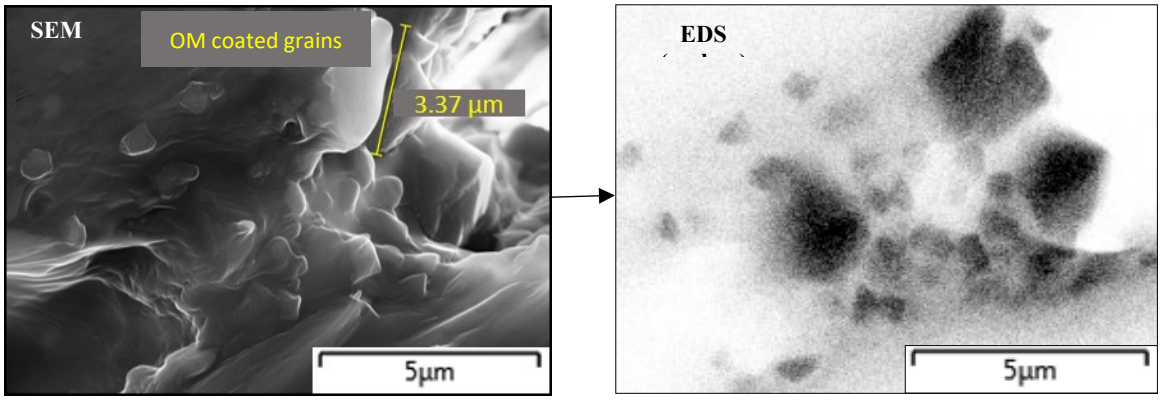

(a) (b)

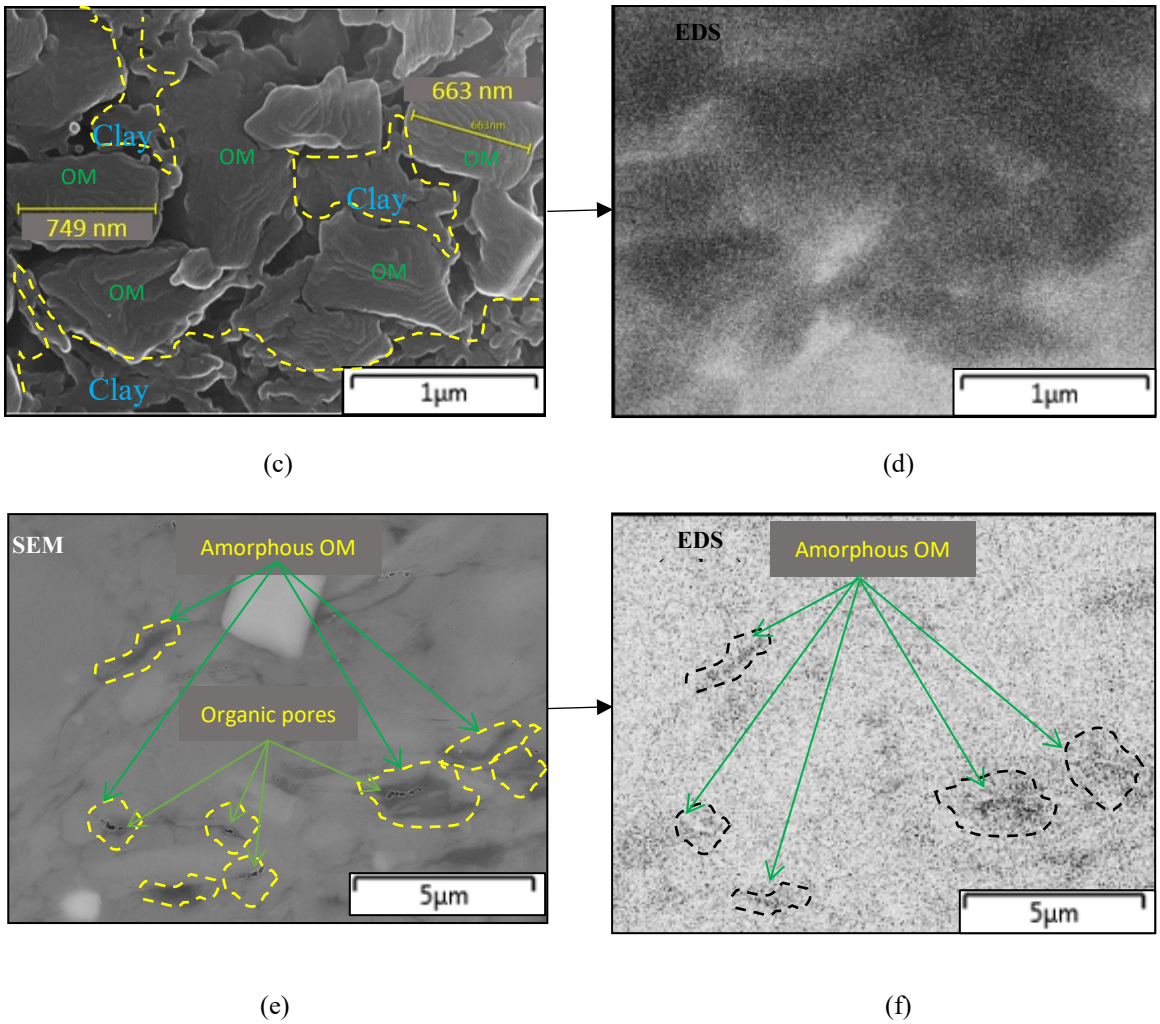

Figure 8: (a) SEM of organic carbon coated grains; (c) SEM of fragments of OM in clay layers; (e) SEM of amorphous OM in the rock matrix containing organic pores; (b),(d) and (f) are the carbon EDS images of (a), (c) and (e) respectively.

Organic and Inorganic Pores: Pores inside the organic matters are the organic pores, and mineral-hosted pores are the inorganic pores. Duvernay rock has both inorganic and organic pores. From the SEM images, it was found that the organic pores are very dominant in the Duvernay rock sample than the inorganic pores.

The organic pore is a very common type of pore system in shale formation (Passey et al., 2010; Curtis et al., 2011). Duvernay pores within the organic matter created sponge like structures (Figure 9(a)). Different sizes of pores in the OM created this sponge like structure. The organic

pore size combines with the vitrinite reflectance data may describe the thermal maturity of OM to produce hydrocarbon (L.M. Anovitz, K.C. Littrell., 2014; Tang, Xianglu et al., 2016). Some pores were connected to each other (Figure 9 (a), (b), (c), and (d)). Connected organic pores can create a large round shaped pore or an elongated linear groupings of pores. Elongated linear groupings of organic pores are usually around 500 nm to 1µm in length.

Inorganic pores are not very common in Duvernay rocks. A very few of them were identified with SEM images (Figure 9(b)). Duvernay formation contains clay to silt sized grains deposited during the maximum transgressive stage. The depositional environment and the later overburden pressure may turn this formation into a compacted shale formation. This may cause the lack of inorganic pores in the Duvernay formation.

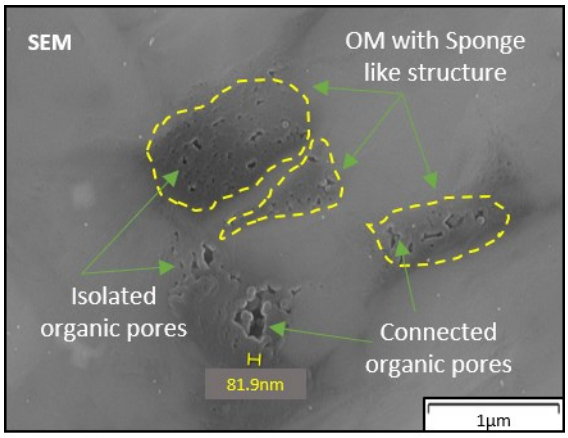

(a)

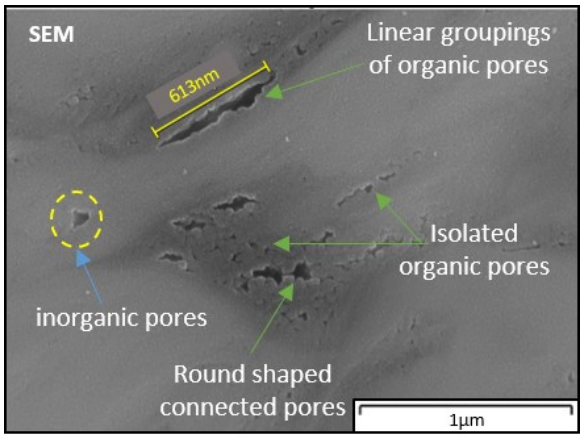

(b)

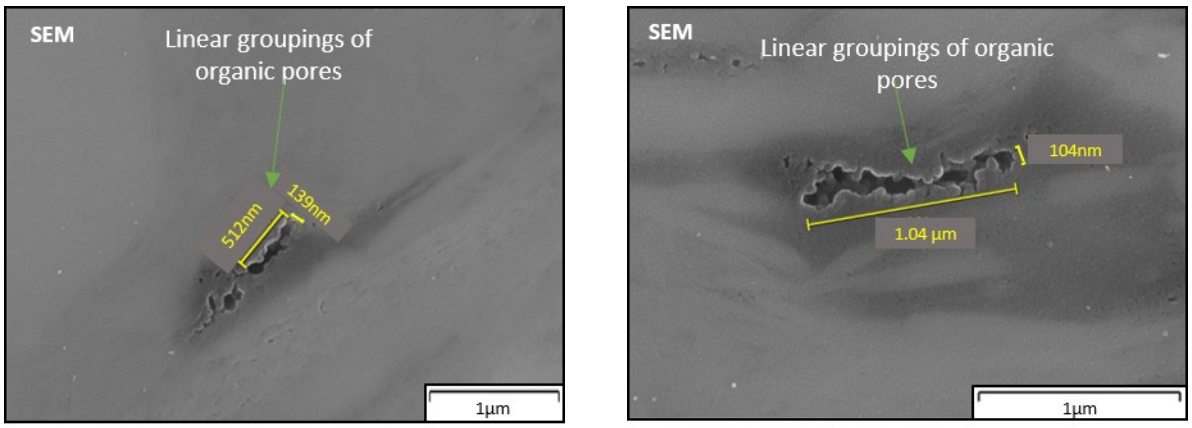

(c) (d)

Figure 9: SEM images of (a) OM creating sponge like structures on rock matrix; (b) isolated and connected organic pores, presence of inorganic pores; (c) and (d) linear grouping of organic pores

3.3 Conclusions

This study demonstrates the lithology, petrology, and petrofacies of the Duvernay rock. From the thin section and SEM-EDS images, we extracted detail information about the formation. The mineral content, the size and shape of grains, distinct features of the rock sample and the presence OM were explained by analyzing both thin sections and SEM-EDS images. Rock texture and some certain sedimentary features such as lamination and the presence of bioclast gave us the clear picture of depositional environment of the formation. From the thin sections, it was found that Duvernay rock contains clay to silt sized mineral grains. Among them, quartz and feldspars are the dominant minerals with the presence of carbonates, clay minerals (mica/illite) and pyrite. Distinct layers of OM were very noticeable which leading to explain the quality of the source rock in petroleum perspective. Furthermore, the SEM-EDS images were taken to identify the pore type, pore system and the presence and distribution of OM. It was found that most of the Duvernay pores are organic pores indicates the possible oil wet behavior of the rock. The sponge like structure of

OM with the presence of connected pores may demonstrate the maturation of the OM to produce hydrocarbon.

Chapter 4

Investigating the wettability of Ireton and Duvernay Formations and the functional dependence of Duvernay wettability on its rock properties

In this chapter, we characterized the wettability of organic shale samples from a single well completed in the Duvernay Formation which is a source rock reservoir. We presented the results of air-liquid contact angle and spontaneous imbibition experiments on the core plugs. The crossplots of petrophysical properties and SEM/EDS analyses were used to explain the results of wettability measurements. The effect of heating on rock wettability is also described. Finally, the dependence of rock wettability on petrophysical and geochemical properties was investigated by comparing the as received and heated samples results.

4.1 Materials

4.1.1 Rock Samples

To investigate the wettability, we have used 10 pairs of twin core plugs drilled from a single well on Ireton and Duvernay formations. These samples were collected from Kaybob region. The petrophysical and geochemical characteristics of the samples were described in chapter 2. All the characteristics are assumed to be similar for a twin pair. Among the 10 pairs of twin core plugs, one pair is from Ireton formation, and the rest of the nine pairs are from Duvernay Formation. The depth, mass, length, diameter, and volume of Ireton and Duvernay samples are listed in the

following Table 6. The type of the experiments are done with the corresponding samples are also listed in the Table 6.

Table 6: Depth, mass, length, diameter, and volume of Ireton and Duvernay samples.

Formation name	Sample ID	Dry mass, g	Length, cm	Diameter, cm	Volume, cm^3	Imbibition test	Soaking test	Co-current imbibition
Ireton	**AOK1-1**	103.705	7.62	2.54	38.61	✓	-	-
	AOK1-2	101.482	7.62	2.54	38.61	✓	-	-
Duvernay	**AOK2-1**	105.733	7.62	2.54	38.61	✓	✓	-
	AOK2-2	97.256	7.62	2.54	38.61	✓	✓	-
	AOK3-1	99.783	7.62	2.54	38.61	✓	✓	-
	AOK3-2	100.136	7.62	2.54	38.61	✓	✓	-
	AOK4-1	103.146	7.62	2.54	38.61	✓	✓	-
	AOK4-2	100.842	7.62	2.54	38.61	✓	✓	-
	AOK5-1	97.713	7.62	2.54	38.61	✓	✓	-
	AOK5-2	97.112	7.62	2.54	38.61	✓	✓	-
	AOK6-1	95.797	7.62	2.54	38.61	✓	✓	✓
	AOK6-2	99.393	7.62	2.54	38.61	✓	✓	✓
	AOK7-1	99.437	7.62	2.54	38.61	✓	✓	✓
	AOK7-2	98.067	7.62	2.54	38.61	✓	✓	✓
	AOK8-1	99.990	7.62	2.54	38.61	✓	✓	✓
	AOK8-2	98.780	7.62	2.54	38.61	✓	✓	✓
	AOK9-1	96.501	7.62	2.54	38.61	✓	✓	-
	AOK9-2	98.411	7.62	2.54	38.61	✓	✓	-
	AOK10-1	100.590	7.62	2.54	38.61	✓	-	-
	AOK10-2	99.732	7.62	2.54	38.61	✓	-	-

4.1.2 Reservoir Fluids

In this section, we present the physical properties of reservoir oil and brine. We use reservoir oil and brine for evaluation of wettability through spontaneous imbibition experiments.

Produced oil and brine were collected from a well next to the cored well. The produced fluids are filtered to separate solid contaminations before measuring physical properties. The physical properties of oil and brine are listed in Table 7. We measure the density by Anton Paar instrument. The densities of brine and oil are 1.09 and 0.80 g/cm^3, respectively. We measured the viscosity using concentric cylinder rheometer. The viscosities of brine and oil are 1.38 cP and 2.97 cP, respectively. We measured the surface tension using Attension Sigma 700 (Biolin Scientific) instrument and ring method. The surface tensions of produced oil and brine are 24.7 and 40.0 mN/m, respectively. The surface tension of brine increases when salinity increases. In other words, the surface tension of produced brine with high salinity should be higher than deionized water (72 mN/m). As reported in Table 7, the surface tension of produced brine is 40.0 mN/m. The slickwater, used as fracturing fluid in the Duvernay wells, contains surfactant that reduces surface tension and facilitates fracture-face clean up after fracturing. During fracturing operation, a portion of fracturing fluid mixes with the formation brine and, thus, the produced flowback brine has lower surface tension than the original formation brine, as listed in Table 7.

Table 7: Physical properties of produced oil and brine.

Fluids	Density (g/cm^3)	Viscosity (cP)	Surface tension (mN/m)
Produced brine	1.09	1.38	40.0
Oil	0.80	2.97	24.7

4.2 Methodology

In this section, we present the procedure of conducting experiments for evaluation of wettability. As-received core samples are partly-saturated with reservoir oil and brine as listed in Table 3. To investigate the effect of initial liquid saturation on spontaneous imbibition and contact angle we heat four samples and reduce the initial oil and brine saturations.

4.2.1 Sample Preparation

As-received samples: Twin core plugs of AOK1, AOK4, AOK6, AOK7, AOK8, and AOK10 are as-received samples. These core plugs were not heated before air-liquid imbibition and air-liquid contact angle experiments. As discussed previously, as-received samples are not well-preserved, and there is an uncertainty in water and oil saturations listed in Table 3.

Heated samples: We heat the twin core plugs of AOK2, AOK3, AOK5, and AOK9 at a temperature of 100 ºC and record the change in mass of the samples. Figure 10 shows the wt% vs. time. wt% is calculated by dividing the mass change by initial mass of the sample. By heating, we can assume that the initial water and oil saturations in heated samples are lower than those in as-received samples.

$$\text{wt\%} = \frac{\text{Heated mass} - \text{Initial mass}}{\text{Initial mass}} \times 100 \quad (4)$$

As shown in Table 3, the water saturation is in the form of sub-irreducible saturation and ranges between 2.89 %PV (AOK2) to 11.21 %PV (AOK9) before heating the core plugs. On the other hand, oil saturation is higher than water saturation and ranges 31.38 %PV (AOK9) to 47.55 %PV

(AOK5). Therefore, the wt% shown in Figure 10 is mainly contributed to the reduction of oil saturation.

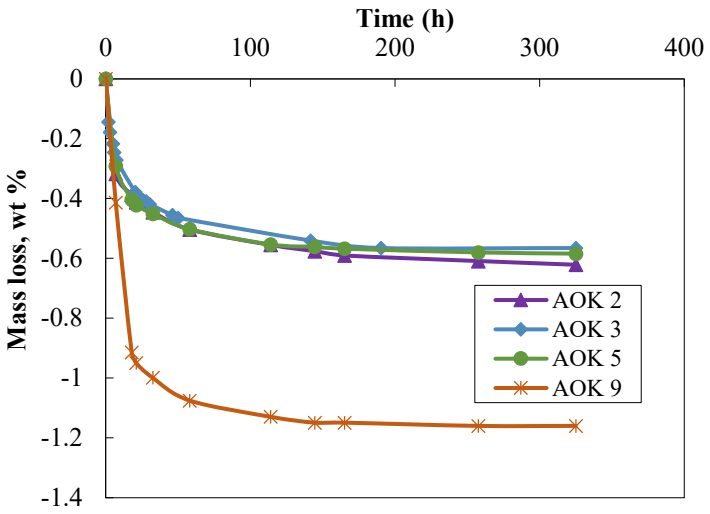

Figure 10: wt% of heated samples vs. time. The heating temperature is 100^{0}C.

4.2.2 Wettability Measurement

In this section, we present the procedures of air-liquid contact angle and spontaneous imbibition tests. Air is in contact with liquid (oil or brine) in both contact angle and spontaneous imbibition experiments. These experiments are conducted for evaluating the wettability of Duvernay core samples in an air-liquid system.

4.2.2.1 Air-liquid contact angle measurement

We measure air-liquid contact angles using the high-resolution camera of Attension THETA (Biolin Scientific) instrument Figure 11. To measure the contact angle, we place a droplet of oil or brine on the polished surface of the samples. The camera captures the profile of droplet until reaching the equilibrium state. To reduce the effect of droplet size on contact angle measurements, we fixed the volume of the droplet to 10 µL using a special syringe and calibrated THETA's

software. We measure and compare the equilibrium contact angle on both as-received (AOK1, AOK4, AOK6, AOK7, AOK8 and AOK10) and heated (AOK2, AOK3, AOK5, and AOK9) samples. We have measured the contact angle twice for heated samples (before and after heating) to investigate the effect of heating on air-liquid contact angle.

(a) **(b)**

Figure 11: (a) Brookfield viscometer (b) Sigma 700 instrument for measuring the surface tension by ring method.

4.2.2.2. Air-liquid spontaneous imbibition experiments

In this process, samples are fully immersed into a liquid. So, samples are open with all faces for imbibition. We conduct air-brine and air-oil spontaneous imbibition tests on as-received (AOK1, AOK4, AOK6, AOK7, AOK8, and AOK10) samples. We have 6 pairs of as-received core plugs. The depth difference between core samples of each pair is less than 1 cm, and we can assume that the core samples have similar petrophysical properties. We immerse six as-received core plugs in

brine and the other 6 core plugs in the oil. All heated twin core plugs (AOK2, AOK3, AOK5, and AOK9) are immersed only into the oil.

During imbibition tests, we record the mass of rock using a digital balance with 0.001 g accuracy. The initial mass of rock is subtracted from recorded mass to calculate the imbibed mass of liquid. Then, we calculate the imbibed volume by dividing the imbibed mass by the liquid density. After reaching an equilibrium state, the final imbibed volume of liquid is divided by the effective pore volume to calculate the final normalized imbibed volume of oil (I_o) and brine (I_w) (Eq.5 and Eq.6 respectively). Finally, the oil index (WI_o) is calculated by using Eq.7. Higher WI_o represents higher oil wetting affinity compared to brine.

$$I_o = \frac{\text{Final imbibed volume of oil}}{\text{Pore volume}} \times 100 \quad (5)$$

$$I_w = \frac{\text{Final imbibed volume of brine}}{\text{Pore volume}} \times 100 \quad (6)$$

$$\text{Oil wetting affinity index, } WI_o = \frac{I_o}{I_o + I_w} \quad (7)$$

4.4 Results

Results and discussions are presented in three parts.

A. First, we present the results of air-liquid contact angle and air-liquid spontaneous imbibition experiments of as received samples. Then we discussed the contact angle and imbibition results for evaluating the wettability of Ireton and Duvernay as received samples.

B. In the second part, we represent the air-liquid contact angle and air-liquid spontaneous imbibition of Duvernay heated samples. After that, the effect of heating on Duvernay wettability is explained.

C. In the third part, some correlations between I_o and mineralogy, petrophysical, geochemical properties are shown to investigate the functional dependence of wettability.

4.4.1 Evaluation of wettability of Ireton and Duvernay as received samples

In this part, we present the results of wettability measurements on as-received core plugs. We use spontaneous imbibition experiments and define I_o and I_w (Eq. 5-6).

Air-liquid contact angle results

When the oil droplet contacts with the clean core surface, it completely spreads on the rock surface ($\theta=0^o$) (Figure 12 (a) and (c)). In Figure 12 (a) represents the oil contact angle measurement of Ireton sample and Figure 12 (c) represents the oil contact angle of Duvernay sample. However, brine retains its identity as droplets, for example, the contact angle of 16º and 67º in Figure 12 (b) and (d) Figure 12 (b) represents the brine contact angle of Ireton sample and Figure 12 (d) represents the brine contact angle of Duvernay sample. The measured contact angle of oil on all samples is zero, and that of brine is listed in Table 7.

These data indicate that the affinity of the Duvernay samples to oil is higher than that to brine. As is evident in Table 8 and Figure 12 (b), AOK1 (Ireton sample) has the minimum brine contact angle among the samples. Table 2 shows that AOK1 has a maximum clay content of 59 wt%. Clay minerals have the strong affinity for water uptake, and it may be one reason for minimum contact angle of brine on AOK1 surface. Another reason for minimum contact angle of brine may be the

high initial water saturation of AOK1. As shown in Table 3, as-received sample of AOK1 has maximum water saturation of 54.6% P.V among all samples. High water saturation in the rock increases the affinity of rock for uptake of brine droplet and consequently reduces the contact angle.

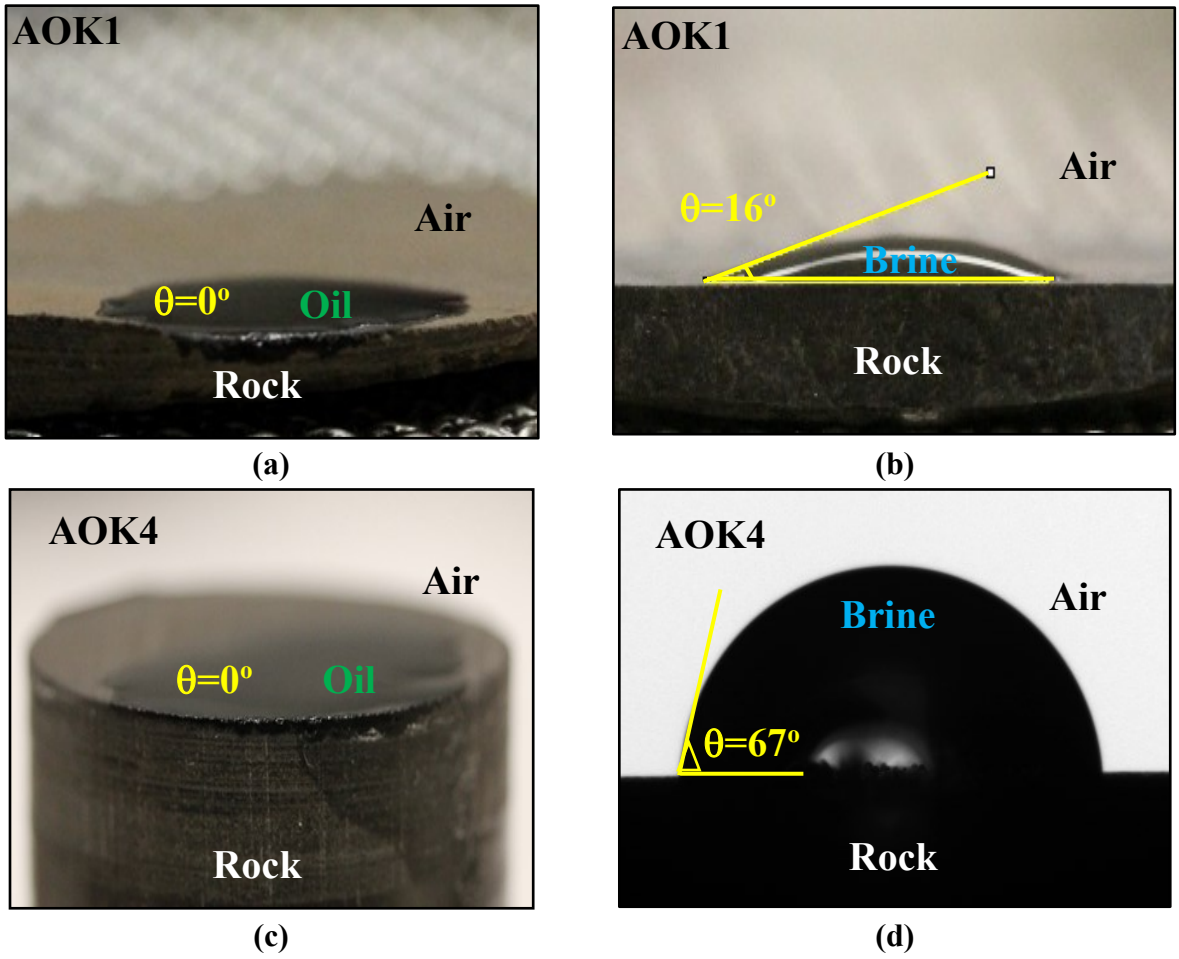

Figure 12: Air-liquid contact angles of oil (a) and (c); air-liquid contact angle of produced brine (b) and (d) on the polished surface of Ireton (AOK1) and Duvernay (AOK4) sample. The volume of the droplet is 10 µL.

Table 8: The results of air-liquid contact angles on the polished surface of as-received samples.

As-received sample ID	Oil contact angle (degree)	Brine contact angle (degree)
AOK1	0.0	16.08
AOK4	0.0	67.15
AOK6	0.0	89.06
AOK7	0.0	74.21
AOK8	0.0	78.22
AOK10	0.0	57.21

Air-liquid spontaneous imbibition results

In Figure 14 (a) we observed that the weight of AOK1 sample (Ireton) immersed in the oil decreases versus time. At the end of the test, small droplets of brine were accumulated at the bottom of the cell (Figure 13). As noted before, the as-received AOK1 sample has maximum initial water saturation of 54.6% P.V. It seems that oil has displaced both in-situ brine and air. Since oil density is lower that brine, the weight of sample decreased when brine is displaced by oil. Because of the very low amount of displaced water, we were unable to calculate the volume of displaced brine; thus, we could not calculate the imbibed volume of oil (I_o). Figure 14 (b) shows that the cumulative imbibed mass of brine which is higher than the cumulative imbibed mass of oil.

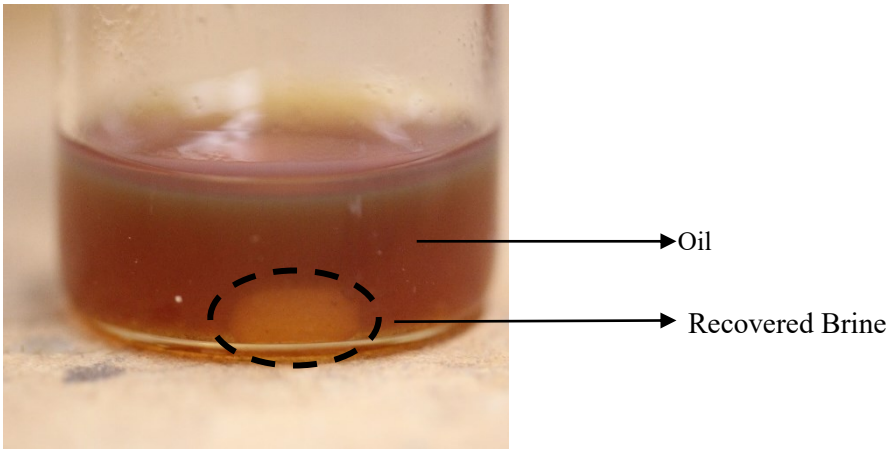

Figure 13: Droplets of displaced brine from Ireton sample during air-oil spontaneous imbibition

Figure 14 (c) and (d) show the normalized imbibed volume oil and brine of Duvernay samples, respectively. We calculate normalized imbibed volume by dividing the imbibed volume by the effective pore volume of the sample. Effective pore volume is calculated using effective porosity of core samples listed in Table 3. As shown in Figure 14 (c) and (d), the normalized imbibed volume of oil is higher than that of brine for all samples. Table 9 lists I_o and I_w for as-received samples. The results of air-liquid imbibition tests suggest that the wetting affinity of the Duvernay samples to oil is higher than that to brine. This agrees with air-liquid contact angle results that show higher contact angle of brine compared with that of oil.

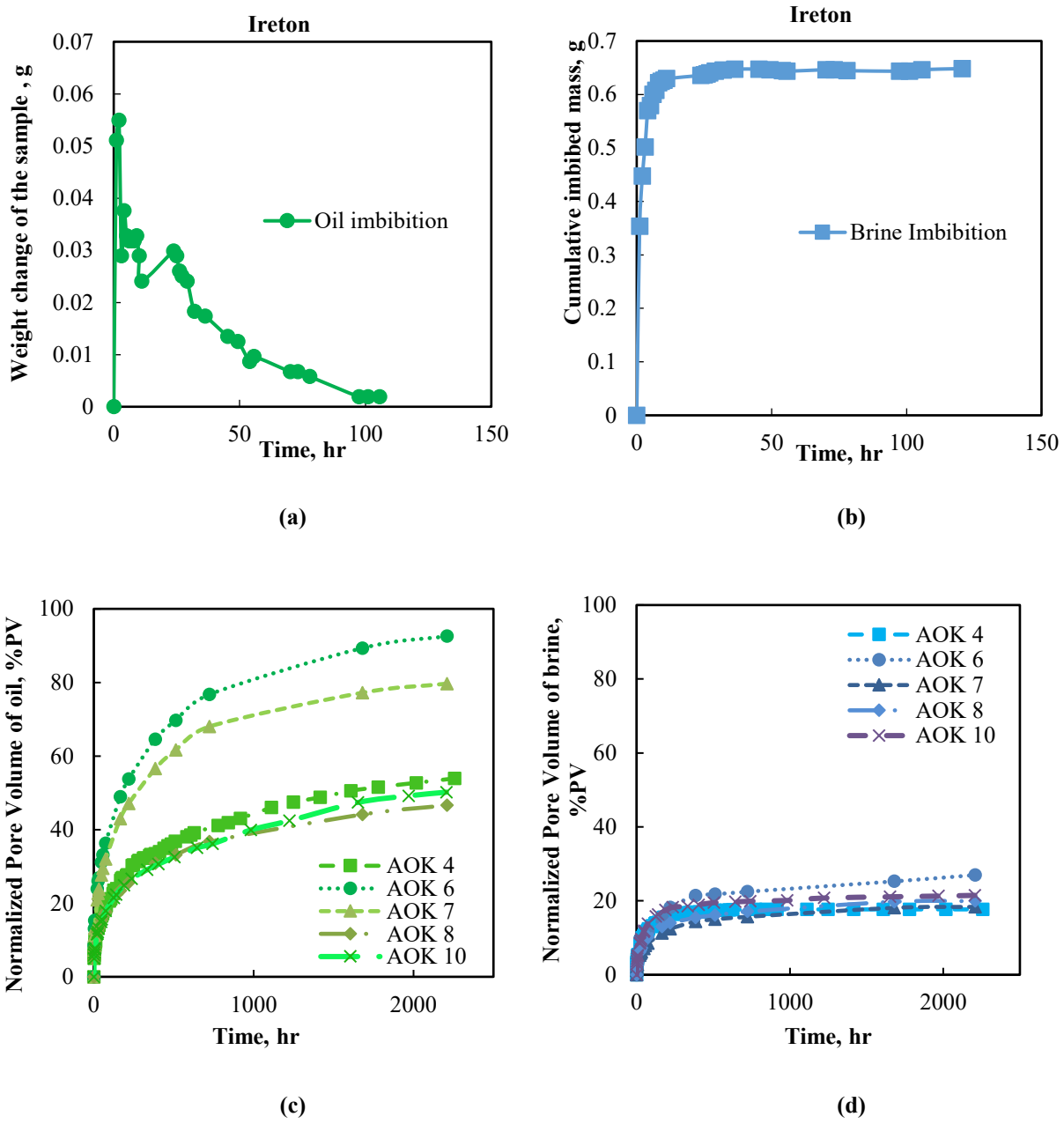

Figure 14: (a) Weight change of the sample vs time when imbibing oil and (b) Cumulative Imbibed mass of brine vs time for Ireton as-received sample; normalized imbibed volume of (c) oil and (d) brine vs. time for Duvernay as-received samples

Table 9: Equilibrium imbibed volume of oil (Io) and brine (Iw) for as-received samples.

As-received sample ID	I_o (%PV)	I_w (%PV)	WI_o
AOK1	-	64.83	
AOK4	51.01	17.68	0.74
AOK6	91.26	25.81	0.78
AOK7	63.23	14.84	0.81
AOK8	46.61	20.87	0.70
AOK10	54.49	22.73	0.71

Wettability of Ireton: The contact angle data of Ireton samples show that oil droplets completely spread on the surface of the rock; however, brine retains as a droplet on its surface (Table 8). This observation means that the Ireton samples have more affinity to oil than brine. On the contrary, the brine imbibition data of Ireton samples show that the samples have more affinity to brine than oil (Figure 14 (a) and (b)) because the imbibed mass of brine was much higher than that of oil. Conversely, oil could replace the existing brine in the sample during oil imbibition.

To describe the wettability of Ireton caprock, the petrophysical data can be analyzed. From the XRD data of Ireton samples, it was observed that Ireton sample contains 59% of clay minerals. Inorganic minerals, especially clay minerals, is the reason for hydrophilic nature of rock (Chenevert, 1970). The Ireton sample mostly contains illite, mica, and smectite that are mainly hydrophilic and kaolinite (2wt %) which is a hydrophobic clay mineral (Buntignies et al., 1997; Jerauld and Rathmell 1994). The presence of clay minerals may be the reason for higher brine imbibition of rock that represents water wet behavior of rock. Rock eval data show that Ireton

Formation also contains 0.94% of TOC. The presence of this organic content may cause a little oil uptake in oil imbibition. In another study by Alpine and Larter (2005), it was found that shale caprock may not remain as water wet when exposed to oil components. Oil penetrates into rock formation water, changes the wettability, and creates oil wet path by the sorption of the hydrophobic organic compound that causes caprock leakage during petroleum migration. Therefore, in this study, Ireton shale caprock may show the similar mechanism in the oil imbibition. Oil gets exposed to formation water, and, as a result, the surface creates oil wet path by imbibing oil and displacing the formation water.

Wettability of Duvernay: The results of wettability measurements show that the Duvernay samples have a higher wetting affinity to oil compared with brine. They imbibe more oil than the (I_o>I_w) (Table 9). Moreover, the higher value of WI_o (above 0.7) declares that the samples have more wetting affinity to oil than brine. To explain this observation, we further investigate the crossplots of petrophysical properties. We also use SEM/EDS analyses to characterize the pore structure and explain the strong oil-wetness of shale samples.

Shale matrix is mainly comprised of inorganic minerals such as quartz, calcite, K-feldspar, and clay (Table 2) and organic matter (Table 4). Inorganic minerals can be hydrophilic, especially when clay minerals are present (Chenevert, 1970; Hensen and Smit, 2002). Conversely, organic matter is expected to have a higher wetting affinity towards oil (Mitchell et al., 1990). The distribution of pores within inorganic minerals and/or organic matter affects wettability of shale, and consequently spontaneous imbibition. Figure 15 (a) and Figure 15 (b) show the crossplots of effective porosity and pressure-decay permeability vs. TOC content, respectively. The data points are shown in Figure 15 (a) and (b) correspond to 20 TRA core samples in the cored well. **Figure**

15 (a) shows that the effective porosity increases by increasing the TOC content. This correlation suggests that majority of connected pores hosted by the organic matter of the rock, and organic pores play a significant role in Duvernay Formation. Figure 15 (b) shows that the samples with higher TOC content have generally higher pressure-decay permeability. This correlation suggests that the pores within organic matter are well-connected. Only Duvernay samples from AOK2 to AOK9 (8pairs) were considered for this correlations. As AOK1 and AOK10 are representatives of the Ireton Formation and carbonate layer of Duvernay formation, respectively. The sample properties of AOK1 and AOK10 are different from those of AOK2 to AOK9, and the properties will not be comparable with each other. Yassin et al. (2017) investigated the crossplots of effective porosity and pressure-decay permeability for 130 data points collected from Lower Duvernay Formation. The authors presented similar positive correlations of effective porosity and pressure-decay permeability with TOC content; suggesting the significant role of organic porosity in the Duvernay shale samples.

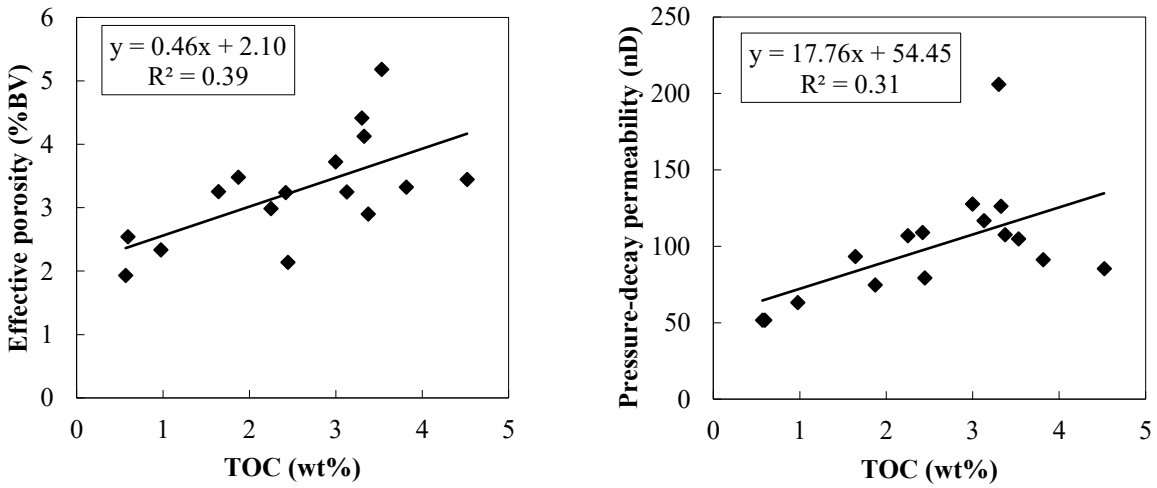

Figure 15: The crossplots of (a) effective porosity and (b) pressure-decay permeability vs. TOC content for 16 Duvernay core plugs. The positive correlations of effective porosity and pressure-decay permeability suggest that majority of connected pores hosted by organic contents.

The SEM images of some Duvernay sample explained at this section. AOK4 and AOK8 are shown in Figure 16(a) and 16(b), respectively. The organic matter and different inorganic minerals are detected by EDS analysis. As shown in Figure 16(a) and 16(b), most pores with average pore sizes smaller than 200 nm are present within the organic matter. The abundance of organic pores with a strong wetting affinity towards oil (Mitchell et al., 1990) may explain higher spontaneous imbibition of oil compared with that of brine (Figure 14 (c) and Figure 14(d)). The significance of organic pores demonstrated in Figure 16(a) and 16(b) is in agreement with Figure 15(a) and Figure 15 (b) which show that the samples with higher TOC content have higher effective porosity and pressure-decay permeability. The analyses of SEM images also show some pores within inorganic minerals. Figure 17 (a) shows a SEM image of a Duvernay sample (AOK2) incorporated with an elemental analysis of carbon, silicon, and oxygen (Figure 17 b-d). The black areas correspond to the higher concentration of element. As shown in carbon map (Figure 17 b), the surface area of many grains is coated by organic matter. Coating the grains by organic matter may change the wettability of inorganic pores from water-wet to oil-wet. There are high concentrations of silicon and oxygen elements (Figure 17(c) and 17(d) on the bottom left of Figure 17 (a) that correspond to quartz mineral. This area lacks organic matter and contains large micropores with average diameters larger than 700 nm. These pores within inorganic minerals such as quartz may act as conduits for brine imbibition. The analyses of many SEM images show both organic and inorganic pores in Duvernay shale samples. However, the number of pores within inorganic minerals is much less than those within organic matter. Yassin et al. (2017) analyzed several SEM images of samples from the Lower Duvernay Formation. They also observed the abundance of nanopores within organic matter and large micropores within inorganic minerals. The authors used spontaneous imbibition data and defined pore wettability index (PWI) using Handy's (1960) model.

Comparison of PWI for oil and brine indicated that brine preferentially flows through larger pores and fills them first. They showed that faster brine imbibition in large hydrophilic micropores (inorganic pores in Figure 17 (a)) and negligible brine uptake in small hydrophobic nanopores (Figure 16 (a) and 16(b)) may explain early equilibrium of brine compared with late equilibrium of oil as shown in Figure 14(c) and Figure 14 (d).

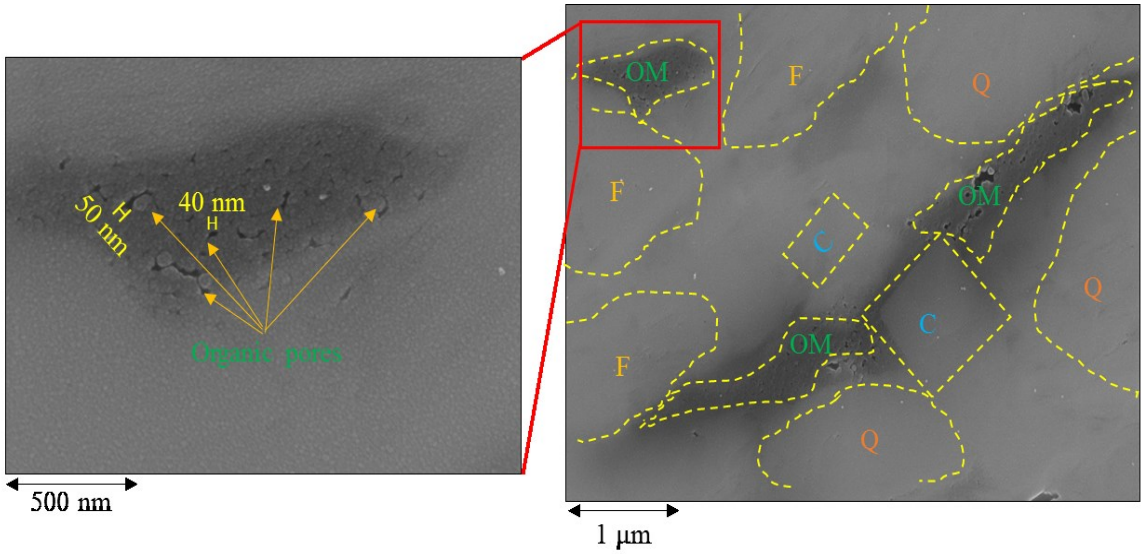

(a)

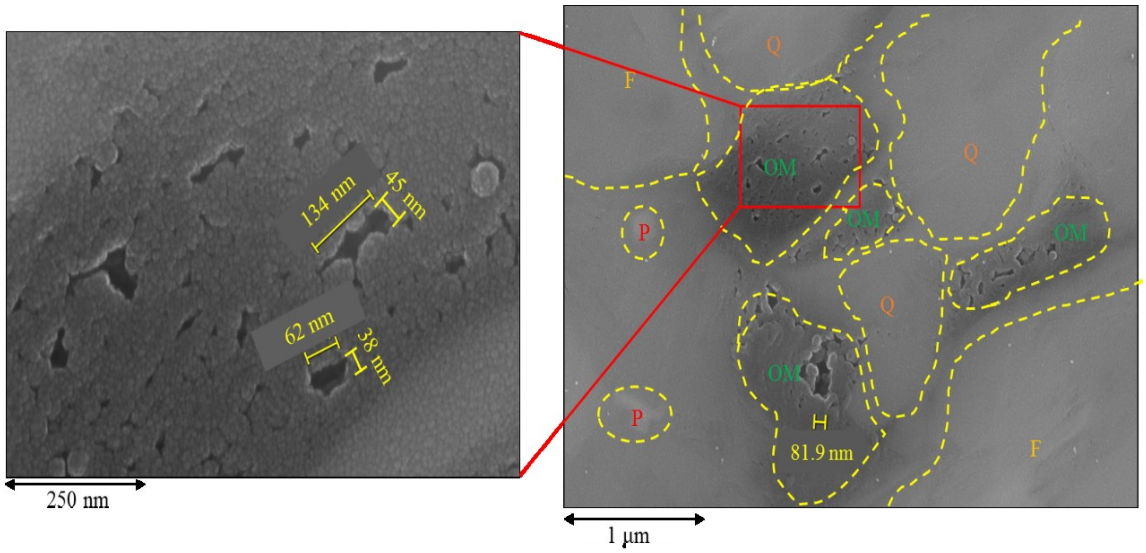

(b)

Figure 16: SEM images of (a) AOK4 and (b) AOK8 samples. Organic pores with average diameters less than 200 nm may explain higher spontaneous imbibition of oil compared with that of brine. Q, F, C, P, and OM stand for quartz, feldspar, calcite, pyrite, and organic matter, respectively.

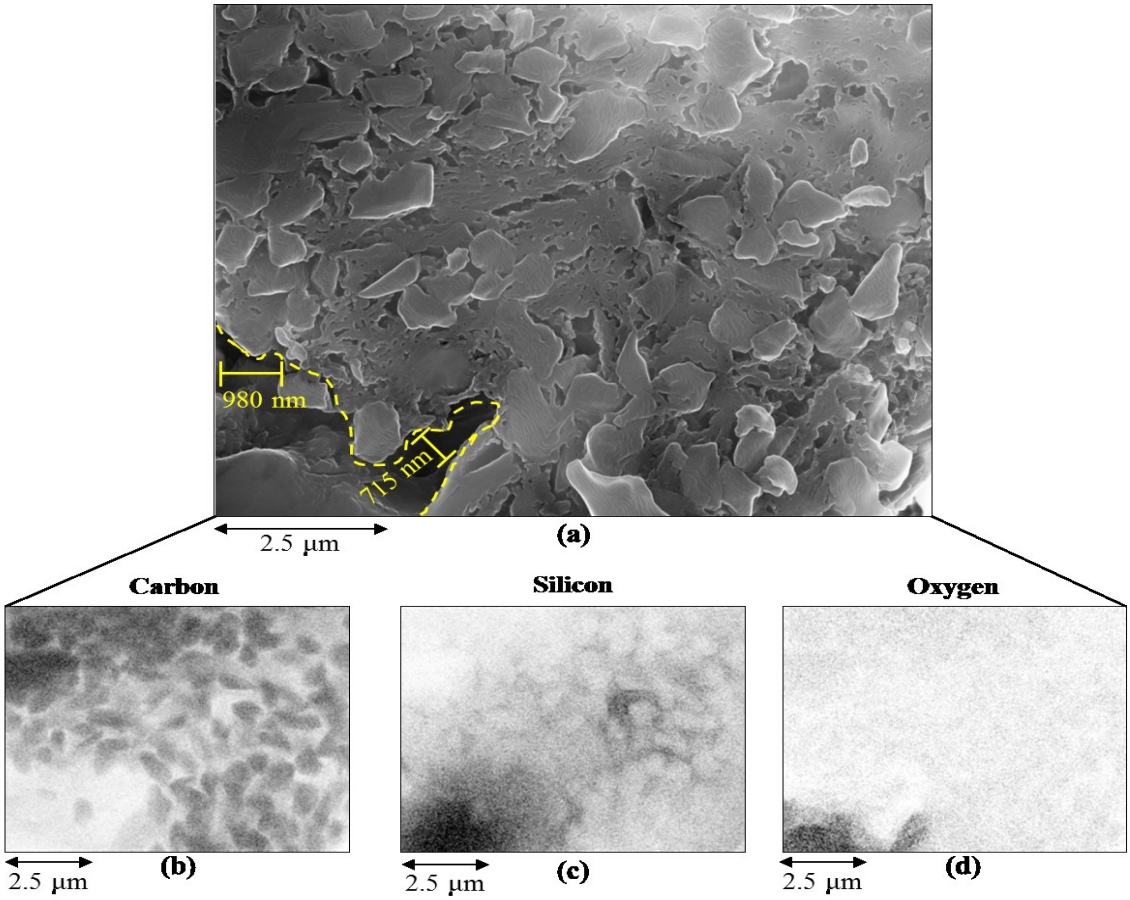

Figure 17: (a) SEM image of AOK1. The elemental map of (b) carbon, (c) silicon, and (d) oxygen measured using energy-dispersive X-ray spectroscopy (EDS) analysis. Elemental map of carbon shows several grains coated by organic matter. High concentrations of silicon and oxygen at the bottom left represents quartz mineral. Inorganic micropores within quartz may act as conduits for brine imbibition.

Overall, the results of wettability experiments show that the wetting affinity of samples to oil is higher than that to brine. Significant organic porosity confirmed by 1- crossplots of effective porosity and pressure-decay permeability vs. TOC and 2- SEM/EDS analyses may explain strong wetting affinity of the Duvernay samples to oil.

4.4.2 Evaluation of Wettability on Duvernay Heated Samples:

Air-liquid contact angle: We have measured the air-liquid contact angle of Duvernay heated samples (AOK2, AOK3, AOK5, and AOK9). We have measured the contact angle of these samples both before heating and after heating. Figure 18 (a-c) compare the contact angles of brine droplets equilibrated on AOK2, AOK5, and AOK9 samples before and after heating. Table 10 represents the list of contact angles of all heated samples AOK2, AOK3, AOK5, and AOK9 before and after heating. The results show that the brine contact angles after heating are smaller than that before heating. Oil contact angles before and after heating the samples are similar and are equal to 0°. As mentioned before in Table 3, water saturation in as-received shale samples is very low (2.89-11.21 %PV). Therefore, the weight loss after heating is mainly contributed to reducing oil saturation. Lower oil saturation in heated samples may explain the reduction in brine contact angles as shown in Figure 18.

Table 10: Before heating and after heating contact angles of oil and water on Duvernay heated samples

Heated Sample ID	Before heating		After Heating	
	Oil	Water	Oil	Water
AOK 2	0.00	68.79	0.00	53.34
AOK 3	0.00	63.85	0.00	41.87
AOK 5	0.00	72.49	0.00	37.06
AOK 9	0.00	48.5	0.00	36.59

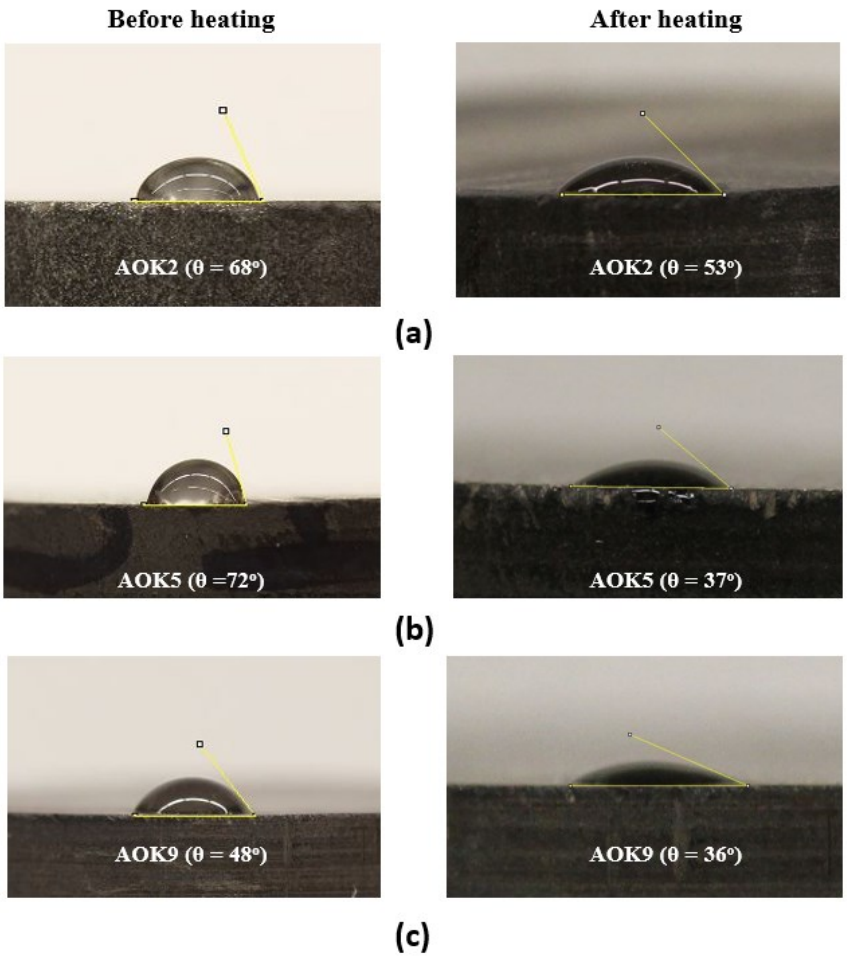

Figure 18: Air-brine contact angles on the polished surface of (a) AOK2, (b) AOK5, and (c) AOK9 before and after heating.

Air-oil spontaneous imbibition: After heating, we immerse them only into oil for spontaneous imbibition of oil. These samples were mainly prepared for the soaking experiment will be described on Chapter-6. At the same time, we can investigate the effect of heating on Duvernay wettability. Figure 19 shows the normalized imbibed volume of oil vs. time for heated samples. Comparing Figure 19 with Figure 14 (c) shows that heated core plugs have higher oil imbibition than as-received samples. This is because heating the samples evaporates the initial oil in the

samples. Therefore, there is more pore volume available for oil imbibition. Table 11 lists the values of I_o for the heated samples.

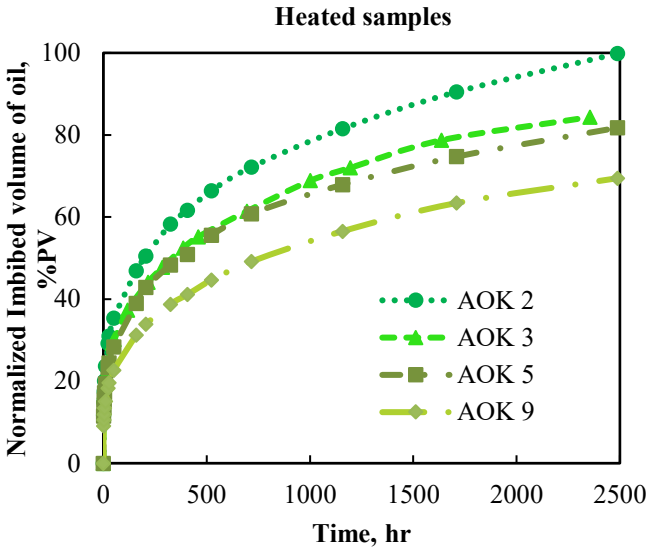

Figure 19: The normalized imbibed volume of oil vs. time for heated samples.

Table 11: The results of air-oil spontaneous imbibition tests on heated samples.

Heated sample ID	I_o (%PV)
AOK 2	100.0
AOK 3	79.29
AOK 5	79.14
AOK 9	68.12

4.5 Discussions

In this section, the normalized imbibed volume of oil (I_o) for both heated and as-received core plugs is plotted against the rock-eval pyrolysis data (TOC%, S1 and OI) to find the possible

correlations. The values of I_o for as-received and heated samples are also plotted against the clay content to understand the role of clay content on oil imbibition. Only Duvernay samples from AOK2 to AOK9 (8pairs) were considered for this section as AOK1 and AOK10 are representatives of the Ireton Formation and carbonate layer of Duvernay formation, respectively. The sample properties of AOK1 and AOK10 are different from those of AOK2 to AOK9, and the I_o results will not be comparable with each other.

4.5.1 Io vs. TOC Content

I_o for both heated and as-received samples are plotted against TOC content (Figure 20). In Figure 10, it was shown that the samples had initial oil and water saturation that can be partially evaporated by heating. To observe the effect of initial saturation between the heated and as-received samples, we plotted them separately into two graphs. In both cases, the results show that I_o decreases with increasing TOC content. The effect of initial oil saturation is observed when the I_o of as-received samples is plotted against TOC content (Figure 20 (a)). Among all of the samples, AOK4 (red marked) has comparatively high oil saturation (31.75%) whereas other samples have initial oil saturation within the range of 23.98-25.61% (Table 1). On the other hand, there is no effect of initial saturation on the heated samples (Figure 20 (b)). Thus, a further investigation is needed to examine the effect of initial saturation on oil imbibition.

Organic matter has a high wetting affinity towards oil (Borysenko et al., 2009). The presence of organic matter such as kerogen can enhance oil imbibition and lead to the positive correlation between normalized imbibed volume (I_o) and TOC content (Elijah et al., 2011). In another study (Yassin et al., 2017) on Lower Duvernay samples, it was found that TOC content had a positive correlation with I_o. However, we observed a negative correlation between Io and TOC content for

Upper Duvernay samples in this study (Figure 20). To explain this contradiction, we should not only consider the effect of TOC content of the rock, but also the maturity of kerogen, the abundance of organic pore volume, and the availability of organic pores especially for a source rock like Duvernay Formation. The possible explanations are discussed in the next section.

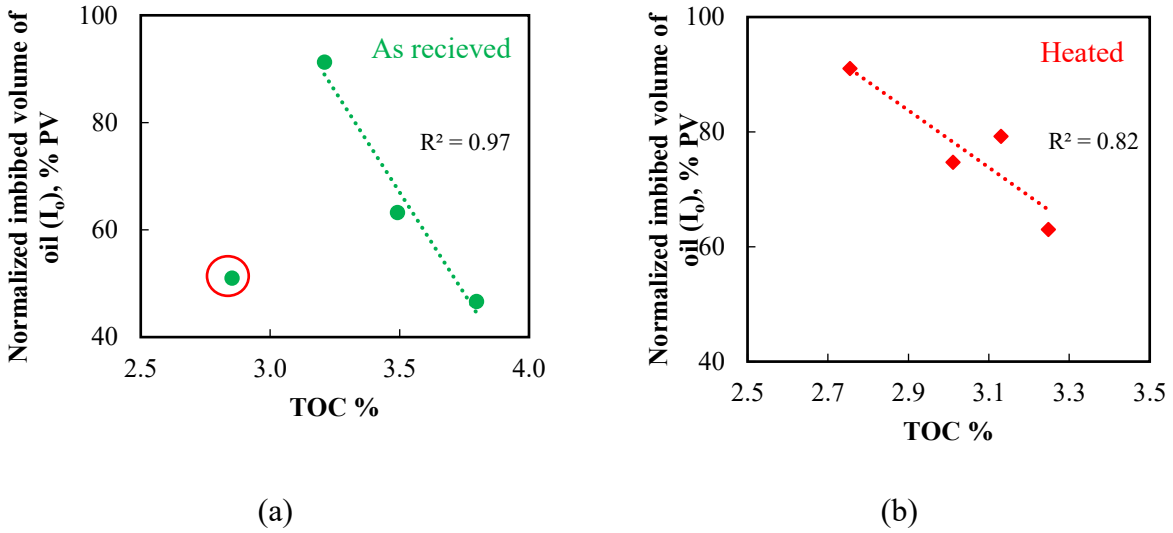

Figure 20: Correlation between the normalized imbibed volume of oil (Io) and TOC content of (a) as-received and (b) heated samples. In figure (a) the red marked sample has comparatively high initial oil saturation and does not participate into the trendline with the other samples shows the effect of initial saturation on imbibed volume of oil.

Effect of kerogen maturity on wettability

Several studies demonstrated the importance of the thermal maturity of kerogen on rock wettability (Elijah et al., 2011; Hu et al., 2014; Peng et al., 2015; Buckley, 2001). The kerogen type of the Duvernay Formation is Type II which can produce both oil and gas. Yassin et al., (2017) used the Lower Duvernay samples (depth 3095-3963 m) that contain average 4.5 wt.% of TOC and have the thermal maturity to produce gas. On the other hand, the Upper Duvernay samples (depth 2780-

2804 m) contain average TOC content of 3.3 wt.% and the thermal maturity to produce oil (Figure 3(a) and 3(b)). Therefore, Lower Duvernay samples are more mature than Upper Duvernay samples. Hu et al., 2014 found that kerogen becomes more oil-wet in high maturity, mixed-wet at intermediate maturity, and water-wet at very low maturity. Similarly, due to the high maturity and high oil wetting nature of kerogen, Lower Duvernay samples imbibe more oil. However, samples imbibed comparatively low volume of oil (I_o) due to the intermediate thermal maturity of Upper Duvernay kerogen. Thus, the thermal maturity of kerogen has an influence on the wettability of Duvernay samples.

These discussions suggest that there may be a correlation between wettability and the rock maturity. To confirm this hypothesis, we plot the oil affinity index (WI_o) versus oxygen index (OI) for Upper Duvernay samples. In Van-krevelan diagram, hydrogen index (HI) and oxygen index (OI) (data extracted from rock-eval pyrolysis) represent the kerogen type and maturity, respectively. HI and OI represent the hydrogen-carbon and oxygen-carbon ratio of the rock, respectively. In Van-krevelan diagram, low O/C ratio represents the high maturity of kerogen and vice versa (Tissot and Welte, 1984). As a consequence, considering OI as a representative of rock maturity (Hu, Y., et al., 2014), we have found that WI_o decreases with increasing OI (Figure 21); it means that the samples with higher maturity have a higher wetting affinity to oil and vice versa.

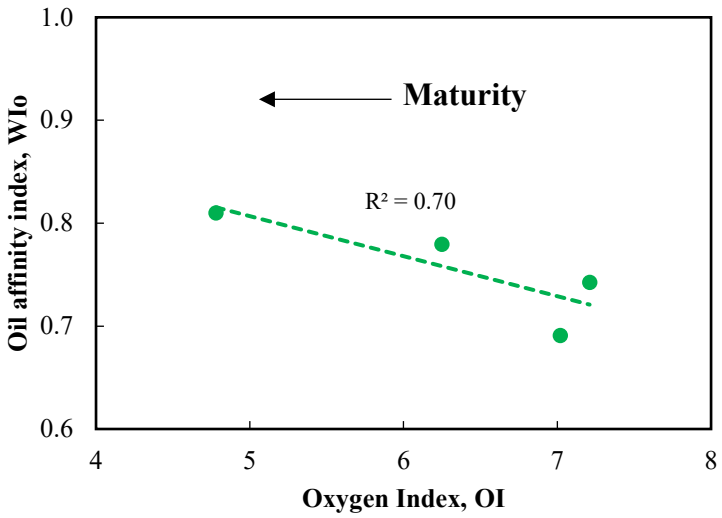

Figure 21: Oil affinity index (WIo) vs oxygen index (OI)

Effect of the storage availability of organic pores on Io

The wettability of kerogen may depend on the abundance of organic pore volume (Elijah et al., 2011; Munson, 2015) and the availability of organic pores to imbibe oil. Organic pores in the kerogen can be isolated, discrete sponge like structures, or complex cluster of pores (Kitty L. Milliken, 2013*)*. The number of organic pores increases by increasing the thermal maturity as kerogen converts to hydrocarbon (Cao and Zhou 2015; Munson, 2015). For instance, the Lower Duvernay samples have a high level of maturity for gas production and contain average porosity of 4.2 %BV (Yassin et al., 2017) while the Upper Duvernay samples have a lower level of maturity for oil production and contain average porosity of 3.3 %BV (Table 3). According to Yassin et al. (2017) and the SEM images (Chapter-3), we have found that most of the Duvernay pores are organic pores. Therefore, it can be assumed that the Lower Duvernay samples have more organic pore volume than the Upper Duvernay samples.

Also, the storage availability of the organic pore for oil imbibition needs to be considered. The organic pores function as a storage of hydrocarbon that has been produced from the rock (Akkutlu et al., 2011; Xiaong et al., 2012). Similarly, Upper Duvernay samples reaches the required thermal maturity, results in hydrocarbon expulsion by producing oil, and leaves the pores within the kerogen (Cao, Q. and Zhou, W. 2015). Moreover, the produced oil stays in this pore system of kerogen (Curtis et al., 2011). Consequently, if the thermally produced oil stays in the pore system of kerogen, there will be less organic pores available for oil imbibition. This might be a reason for the negative correlation of I_o versus TOC content for Upper Duvernay samples. On the other hand, Lower Duvernay samples (Yassin et al., 2017) kerogen is highly matured and produces gas. Thus, the organic pores of dry Lower Duvernay samples were empty and more available for oil imbibition. Consequently, more TOC% of Lower Duvernay samples means more organic pores and more rooms to imbibe oil. Therefore, the storage availability of organic pores may affects the wettability of Duvernay samples.

From the above discussions, we can conclude that only TOC% cannot solely control the oil imbibition. Besides TOC% we should also consider the thermal maturity of kerogen, organic pore volume, and it's storage availability while describing the controlling factor of oil imbibition.

4.5.2 I_o vs. Clay Content

Figures 22 (a) and (b) show that the total imbibed volume of oil decreases with increasing clay content due to the hydrophilic characteristics of clay minerals (Chenevert, 1970; Hensen and Smit, 2002). Moreover, among all the clay minerals illite/mica shows a strong negative correlation with I_o for both as-received and heated samples (Figures 22 (c) and (d)). The hydrophilic nature of

illite/mica (Buntignies et al., 1997; Jerauld and Rathmell 1994) may contribute to this negative correlation. Thus, we conclude that the clay content may also influence the oil imbibition.

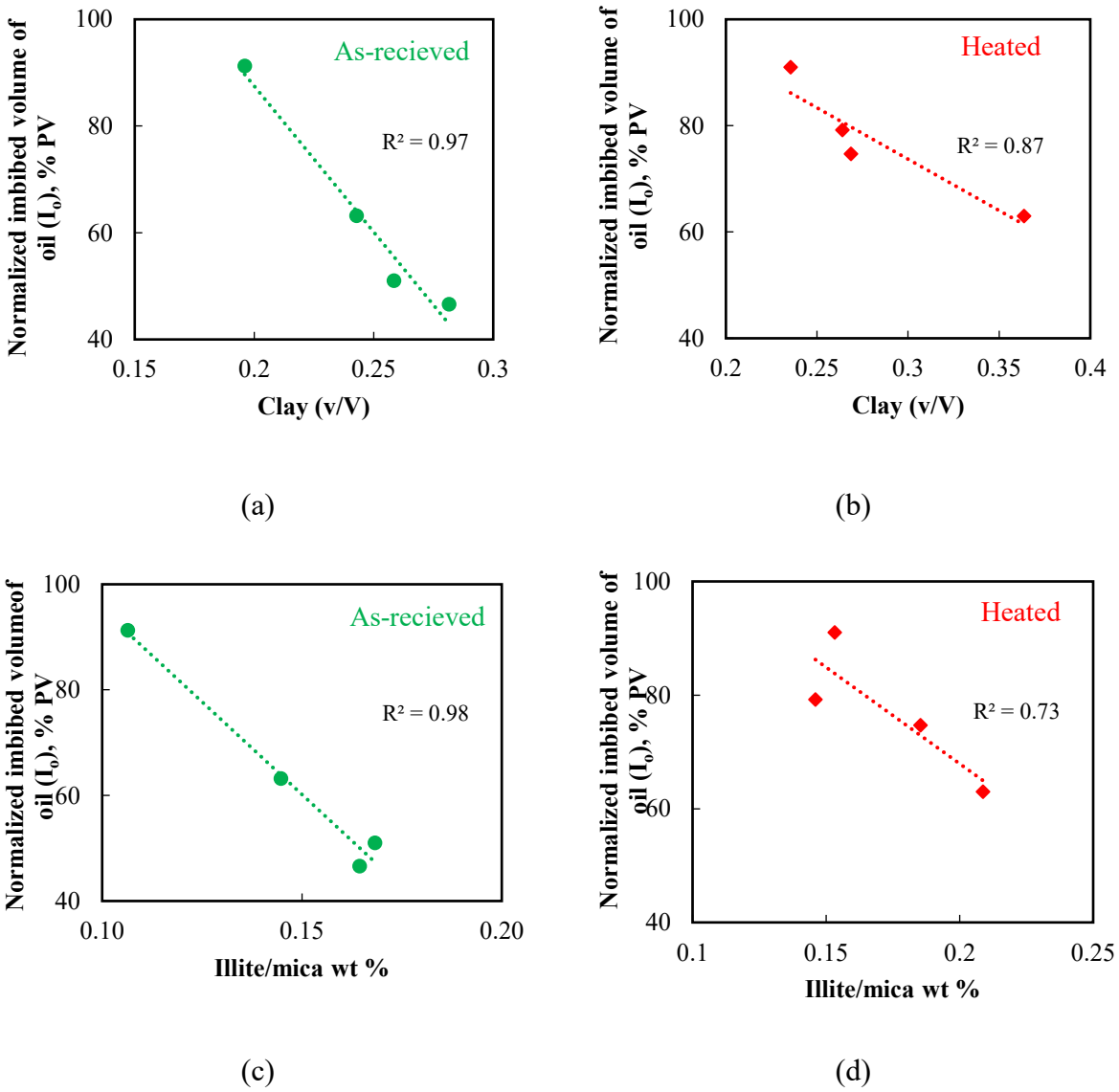

Figure 22: Correlation between the normalized imbibed volume of oil (Io) and clay (v/V) of (a) as-received and (b) heated samples. Normalized imbibed volume of oil (Io) vs. wt% of illite/mica for (a) as-received and (b) heated samples.

4.6 Summary

The key findings of this chapter are summarized as follows:

1- The results of air-liquid contact angle on Ireton core plug show that the wetting affinity to oil is stronger than that to brine. However, the air-liquid spontaneous imbibition result shows that imbibed mass of brine is higher than that of oil. It was also observed that, imbibed oil could replace the brine that was initially present in the rock sample. Replacing the initial brine in presence of oil agrees with the contact angle results which indicate that the sample is more affinity to oil than brine. Moreover, high I_w of Ireton sample represents more affinity to water which can be supported by the high clay content of Ireton samples.

2- The results of both air-liquid contact angle and air-liquid spontaneous imbibition tests on Duvernay core plugs show that the wetting affinity of as-received samples to oil is much stronger than that to brine. The organic porosity supported by both the positive correlations of effective porosity and the pressure-decay permeability vs. TOC content may explain high oil-wetness of shale samples. Organic porosity is also in agreement with SEM/EDS analyses indicating that the majority of pores are within organic matter.

3- High I_o in the air-oil imbibition tests indicates that oil has a high chance to be imbibed into both hydrophobic organic nanopores and hydrophilic inorganic micropores. Brine has a low wetting affinity towards hydrophobic organic pores. Low I_w in air-brine imbibition tests suggests that brine may only fill hydrophilic inorganic pores.

4- The effect of heating was analyzed by comparing the results of Duvernay as-received and heated samples. The result of air-liquid contact angle shows that the samples gain more affinity to brine after heating. Similarly, the result of the air-liquid spontaneous imbibition shows that samples gain more affinity to oil after heating. One possible reason could be the

initial saturation of the sample. As-received sample contains reservoir fluids that can be evaporated by heating. Thus, the higher pore volume of the samples becomes available for imbibition and shows more affinity to liquid (both oil and water).

5- Wettability is not solely dependent on the TOC content of the rock. The maturity of kerogen also needs to be taken into account to explain rock wettability. It was found that the samples with high thermal maturity imbibe more oil and have more affinity to oil and vice versa.

6- The organic pore volume of rock and the storage availability of pores may also affect the oil imbibition. The sample has less ability to imbibe oil if a high amount of produced hydrocarbon already fills up most of the organic pores of the rock.

7- Clay content may be another factor in controlling oil imbibition. Due to the hydrophilic behavior of clay, samples may imbibe less oil with increasing clay content.

Chapter 5

Co-current Spontaneous Imbibition Data for Calculation of Oil/Water Capillary Pressure Ratio

In this chapter, we present the procedure of conducting co-current imbibition experiments for the wettability evaluation and calculation of oil/water capillary pressure. We use Handy's model and Young-Laplace equation to for calculating the capillary pressure ration of oil and water. Then, we discuss the potential driving force for higher oil imbibition in Duvernay shale samples.

5.1 Methodology

5.1.1 Samples preparation

In this part, we selected three core plugs named AOK6-1, AOK7-1, and AOK8-1. These samples were previously used for air-brine spontaneous imbibition in Chapter 4. To dry out these brine-saturated samples, we heat them at 100^{o}C and measure their weight periodically. We heat the samples until there is no weight change.

For this experiment, we used three samples from three different depths. We decided to half-cut our plugs so that they will be twin plugs and their characteristics will be similar. The diameter, length and initial mass (after heating) of twin samples are listed in Table 12.

Table 12: Length, diameter, and mass of three twin plugs

Sample ID	Length (cm)	Diameter (cm)	Initial mass (g)
AOK 6 1 (a)	7.62	2.54	43.88
AOK 6 1 (b)	7.62	2.54	43.90
AOK 7 1 (a)	7.87	2.53	47.08
AOK 7 1 (b)	7.87	2.53	49.74
AOK 8 1 (a)	7.87	2.53	47.98
AOK 8 1 (b)	7.87	2.53	49.54

5.1.2 Air-liquid co-current spontaneous imbibition experiments

We conducted air-brine and air-oil co-current spontaneous imbibition tests on three pairs of heated twin core plugs (AOK6-1, AOK7-1, and AOK8-1). We did not fully immerse these plugs in oil and brine. Twin samples were placed on the imbibition fluids for one-dimension (1D) co-current imbibition. In this imbibition process, only one face of the plug is open for imbibition as shown in Figure 23. We place the sample on the imbibition fluid (oil or brine) separated by a mesh. So, the fluid flows upward through the core plug and saturate it. Core plugs AOK6-1(a), AOK7-1(a), and AOK8-1(a) were placed on oil for air-oil imbibition, and AOK6-1(b), AOK7-1(b), and AOK8-1(b) were placed in brine for air-brine imbibition.

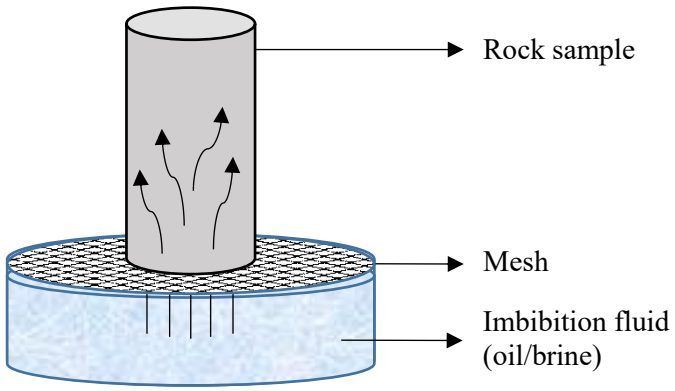

Figure 23: Schematic of set-up used for co-current spontaneous imbibition test.

During imbibition tests, we record the mass of rock using a digital balance. The initial mass of rock is subtracted from recorded mass to calculate the imbibed mass of liquid. Then, we calculate the imbibed volume by dividing the imbibed mass by the liquid density. After reaching the equilibrium state, the final imbibed volume of liquid is divided by the effective pore volume to calculate the final normalized imbibed volume of oil (I_o) and brine (I_w) (Eq.7 and Eq.8 respectively).

$$I_o = \frac{\text{Final imbibed volume of oil}}{\text{Pore volume}} \times 100 \quad (8)$$

$$I_w = \frac{\text{Final imbibed volume of brine}}{\text{Pore volume}} \times 100 \quad (9)$$

5.2 Imbibition Results

Figure 24 (a) and 24 (b) show I_o and I_w of samples respectively. We calculate the final normalized imbibed volume by dividing the imbibed volume by the effective pore volume of the sample. Effective pore volume is calculated using effective porosity of core samples listed in Table 3. As shown in Figure 24 (a) and 24(b), the normalized imbibed volume of oil (I_o) is higher than that of brine (I_w) for all plugs. The results of air-liquid imbibition tests suggest that the wetting affinity of the core plugs to oil is higher than that to brine. This is in agreement with air-liquid contact angle results and counter-current air-liquid (fully immersed) imbibition experiments that we presented in Chapter 4. Table 13 lists I_o and I_w of the core plugs.

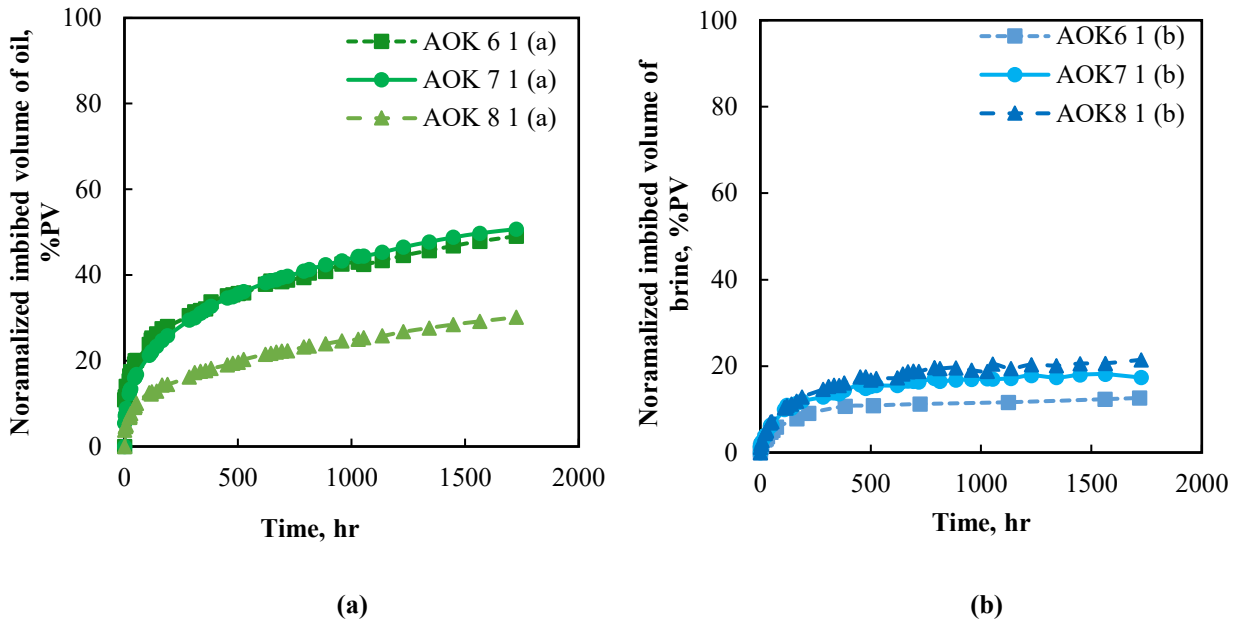

Figure 24: Normalized imbibed volume of (a) oil and (b) brine versus time for three binary plugs (AOK6-1, AOK7-1, and AOK8-1).

Table 13: Equilibrium imbibed volume of oil (Io) and brine (Iw) for three binary plugs (AOK6-1, AOK7-1, and AOK8-1).

Sample ID	I_o (%PV)	I_w (%PV)
AOK6-1	49.06	12.63
AOK7-1	50.72	17.35
AOK8-1	30.16	21.47

5.3 Calculating Capillary-Pressure Ratio

5.3.1 Handy's Model

Handy (1960) proposed a model for one-dimensional piston-like spontaneous imbibition process. According to his model, at the early stage of imbibition, there is a proportional relation between the spontaneous imbibed mass of liquid and the square root of time (√t). Thus, we plot the

cumulative imbibed mass of oil and brine (Figure 25 (a) and (b) respectively) versus square root of time (√t). We considered the initial 144 hours (12 √hr) as the early stage of imbibition. According to Lan et al. (2014), the early stage of imbibition defines the imbibition rate of the sample. The imbibition rate primarily depends on the effective permeability of the sample and the viscosity of the fluid. Thus, the slope was calculated by using early imbibition data as shown in Figure 25 (c) that represents the rate of oil and brine imbibition.

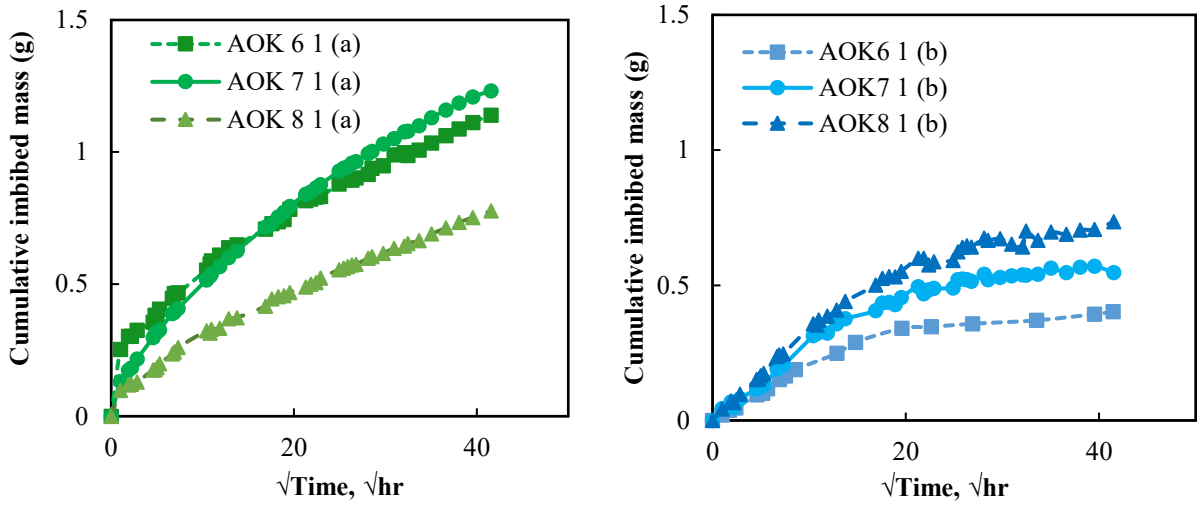

(a) **(b)**

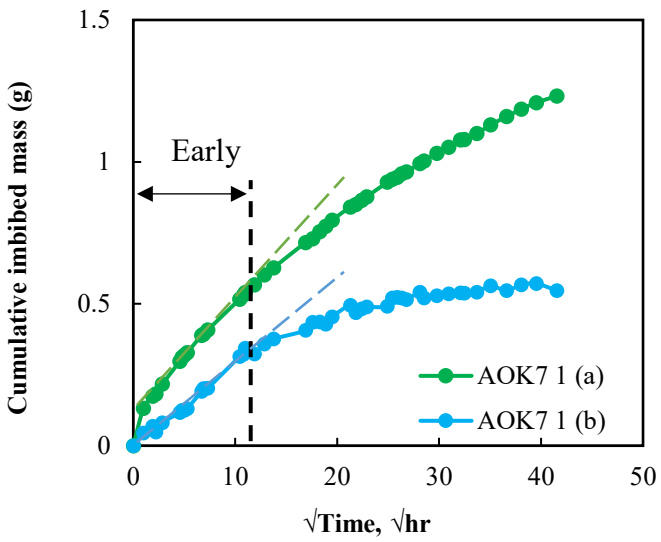

(c)

Figure 25: Cumulative imbibed mass of (a) oil and (b) brine versus square root of time; (c) Calculating the slope of oil and brine imbibition using the plot of the cumulative imbibed mass of oil and brine versus square root of time.

According to Handy's model (1960), the imbibed mass of liquid is proportional to the square root of time and the mathematical expression for the imbibed mass of wetting fluids,

$$M = \sqrt{\frac{2S_A^2 K \emptyset S_{wf} \rho^2 P_c}{\mu}}\sqrt{t} \qquad (8)$$

where S_A is the cross-sectional area of the sample, S_{wf} is the front saturation of the liquid, K is the permeability of each sample, ø is the porosity of each sample, ρ is the density of the liquid, P_c is the capillary pressure, μ is liquid viscosity, and t is the imbibition time. The slope of each imbibition data (m) is calculated by,

$$m = \sqrt{\frac{2S_A^2 K \emptyset S_{wf} \rho^2 P_c}{\mu}} \qquad (9)$$

We assume m_o and m_w as the slope of oil and brine imbibition graphs, respectively. Now, for a pair of a twin core plug, the ratio of the m_o/m_w is,

$$\frac{m_o}{m_w} = \sqrt{\frac{K_o \emptyset_o S_{wfo} \rho_o{}^2 P_{co} \mu_w}{K_w \emptyset_w S_{wfw} \rho_w{}^2 P_{cw} \mu_o}} \tag{10}$$

or,

$$\left(\frac{P_{co}}{P_{cw}}\right)im = \left(\frac{m_o \rho_w}{m_w \rho_o}\right)^2 \frac{\mu_o}{\mu_w} \tag{11}$$

For a pair of twin plug, we assume $S_{wfo} = S_{w\,f\,w}$; $ø_o = ø_w$ and $K_o = K_w$. The density and viscosity of the oil and brine are given in Table 7. Thus, the capillary pressure ratio is calculated using the slope ratio of imbibition graph.

5.3.2 Young-Laplace equation

Another way to calculate the capillary pressure is the Young-Laplace equation,

$$P_c = \frac{4\sigma\cos\theta}{D} \tag{12}$$

Here, σ is surface tension between air and liquid; θ= the air-liquid contact angle and D= the diameter of the pore. If we consider that both oil and brine can flow through the same pore network, we can assume D_w=D_0, then the capillary pressure ratio is calculated by the following equation,

$$\left(\frac{P_{co}}{P_{cw}}\right)YL = \frac{\sigma_o \cos\theta_o}{\sigma_w \cos\theta_w} \tag{13}$$

The surface tension of oil and brine as well as the air-liquid contact angles are listed in Table 7 and Table 8, respectively.

5.4 Discussions

The calculated capillary pressure ratio from both imbibition data (Handy's model) and the Young-Laplace equation for the three twin plugs are listed in Table 14. The results show that the capillary pressure ratio for both $\left(\frac{Pco}{Pcw}\right)_{im}$ and $\left(\frac{Pco}{Pcw}\right)_{YL}$ for all samples is greater than one, suggesting that the capillary pressure of oil is higher than that for brine.

Table 14: Oil and water capillary pressure ratio for each twin plug.

Twin Sample	$(P_{co}/P_{cw})_{im}$	$(P_{co}/P_{cw})_{YL}$
AOK 6-1	13.19	5.91
AOK 7-1	9.35	2.27
AOK 8-1	2.17	2.01

Figure 26 shows the crossplot of capillary pressure ratio $\left(\frac{Pco}{Pcw}\right)_{im}$ versus $\left(\frac{Pco}{Pcw}\right)_{YL}$. According to this figure, there is a difference between two capillary pressure ratio values. Capillary pressure ratio calculated by imbibition data is always higher than the capillary ratio calculated by Young-Laplace equation. The differences between $\left(\frac{Pco}{Pcw}\right)_{im}$ and $\left(\frac{Pco}{Pcw}\right)_{YL}$ may be explained by the assumption we used in Handy's model (Lan et al., 2014; Habibi et al., 2016). We assumed that both oil and brine flow through the same pore networks and capillary pressure is the only driving force for oil and brine imbibition. Another reason for this difference might be the presence of organic matter in the pore network which was not considered when deriving the Young-Laplace equation to calculate capillary pressure. According to Lan et al. (2014), one possible reason is the adsorption of oil on the surface of organic matter that leads to higher oil imbibition and consequently, higher calculated capillary pressure.

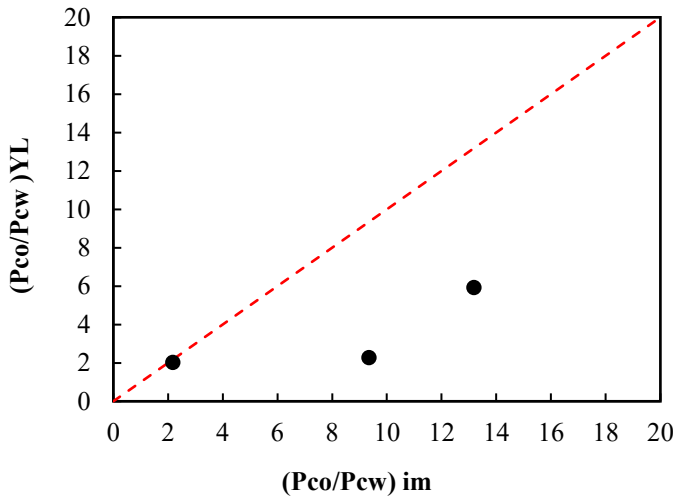

Figure 26: (Pco/Pcw)im versus (Pco/Pcw)YL of three twin plugs. Theoretically, the crossplots of (Pco/Pcw)im and (Pco/Pcw)YL should be linear. According to the plot, capillary pressure is not the driving factor of oil imbibition. The presence of organic matter and the oil adsorption on the surface of organic matter may result high calculated capillary pressure.

5.5 Conclusions

In this chapter, the Handy's model was used to calculate the capillary pressure using the co-current imbibition data for oil and brine. Then, the capillary pressure ratio was calculated. We also calculated the capillary pressure ratio of oil and brine by Young-Laplace equation. After comparing both capillary pressure ratio, the following observations were discussed.

1. Capillary pressure ratio value of oil and brine imbibition calculated from imbibition data and the Young-Laplace equation is greater than one, suggesting higher capillary pressure of oil compared with that of brine.

2. The capillary pressure ratio calculated by Young-Laplace equation shows a lower value than the capillary pressure ratio calculated by imbibition data (Handy's model). The

comparison between the values of capillary pressure ratio proves that the capillary pressure is not the only driving factor for oil imbibition. The presence of highly mature organic content may accelerate the oil uptake into the samples. Moreover, oil adsorption may occur on the surface of the organic matter and defined as a main driving force of higher oil imbibition of Duvernay samples.

Chapter 6

Rock-Fluid Interactions in the Duvernay Formation: Evaluation of Soaking Fluids and Imbibition Oil Recovery

In this chapter, we conduct soaking tests using Duvernay oil-saturated samples and soaking fluids with different compositions and physical properties. We compare the soaking fluids in terms of oil RF and explain the results by analyzing liquid-liquid contact angles and IFT of soaking fluids. Finally, we characterize the mechanisms controlling oil recovery from shales by imbibition process.

6.1 Materials

6.1.1 Core samples

In this experiment, we have used all the oil saturated samples (AOK2_1, AOK2_2, AOK5_1, AOK5_2, AOK9_1, AOK9_2, AOK3, AOK4, AOK5, AOK6, AOK7, AOK8, AOK9) those we have used for the air-oil imbibition experiment. To ensure the repetitive oil recovery result, we have half-cut three twin plugs (AOK2_1, AOK2_2, AOK5_1, AOK5_2, AOK9_1, and AOK9_2). Table 15 shows the list of full-length and half cut samples.

Table 15: The list of the length of the sample.

Full length (as received samples)	Length	Half cut (heated samples)	Length
AOK 3	3 inch	AOK 2_1	1.5 inch
AOK 4	3 inch	AOK 2_2	1.5 inch
AOK 6	3 inch	AOK 5_1	1.5 inch
AOK 7	3 inch	AOK 5_2	1.5 inch
AOK 8	3 inch	AOK 9_1	1.5 inch
		AOK 9_2	1.5 inch

6.1.2. Soaking fluids

In this section, we present the composition and physical properties of different soaking fluids. We use the soaking fluids in liquid-liquid spontaneous imbibition tests and investigate the performance of soaking fluids on oil recovery factor (RF). In liquid-liquid spontaneous imbibition experiments, we immerse oil-saturated samples in soaking fluid. As soaking fluid imbibes into the rock, oil is produced and accumulated at the top of the Amott cell. We measure the produced oil volume vs. time and calculate oil RF. We use the 1- Produced brine, 2- deionized water (DW), 3- deionized water with surfactant (DW+Surfactant), 4- deionized water with clay stabilizer (DW+Clay stabilizer), and 5- slick water as soaking fluids. The procedure of preparing slick water is more complicated than other soaking fluids and presented as follows,

1- Mix 1 ml of polyacrylamide friction reducer in 1 L of deionized water and agitate the solution for 30 seconds. Polyacrylamide provides a reduction in the friction pressure at the surface and reduces the energy required to pump fluid/sand.

2- Mix 1 ml of clay stabilizer in 1 L of solution prepared in the first step and agitate the solution for 30 seconds. Clay stabilizer provides clay stabilization in formation by inhibiting clay swelling.

3- Shake and mix 0.15 ml of scale inhibitor in 1 L of solution prepared in the second step and agitate the solution for 30 seconds. Scale inhibitor is an important additive in fracturing fluid to prevent mineral scale depositions during hydraulic fracturing, shut-in, and flowback stages (Yue et al., 2014).

To make DW+Surfactant, we dissolve 1 ml of surfactant in 1 L of deionized water and agitate the mixture for 30 seconds to prepare a homogeneous solution. This commercial surfactant supplied by a fracturing company is used as an additive for making slick water and cross-linked gel fracturing fluids. To make DW+Clay stabilizer, we dissolve 1 ml of clay stabilizer in 1 L of deionized water and mix them by agitation. The clay stabilizer is also supplied by the fracturing company and is used for inhibiting clay swelling in fracturing operations. Table 16 lists the physical properties of soaking fluids used in this study.

Table 16: Physical properties of soaking fluids.

Soaking fluid	Density (g/cm^3)	pH	Surface tension (mN/m)	IFT (mN/m)	Viscosity (cP)
Produced brine	1.09	6.40	40.00	20.45	1.38
DW	0.99	7.00	72.93	17.57	0.91
DW+Surfactant	0.99	8.35	25.26	7.52	0.90
DW+Clay stabilizer	0.99	7.42	55.70	17.41	0.94
Slickwater	0.99	6.95	40.84	17.25	4.36

6.2. Soaking experiments

The purpose of conducting soaking experiments is to investigate the ability of soaking fluid to spontaneously imbibe into the rock, already saturated with oil. We immerse the oil-saturated samples in the soaking fluids with different compositions and physical properties (Table 16). Then, we compare oil RF of different soaking fluids and investigate the controlling mechanisms of oil recovery. Prior to conducting soaking tests, we measure and compare liquid-liquid contact angles of soaking fluids and oil on oil-saturated samples.

6.2.1. Liquid-liquid contact angle measurement

We use Attension THETA (Biolin Scientific) instrument (Figure 11), and measure liquid-liquid contact angles of oil and soaking fluids before soaking experiments. To measure the contact angles of soaking fluids, we immerse the oil-saturated sample in kerosene and drop the droplet of soaking fluid on rock sample. The camera's software records the droplet shape until reaching to an equilibrium state. Similarly, we immerse oil-saturated samples in soaking fluids and measure the contact angle of reservoir oil droplet.

6.2.2. Liquid-liquid spontaneous imbibition (soaking) experiments

After liquid-liquid contact angle measurements, we immerse the oil-saturated core plugs in different soaking fluids (Table 16) and measure the produced oil at the top of Amott cell (Figure 27 (a)). For half cut samples, both pieces are immersed into the single soaking fluid. Then we measure the produced volume of oil accumulated at the top of the Amott cell and calculate oil RF

(Figure 27 (b). Table 17 lists the core samples and the corresponding soaking fluids used for soaking experiments.

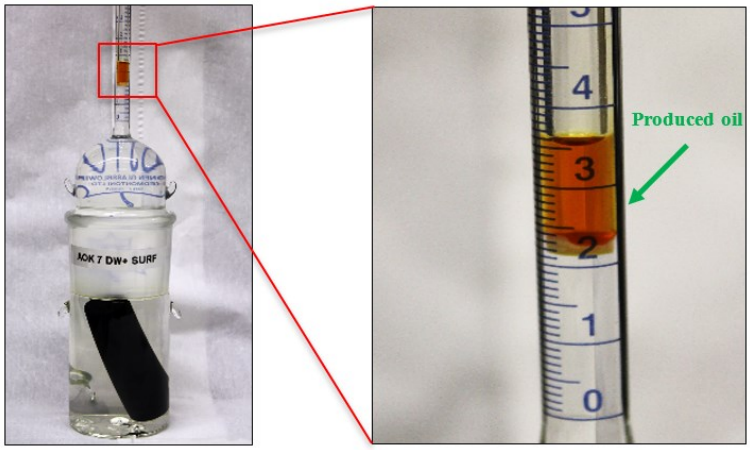

(a)

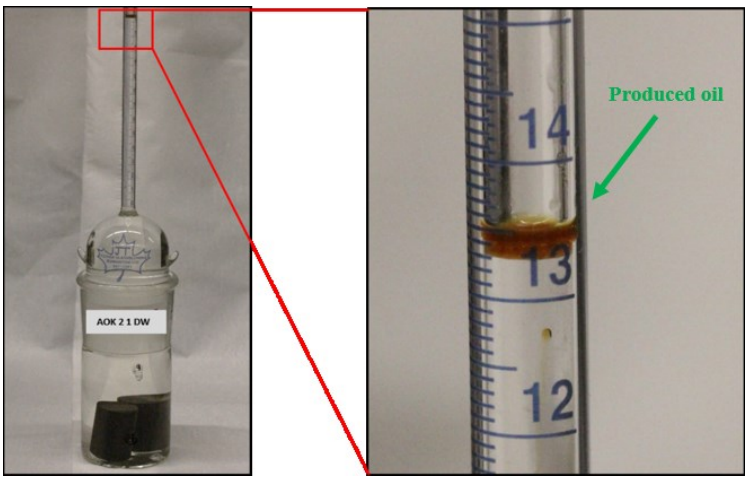

(b)

Figure 27: Amott cells used for soaking experiments. (a) Full length oil-saturated sample is immersed in soaking fluid. The soaking fluid imbibes into the rock and displaces the oil. (b) Half-cut oil-saturated samples are immersed in soaking fluid. The soaking fluid. The soaking fluid imbibes into the rock and displaces the oil.

Table 17: List of core samples and corresponding soaking fluids.

Sample ID	Soaking fluid	Sample ID (twin pairs)	Soaking fluid
AOK 3	Slickwater	**AOK 2_1**	DW
AOK 4	Produced brine	**AOK 2_2**	DW+Surfactant
AOK 6	DW+Clay stabilizer	**AOK 5_1**	DW
AOK 7	DW+Surfactant	**AOK 5_2**	DW+Surfactant
AOK 8	DW	**AOK 9_1**	DW
		AOK 9_2	DW+Surfactant

6.3 Results and Discussions

In this section, we present the results of liquid-liquid contact angles of soaking fluids and oil. Then, we present the results of immersing oil-saturated samples in soaking fluids with different compositions and physical properties. The main objective of soaking experiments is evaluating the key driving mechanisms leading to oil production from oil-wet shales. As received five samples were immersed into different soaking fluids produced brine, deionized water (DW), deionized water and surfactant (DW+Surfactant), deionized water and clay stabilizer (DW+Clay stabilizer), and slick water. From as received results, we investigate the mechanisms controlling oil recovery from shales by imbibition process. Heated three pairs of samples were immersed only into two different fluids. One plug of each pair immersed into DW and another plug into DW+ surfactant. From their results, we investigate the effect of initial oil saturation on oil recovery factor.

6.3.1. Liquid-liquid contact angle results

Figure 28 a, c, e, g, and i present the contact angles of soaking fluids on the polished surface of reservoir oil-saturated samples immersed in kerosene medium. The contact angles of all soaking fluids are larger than 130°. Figure 28 b, d, f, and h show the reservoir oil contact angles on the samples immersed in different soaking fluids. The oil contact angles are less than 90°, and for DW+Clay stabilizer medium, the oil contact angle is 109°. Slick water is an opaque liquid. Therefore, the camera cannot detect the reservoir oil droplet. The results listed in Table 18 show that the contact angles of soaking fluids are higher than oil contact angles; suggesting that the samples have a higher wetting affinity towards oil than that towards soaking fluids. Therefore, the results of liquid-liquid contact angles are in agreement with air-liquid contact angles presented in the previous section (Table 8).

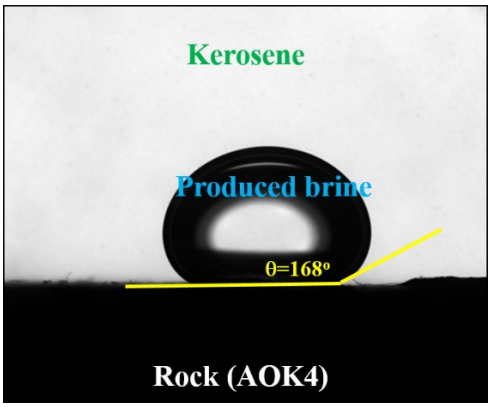

(a)

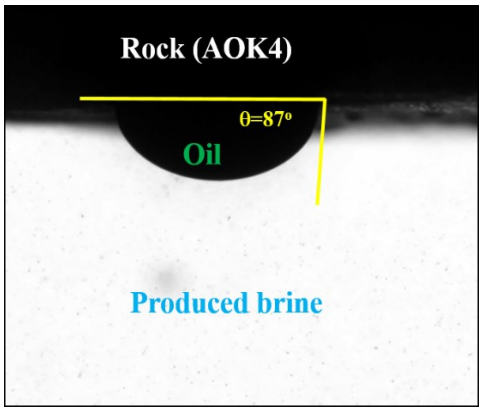

(b)

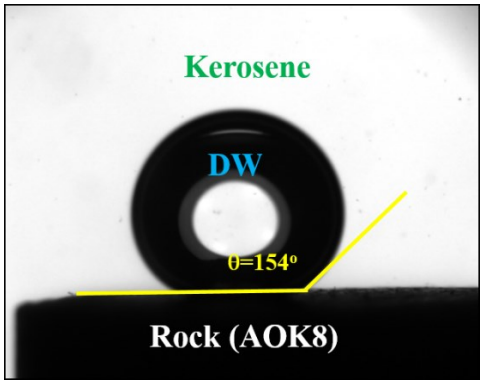
Kerosene
DW
θ=154°
Rock (AOK8)

(c)

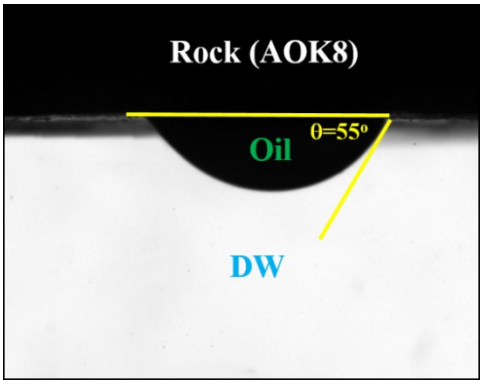
Rock (AOK8)
θ=55°
Oil
DW

(d)

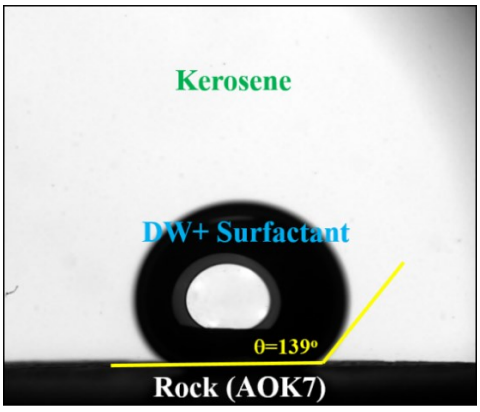
Kerosene
DW+ Surfactant
θ=139°
Rock (AOK7)

(e)

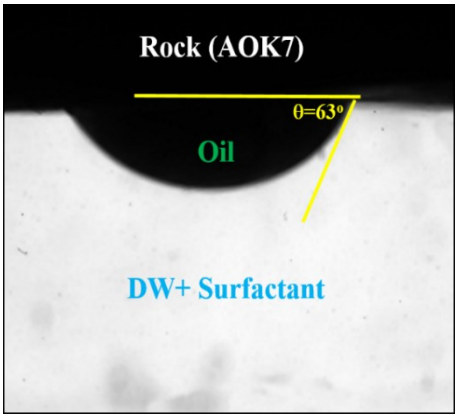
Rock (AOK7)
θ=63°
Oil
DW+ Surfactant

(f)

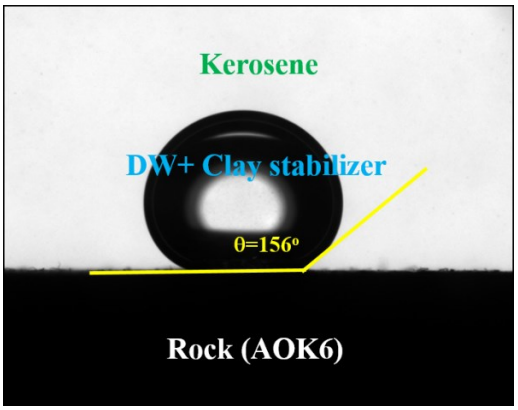
Kerosene
DW+ Clay stabilizer
θ=156°
Rock (AOK6)

(g)

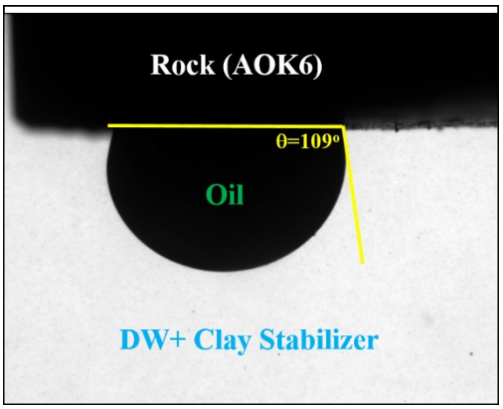
Rock (AOK6)
θ=109°
Oil
DW+ Clay Stabilizer

(h)

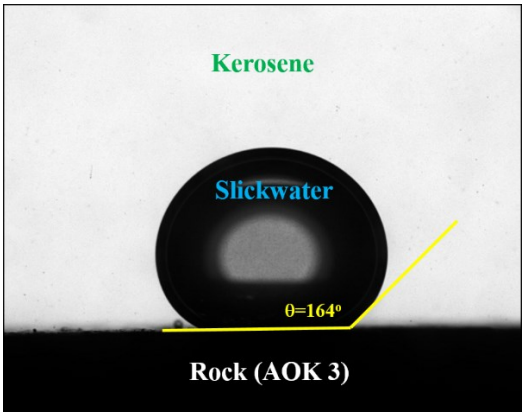

(i)

Figure 28: The contact angles of droplets of (a) Produced brine, (c) DW, (e) DW+Surfactant, (g) DW+Clay stabilizer, and (i) slick water equilibrated on the surface of the rock samples immersed in kerosene. The contact angles of reservoir oil droplets equilibrated on the samples immersed in (b) Produced brine, (d) DW, (f) DW+Surfactant, and (h) DW+Clay stabilizer. The volume of droplet is 10 µL.

Table 18: Liquid-liquid contact angles of soaking fluids and oil in kerosene and soaking fluid mediums, respectively.

Soaking fluid	Contact angle of soaking fluid in kerosene (degree)	Contact angle of reservoir oil in soaking fluid (degree)
Produced brine	168	87
DW	154	55
DW+Surfactant	139	63
DW+Clay stabilizer	156	109
Slickwater	164	-

As listed in Table 18, the contact angles of different soaking fluids in kerosene are different. Produced brine and DW+Surfactant have the maximum and minimum contact angles of 168° and 139°, respectively. Different contact angles indicate different wetting affinity rock to various

soaking fluids. Relatively low values of contact angle for DW+Surfactant may be due to the presence of surfactant that can change the rock-fluid and fluid-fluid forces. To explain different contact angles listed in Table 18, we use Young's (1805) equation:

$$\cos(\theta) = \frac{\gamma_{sk} - \gamma_{ss}}{IFT} \quad (14)$$

where θ is contact angle measured from soaking fluid phase, γ_{sk} is the surface tension between solid surface and kerosene, γ_{ss} is the surface tension between solid surface and soaking fluid, and IFT is the interfacial tension between soaking fluid and kerosene. This equation describes the relationship among rock-fluid and fluid-fluid forces as shown in Figure 29. In this case study, θ is larger than 90° ($-1 < \cos(\theta) < 0$), and consequently $\gamma_{sk} < \gamma_{ss}$. Adding the surfactant to deionized water reduces IFT as listed in Table 16. Based on Eq. 14, the soaking fluids with lower IFT should have higher contact angles. Figure 30 (a) shows the crossplot of soaking fluid contact angle vs. IFT. As is evident, there is a positive correlation between contact angles and IFT, which is in contrary with what we proposed based on Eq. 14. To explain this contradiction, we should also consider the nominator of Eq. 14. γ_{sk} is the surface tension between solid surface of shale and kerosene. If we assume homogeneous surface chemistry for different shale samples, we can consider almost similar γ_{sk} for different experiments. Conversely, γ_{ss} may change by altering the composition and physical properties of soaking fluids. Based on Eq. 14, by reducing γ_{ss}, the contact angle of soaking fluid reduces and the wetting affinity of droplet towards rock increases. To investigate the effect of reducing IFT on γ_{ss}, we plot (γ_{sk}-γ_{ss}) vs. IFT as shown in Figure 30 (b). This crossplot shows that by reducing IFT, the magnitude of (γ_{sk}-γ_{ss}) increases. The value of γ_{sk} is constant and increasing (γ_{sk}-γ_{ss}) means a decline in γ_{ss}. In conclusion, the soaking fluids with lower IFT have smaller γ_{ss}, and consequently lower contact angles (θ).

Adding surfactant to soaking fluid may reduce IFT and γ_{ss}. When the droplet of soaking fluid does not wet the shale sample ($90^o < \theta < 180^o$), the relative changes in IFT and γ_{ss} determines the decline or increase in contact angles (Eq. 14). For example, in this study, if the reduction in γ_{ss} were not significant after adding surfactant, the reduction in IFT would increase the contact angle, and consequently, the rock would be more water-repellant. However, higher reduction in γ_{ss} compared with that in IFT leads to a reduction in contact angle and results in wettability alteration towards more water-wetness (Figure 30 (a)).

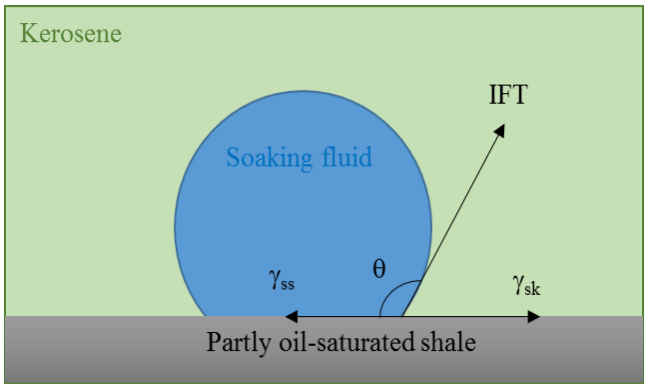

Figure 29: Schematic illustration for a droplet of soaking fluid equilibrated on the surface of the rock immersed kerosene. γsk is the surface tension between solid surface and kerosene, γss is the surface tension between solid surface and soaking fluid, and IFT is the interfacial tension between soaking fluid and kerosene.

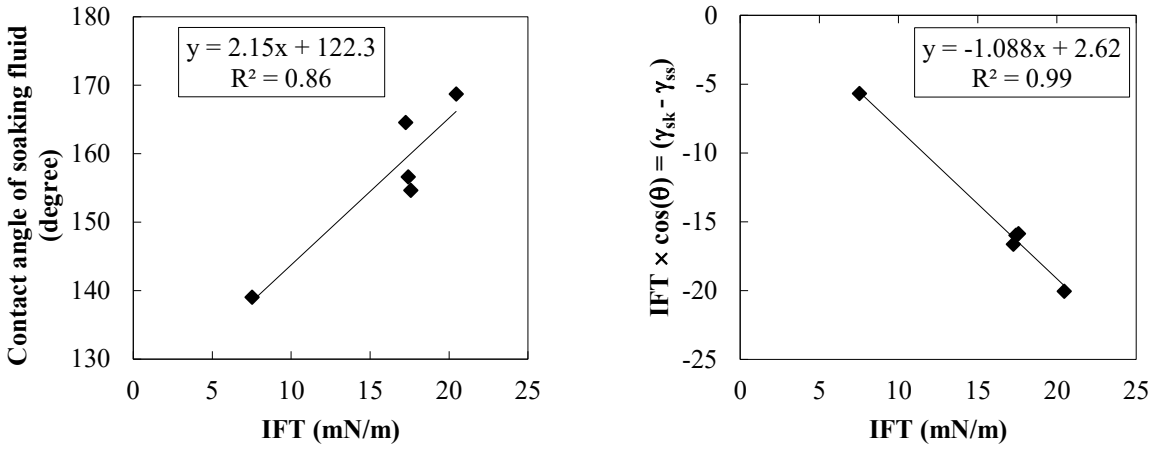

(a) **(b)**

Figure 30: The crossplots of (a) contact angles of soaking fluid vs. IFT and (b) (γsk - γss) vs. IFT. Comparing these two figures and considering Eq. 14 indicates that higher reduction in γss compared with that in IFT leads to a reduction in contact angle, and contact angle, and consequently wettability alteration towards more water-wetness.

6.3.2 Soaking test results of as received samples

As discussed in the previous section, decreasing IFT of the soaking fluids enhances their wetting affinity towards the shale samples. In this section, we immerse the oil-saturated core plugs in the 5 aforementioned soaking fluids and record the volume of produced oil accumulated at the top of Amott cells. Oil RF is calculated by dividing the produced oil volume by the initial oil in the sample. Figure 31 shows the produced oil droplets attached on the surface of the shale samples after immersing in DW. Figure 32 shows the crossplot of oil RF vs. time for all soaking tests. The Produced brine with maximum IFT of 20.45 mN/m and the maximum contact angle of 168° (minimum water-wetness) shows the minimum oil RF of 5.85%. DW+Surfactant with the minimum IFT of 7.52 mN/m and minimum contact angle of 139° (maximum water-wetness) shows maximum oil RF of 25.26%. Capillary pressure is the main driving force for displacing oil by

soaking fluid. On the one hand, lowering IFT reduces the driving capillary pressure; and on the other hand, the rock has the higher wetting affinity to soaking fluids with lower IFT (smaller contact angles) that increases capillary pressure, and consequently spontaneous imbibition of soaking fluid. The competition between IFT and wettability determines the magnitude of the resulting capillary pressure. The quantitative analyses of IFT, contact angle and capillary pressure will be discussed in the next part. The oil RF of other soaking fluids listed in Table 19 lie between the Produced brine and DW+Surfactant.

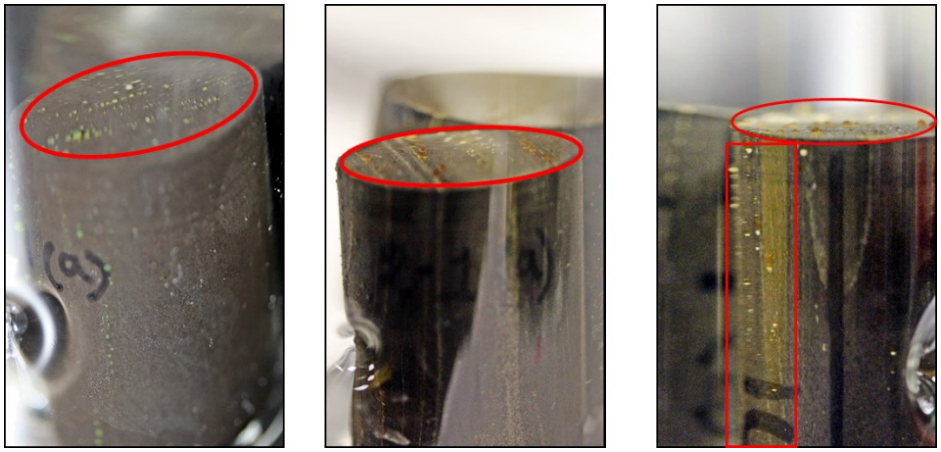

Figure 31: The produced oil droplets (yellow droplets) attached on the surface of the shale samples after immersing in deionized water (DW).

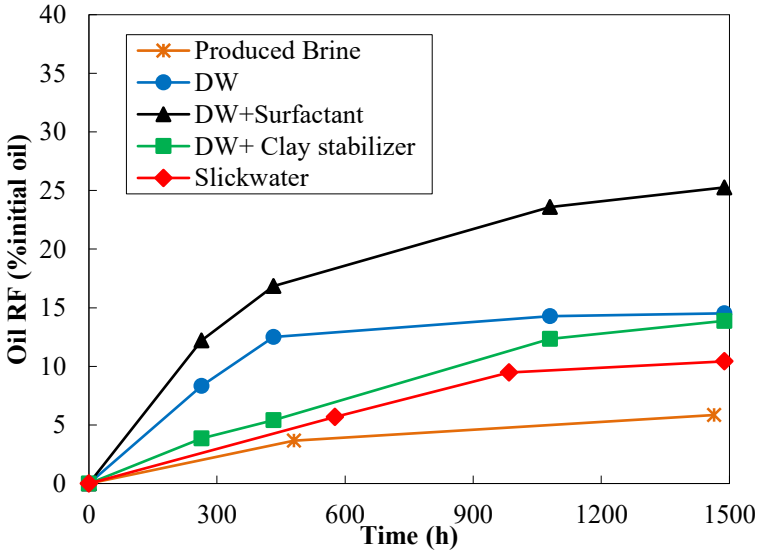

Figure 32: Oil recovery factor for the shale samples immersed in different soaking fluids.

Table 19: Oil recovery factor for different soaking tests.

Sample	Soaking fluid	Oil RF (%initial oil)
AOK4	Produced brine	5.85
AOK8	DW	14.52
AOK7	DW+Surfactant	25.26
AOK6	DW+Clay stabilizer	13.88
AOK3	Slick water	10.42

6.3.3 Discussion of as received soaking tests results

In this part, we discuss the results of liquid-liquid contact angle measurements and soaking tests presented in previous sections. First, we investigate the effects of IFT and contact angle on capillary pressure, and consequently spontaneous imbibition of the soaking fluids. Then, we discuss the effect of buoyancy force as a possible mechanism for oil production in soaking tests. We calculate the dimensionless bond number (N_B) for quantitative comparison of gravity and capillary forces. Then, we compare air-liquid imbibition tests with soaking tests and characterize the type of pores (hydrophobic and hydrophilic) invaded by soaking fluids. Finally, we investigate the effect of initial oil saturation on imbibition of the soaking fluids into oil-saturated samples.

Effects of IFT and contact angle on imbibition oil recovery

In this part, we evaluate the effects of IFT and wettability (liquid-liquid contact angles) on P_c, and consequently on oil production. Figures 33a and 33b show the oil RF versus IFT and contact angle, respectively. In general, the soaking fluids with lower IFT have higher oil RF. Based on Young-

Laplace (1805) equation (Y-L) (Eq. 15), decreasing IFT should decrease the driving P_c and consequently the imbibition rate,

$$P_c = \frac{4 \times IFT \times \cos(\theta)}{D} \quad (15)$$

Where, D is the average pore diameter. Therefore, other reasons such as wettability alteration may be responsible for the negative trend of oil RF versus IFT, observed in Figure 33a. Based on Eq. 15, a reduction in contact angle indicates stronger wetting affinity of rock to soaking fluid and consequently higher spontaneous imbibition and oil production. According to Figure 33b, there is a negative correlation between oil RF and contact angle. This correlation suggests that for soaking fluids with lower IFT, the effect of decreasing oil-wetness may dominate the effect of decreasing IFT. Therefore, the soaking fluids with lower IFT may have higher P_c for spontaneous imbibition, leading to higher oil recovery.

Munson (2015) measured pore size distributions by the N_2 BJH (Barrett-Joyner-Halenda) method and reported a peak pore diameter of approximately 20-70 nm for Duvernay samples from oil-window. We assume average pore diameter of 45 nm for shale samples and plug the values of IFT and contact angle (data in Figures 33a and 33b) into the Y-L equation. P_c calculated by Eq. 15 is negative, suggesting no suction pressure for spontaneous imbibition of the soaking fluids. Furthermore, the absolute value of P_c is lower for the soaking fluid with surfactant compared with that for the surfactant-free fluids. Thus, according to Y-L equation, the P_c, and the subsequent oil recovery, is expected to be lower when surfactant is present in the imbibing fluid, and this contradicts with our experimental observations. Negative P_c, as well as the negative correlation between the absolute value of P_c and oil RF indicate that using contact angle of the soaking fluids in the Y-L equation cannot quantitatively explain the observed high oil recovery when we add surfactant to the soaking fluid. Similar to this study, Nguyen et al. (2014) and Neog and Schechter

(2016) used the results of contact angle measurements as a qualitative tool to explain wettability alteration of shales followed by adding surfactant to the soaking fluid.

It should be mentioned that equilibrium contact angle on the polished surface of shale sample (Figure 28) is different from pore-scale contact angle, and is affected by the surface area fractions of hydrophilic and hydrophobic components. Cassie and Baxter's (1944) equation models the equilibrium contact angle for a surface with varying degrees of heterogeneity. According to this equation, contact angles higher than 90° ($-1<\cos(\theta)<0$) may be explained by the high fraction of the hydrophobic surface area. Therefore, negative P_c calculated by $\theta>90^o$ does not necessarily mean the absence of suction pressure for spontaneous imbibition.

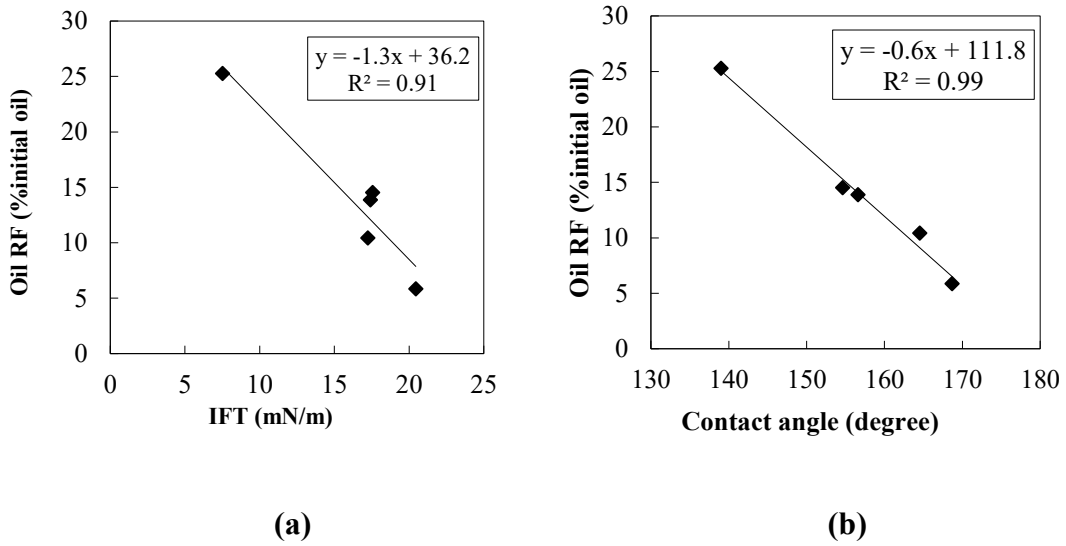

Figure 33: Crossplots of oil recovery factor versus IFT and contact angle of the soaking fluids for tests conducted on the core plugs.

In conventional applications of surfactant flooding for enhanced oil recovery, surfactant is added to the aqueous fluid to reduce the IFT and improve microscopic oil displacement efficiency (E_D) (Sheng, 2010). However, based on Eq. 15, IFT drop due to the addition of surfactant reduces P_c needed for spontaneous imbibition, leading to lower imbibition oil recovery. To explain the

impacts of IFT reduction on oil recovery factor in unconventional reservoirs, we briefly explain different steps of fracturing operations. First, fracturing fluid with high pressure is injected into the formation to create fractures (Step 1). Fracturing fluid pressure is higher than the formation pressure, leading to fracturing fluid leak-off from fracture system into the formation. Then, the well may be soaked for a certain period of time (Step 2). Fracture pressure gets close to formation pressure during the soaking process. After the soaking process, the well is opened to initiate flow-back and production (Step 3). Fracture pressure declines to a value lower than formation pressure during the production period.

During Steps 1 and 3, there is a pressure gradient between fracture and formation which leads to the viscous flow of fracturing fluid and hydrocarbon. Viscous force competes with capillary force during fracturing and production periods. The ratio of viscous force over capillary force is defined as the capillary number (N_{ca}) (Peters, 2012),

$$N_{ca} = \frac{\text{Viscous force}}{\text{Capillary force}} = \frac{\mu \times u}{IFT \times \cos(\theta)} \quad (16)$$

Where, μ is the displacing fluid viscosity, u is the Darcy velocity of the displacing fluid, and IFT is the interfacial tension between the displacing and displaced phases, and θ is the contact angle. By increasing N_{ca}, S_{or} decreases (Lake, 1989; Delshad et al., 1986). Increasing N_{ca} is achieved by increasing viscous force and/or reducing capillary force. Increasing N_{ca} by reducing IFT leads to a decline in S_{or}. The S_{or} can be decreased by decreasing IFT during fracturing (Step 1) and production (Step 3) periods where we have viscous force. Reducing IFT leads to an improvement in E_D. To study the impact of viscous and capillary forces on surfactant-aided oil recovery from unconventional rocks, some researchers conducted core flooding tests and simulated the 3

aforementioned steps (Alvarez et al., 2014; Liang et al. 2017a; Longoria et al., 2017; Penny et al., 2012). During the soaking period (Step 2), fracture pressure gets close to formation pressure. Therefore, spontaneous imbibition by capillary suction may be the dominant mechanism for counter-current transport of oil and fracturing fluid between fracture and matrix. According to Eq. 15, IFT and contact angle affect P_c. Higher IFT and smaller contact angle (stronger water-wet conditions) lead to higher capillary suction. Neog and Schechter (2016) pointed out that if a surfactant changes rock wettability to more water-wet conditions, a reduction in IFT lowers capillary suction, leading to lower imbibition oil recovery. Reduction in IFT after introducing a surfactant in the system is inevitable. Therefore, the balance between IFT reduction and wettability alteration determines the potential of that surfactant for imbibition into the rock (Neog and Schechter, 2016).

In summary, lower P_c during fracturing and production steps may be desirable due to higher N_{ca} that leads to better displacement efficiency (smaller S_{or}). Conversely, higher P_c during the soaking period may be desired to achieve a higher capillary suction of the soaking fluid from the fracture into the formation, leading to improved imbibition oil recovery. Therefore, optimum designing of surfactant solutions for hydraulic fracturing applications requires careful consideration of the combined effects of surfactant and rock-fluid properties during the whole process (Takahashi and Kovscek, 2010).

Effect of gravity force on oil production

Capillary force and gravity force are two dominant forces for oil production from oil-saturated samples immersed in aqueous fluids. Bond number (N_B) is often used to describe the relative effect of gravity and capillary forces (Qi et al., 2016):

$$N_B = \frac{\Delta\rho \times g \times (D/2)^2}{IFT} \quad (17)$$

Here, $\Delta\rho$ is the difference in density of soaking fluid and reservoir oil, kg/m^3; g is the gravity acceleration, m/s^2; D is the average pore diameter, m; and IFT is the interfacial tension between soaking fluid and reservoir oil, N/m. Similar to the previous section, we assume average pore diameter of 45 nm and calculate N_B using Eq. 17. The limiting value of bond number above which the gravity force becomes significant is $1x10^{-5}$ (Chen et al., 2001). The calculated N_B values range from $5.3x10^{-11}$ (DW) to $1.2x10^{-10}$ (DW+Surfactant) which are much smaller than $1x10^{-5}$. Low magnitude of N_B suggests that the role of gravity force for oil production is insignificant compared with that of capillary force. In addition, the data points of oil RF vs. N_B are scattered and do not show any consistent correlation.

Comparison of air-liquid spontaneous imbibition and soaking tests

In order to characterize the pores invaded by soaking fluids, we compare the results of air-liquid imbibition (Chapter 4) and soaking tests. The low imbibed volume of brine in the air-brine imbibition tests (Table 9) suggests that brine has the low wetting affinity towards hydrophobic organic pores (Odusina et al., 2011). This observation suggests that brine may only imbibe into hydrophilic inorganic pores (Lan et al., 2015). Conversely, the relatively high magnitude of imbibed oil volume in the air-oil imbibition tests (Table 9) indicates that oil may tend to imbibe into both hydrophobic organic and hydrophilic inorganic pores.

In soaking tests, we immersed the oil-saturated plugs in different soaking fluids. In order to investigate the wettability of pores invaded by soaking fluids, we compare the imbibed volume of brine (V_b) in air-brine imbibition tests with the produced volume of oil (V_o) (or equivalently imbibed volume of soaking fluid) in soaking tests. Here, V_b is considered as the volume of

hydrophilic pores invaded by brine, in the presence of air. The length and diameter of all core plugs are 7.62 and 2.54 cm, respectively. We assume that the effective porosities of twin core plugs are similar (Table 3). Therefore, twin core plugs have nearly similar pore volumes. As a result, the imbibed volume of brine in imbibition (V_b) and produced oil volume in soaking tests (V_o) are comparable without volumetric normalization. Figure 34 shows that V_o is generally lower than V_b. This result suggests that a portion pores accessible for brine imbibition in the air-brine imbibition tests is not accessible for the imbibition of the soaking fluids in the soaking tests. In other words, $V_o<V_b$ suggests that the soaking fluids probably imbibe into a portion of hydrophilic inorganic pores and expel the oil out. Interestingly, $V_o>V_b$ for DW+Surfactant, which suggests that DW+Surfactant not only displaces the oil from hydrophilic inorganic pores but also displaces a portion of oil from hydrophobic organic pores. This observation indicates that adding surfactant to the soaking fluid may alter the wettability of organic pores towards less oil-wet conditions; leading to the displacement of oil from hydrophobic organic pores. Figures 35a-d schematically illustrate pore-filling mechanism in air-liquid imbibition and soaking tests. Brine may only fill hydrophilic inorganic pores (Figure 35a), while oil may fill both hydrophobic organic and hydrophilic inorganic pores (Figure 35b). After immersing the oil-saturated plug (Figure 35b) in soaking fluid without surfactant, only a portion of oil in inorganic hydrophilic pores may be displaced by soaking fluid (Figure 35c). In other words, soaking fluid can hardly displace the oil from hydrophobic organic pores. As schematically illustrated in Figure 35d, soaking fluid with surfactant may be imbibed and displace the oil from both hydrophilic and hydrophobic pore networks, leading to $V_o>V_b$ (Figure 34).

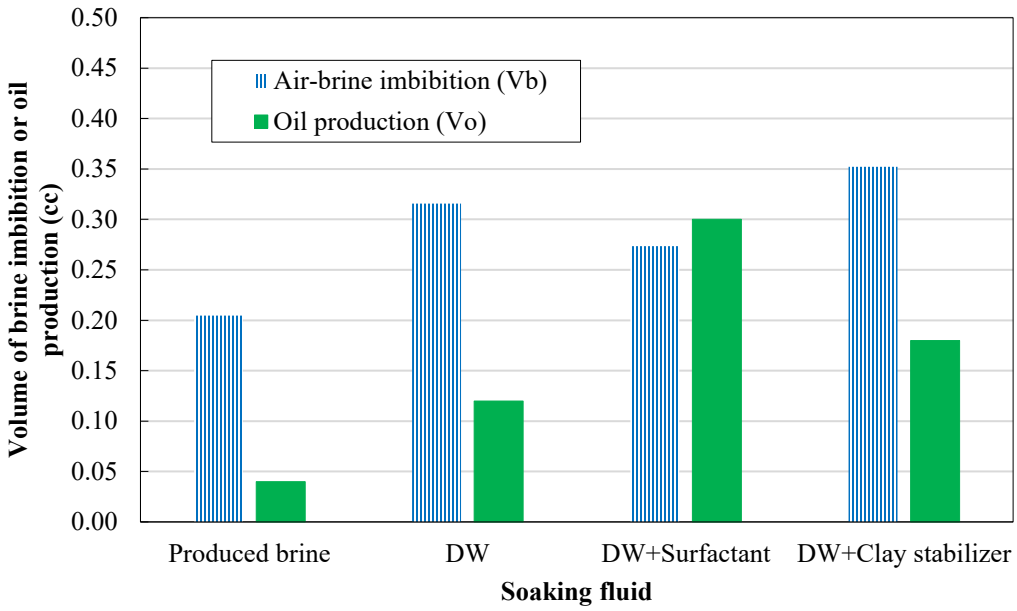

Figure 34: Comparison between imbibed volume of brine (Vb) in air-brine imbibition tests and produced volume of oil (Vo) in soaking experiments. Generally, Vo<Vb suggests that soaking fluid probably imbibes into a portion of hydrophilic inorganic pores and expels the oil out. $V_o > V_b$ in DW+Surfactant suggests that this soaking fluid not only displaces the oil in hydrophilic inorganic pores, but also displaces a portion of oil in hydrophobic organic pores.

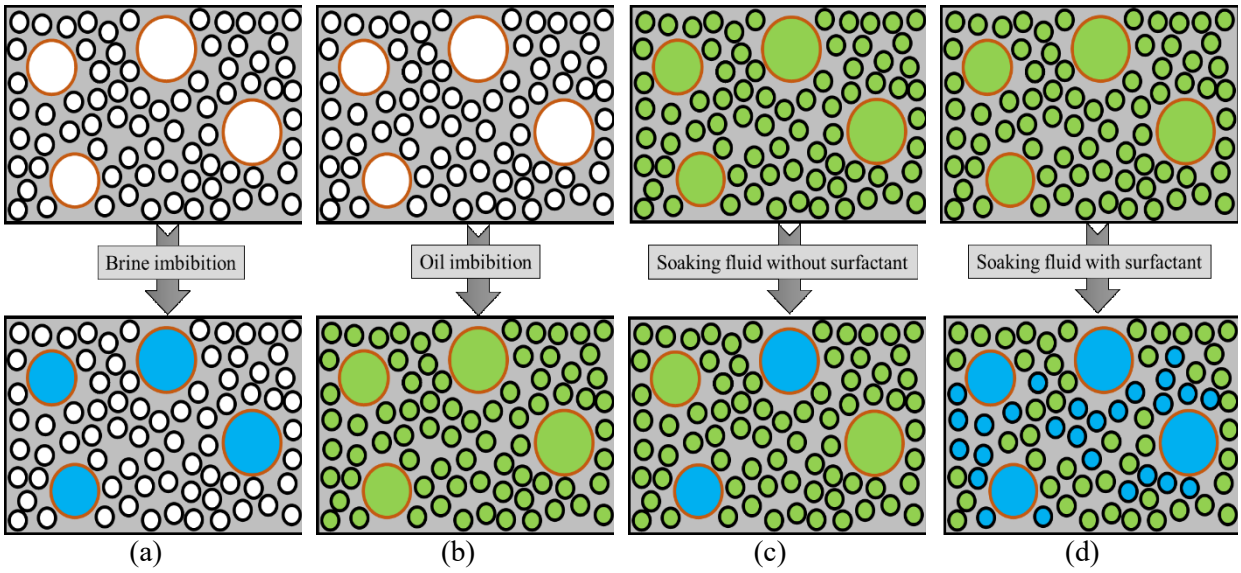

Figure 35: Schematic illustration of imbibition oil recovery at the pore scale. (a) Brine fills hydrophilic inorganic pores of the twin plug in an air-brine imbibition test. (b) Oil fills hydrophobic organic and

hydrophilic inorganic pores of the twin plug in an air-oil imbibition test. (c) After immersing the oil-saturated plugs is soaking fluid without surfactant, only a portion of the oil in hydrophilic pores is displaced. (d) After immersing the oil-saturated plug in the soaking fluid with surfactant, the surfactant solution not only displaces the oil in hydrophilic pores, but also displaces a portion of oil in hydrophobic pores. Small pores with black borders represent hydrophobic organic pores within organic matter. Larger pores with brown borders represent hydrophilic inorganic pores. Green, blue, and white represent oil, brine (in Fig. a) or soaking fluid (in Figs. c and d), and air, respectively. It should be mentioned that we assumed both hydrophilic and hydrophobic pore networks are well-connected to each other. Pore connectivity is not shown in this figure.

6.3.4 Soaking test results of heated samples

In this section, we present the results of soaking tests on heated samples and investigate the effect of initial oil saturation on oil RF. We use the oil-saturated heated samples (AOK2, AOK5, and AOK9), and immerse one half-cut sample in DW and the other one in DW+Surfactant. Figure 36(a) and Figure 36(b) show the oil RF after immersing oil-saturated samples in DW and DW+Surfactant, respectively. The results show that oil RF is higher when surfactant is added to DW. These results are similar to what we observed in soaking experiments on as-received samples (Figure 32). Three sets of samples from three different depths showing similar results for the same experiment also confirm the authenticity of our experiments.

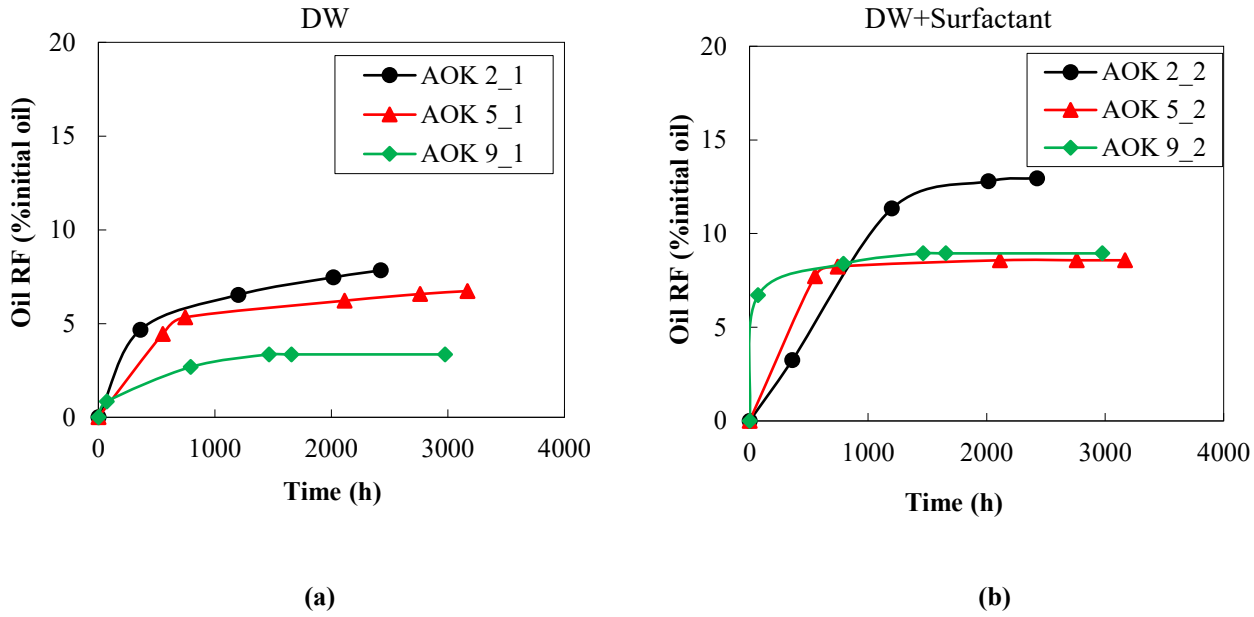

Figure 36: Oil RF for half-cut heated samples immersed in (a) DW and (b) DW+Surfactant.

Effect of initial oil saturation on oil RF

To investigate the effect of initial oil saturation, AOK2, AOK5, and AOK9 samples were heated and oil saturated. In Figure 37 we have plotted the heated samples oil RF vs the initial oil saturation (PV%) for DW (Figure 37(a)) and DW+ surfactant (Figure 37 (b)). We have found that for a certain soaking fluid (DW/ DW+ Surfactant), samples with high initial oil saturation shows high oil RF.

However, the oil RF results of the heated samples and as-received samples show that oil RF is higher for as-received samples compared with heated samples. For examples, oil RFs for the heated samples of AOK2_1 is 7.8% (DW), and AOK2_1 is 12.9% (DW+Surfactant), while, oil RFs for as-received samples of AOK8 and AOK7 are 14.5% (DW) and 25.3% (DW+Surfactant), respectively. The results show that oil RFs for heated samples are almost half of the values for as-received samples. The initial oil saturation of AOK2 is nearly 100% PV, while the initial oil saturation of AOK8 and AOK7 are 46.6 %PV and 79.6 %PV, respectively. The results suggest

that when initial oil saturation is lower, there is more pore space available for spontaneous imbibition of soaking fluid, and this can lead to higher oil RF. Another reason can be explained by the air-oil spontaneous imbibition results discussed on the chapter-4. Air-oil imbibition result shows that the heated samples imbibe comparatively high volume of oil than as received samples and get more affinity oil. Therefore, during the soaking test, soaking fluid cannot replace the initial oil.

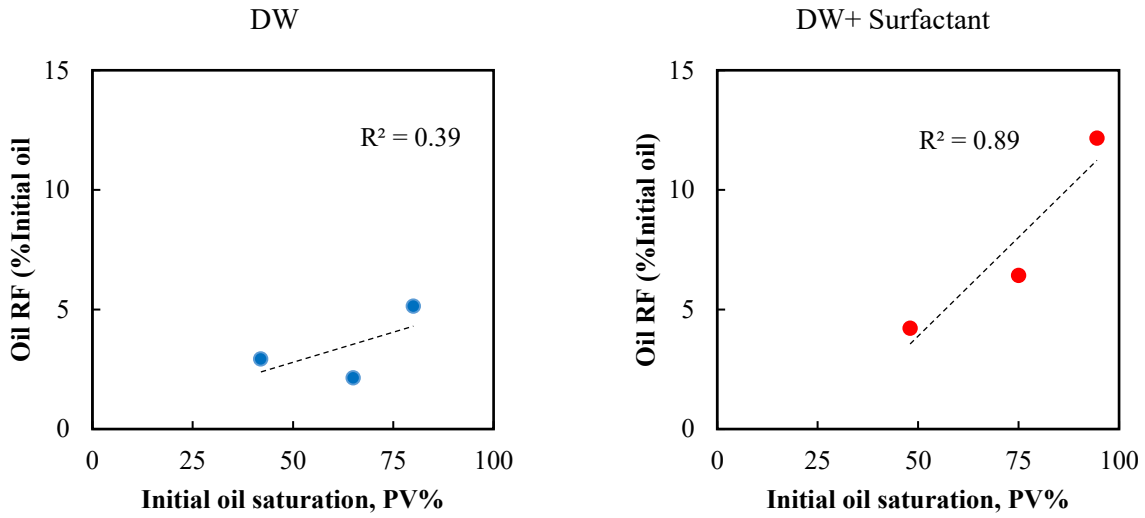

Figure 37: Oil RF vs initial oil saturation (%PV) of heated samples during soaking in (a) DW and (b) DW+ surfactant.

6.4 Conclusions

1- The results of liquid-liquid contact angles show that all soaking fluids are non-wet and have contact angles higher than 130^{o} on the surface of oil-saturated samples. By reducing the IFT, the contact angles of soaking fluids decline; suggesting that the water-wetness of shale to soaking fluids increases.

2- The results of soaking experiments show that the soaking fluids with lower IFT imbibe more and result in higher oil RF. Stronger water-wetness (smaller contact angle) of soaking fluids with lower IFT can compensate the effect of low IFT; leading to higher driving capillary pressure and higher oil RF.

3- Soaking fluid can displace only a portion of oil in inorganic hydrophilic pores and has low chance to displace the oil out of hydrophobic organic pores. Adding surfactant to soaking fluid may alter wettability of organic pores towards water-wetness; leading to higher oil RF.

4- The results of soaking tests on heated samples show that oil RF is lower in samples with higher initial oil saturation. Higher initial oil saturation reduces the pore space available for spontaneous imbibition of soaking fluid and consequently reduces oil RF. Another potential reason could be the heated samples higher wetting affinity to oil.

Chapter 7

Mechanisms of Oil Recovery from Crushed Shale Pack (CSP)

Better quantitative comparison among different soaking fluids can be explained by the soaking test on crushed shale pack (CSP) samples. The Duvernay drilling cuttings were used for making CSP. The CSP samples have comparatively higher porosity, permeability, and the initial oil saturation than the core plugs before the soaking tests. The effect of pore connectivity can be explained by comparing the results of spontaneous imbibition for core plugs and CSP. Moreover, the mechanisms controlling oil recovery from CSP by different soaking fluids can be compared with the core samples.

7.1 Methodology

7.1.1 Preparation of CSP

Drilling cuttings from Duvernay Formation are used as the crushed samples (Figure 38). The as-received drill cuttings are pre-saturated with the reservoir oil and oil-based drilling mud. The average porosity and initial oil saturation of drilling cutting are approximately 37% bulk volume and 80% pore volume, respectively. The drilling cuttings were contaminated with the drilling mud. So, they went through much cleaning processes before the imbibition experiments.

Figure 38: Crushed samples of Duvernay Formation before packing.

The cleaning and packing procedures are described below.

1. The drilling cuttings were centrifuged for 45 minutes to separate the excess oil from cuttings.
2. Then, the soaking cloth was used to dry out the extra oil from the surface of the grains.
3. The grains were washed with toluene using Soxhlet cell for 3-4 days.
4. After washing with toluene, the grains were clean and free from possible impurities. The grains were dried in an open space for 4 days to let the toluene evaporated from the samples.
5. After that, dry clean grains were tightly packed into a Plexiglass tube (Figure 39 (a)) which is open at two ends. Meshes were sealed on both sides of the Plexiglass tube (Figure 39 (b)). The length and diameter of the plexiglass tubes are known (Table 20). Therefore, the bulk volume of the CSP can be calculated.

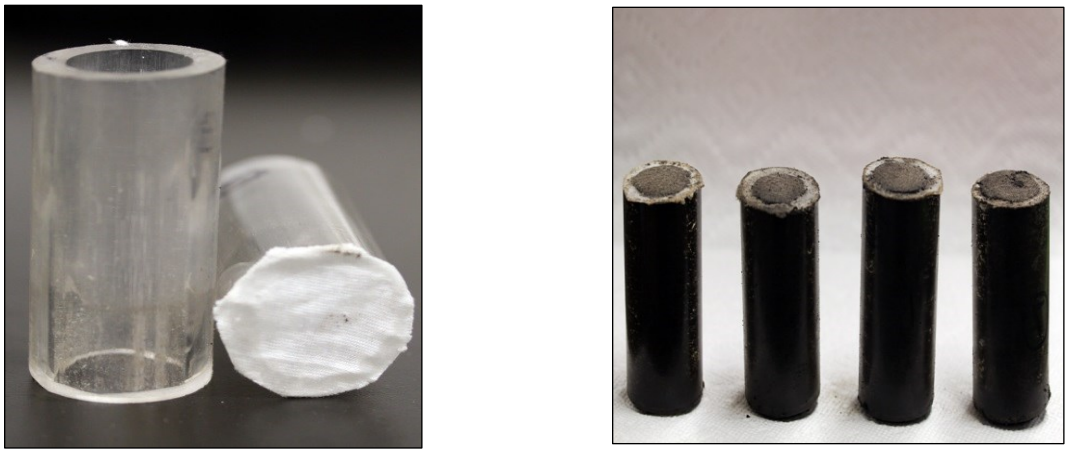

(a) **(b)**

Figure 39: (a) Plexiglass tube (b) CSP samples.

The mass of the powder, length, diameter and the porosity of each tube is listed in Table 20. The porosity is calculated by the following equation,

$$\text{Porosity} = 1 - \left[\frac{\frac{m_{powder}}{\rho_{powder}}}{\frac{\pi D^2 h}{4}}\right] x100 \qquad (18)$$

Here, $\mathbf{m_{powder}}$ is the mass of the dry crushed sample, $\boldsymbol{\rho}_{\mathbf{powder}}$ is the matrix density of the dry crushed sample, **D** is the inner diameter of the tube, **h** is the height of the Plexiglass. The TRA data of Duvernay core sample show that the matrix density of dry rock sample is around 2.6 g/cm^3. We considered this value to calculate the porosity of each CSP samples using Eq18.

Table 20: Dry mass, height, diameter, and porosity of CSP samples.

CSP ID	Mass of crushed samples, g	Length, cm	Diameter, cm	Porosity, fraction
1	69.39	7.70	2.57	0.331507
2	67.16	7.60	2.56	0.339346
3	74.29	7.80	2.62	0.320186
4	70.98	7.70	2.60	0.331878
5	69.88	7.95	2.53	0.328238

7.1.2 Air-oil imbibition

After making CSP samples, they were immersed in oil with only one end open for one-dimensional spontaneous imbibition. The weight of each CSP was measured periodically during the oil imbibition process using a digital balance. The initial mass of CSP is subtracted from recorded mass to calculate the imbibed mass of oil. Then, we calculate the imbibed volume by dividing the imbibed mass by the liquid density. After reaching the equilibrium state, the final imbibed volume of oil is divided by the effective pore volume to calculate the final normalized imbibed volume of oil (I_o).

$$I_o = \frac{\text{Final imbibed volume of oil}}{\text{Pore volume}} \times 100 \quad (19)$$

7.1.3 Soaking tests

We immerse the oil-saturated CSP in different soaking fluids (Table 21) and measure the amount of produced oil at the top of the Amott cell. We have used the similar fracturing fluids that we used in the soaking experiments for core plugs (Chapter- 6). Table 21 lists the CSPs and the

corresponding soaking fluids used for the soaking experiments. The soaking fluid imbibes into the CSP and displaces the oil out. We measure the produced volume of oil accumulated at the top of the Amott cell and calculate oil recovery factor (RF).

Table 21: List of CSP samples and corresponding soaking fluids.

Sample ID	Soaking fluid
Sample 1	DW+Surfactant
Sample 2	Slick water
Sample 3	DW
Sample 4	DW+Clay stabilizer
Sample 5	Produced brine

7.2 Results

In this section, we present the results of immersing oil-saturated CSP samples in soaking fluids with different compositions and physical properties. The main objective of soaking experiments is evaluating the key driving mechanisms leading to oil production from CSP samples and compare the results with those soaking tests conducted on the core plugs (Chapter 6).

7.2.1 Air-oil imbibition

Figure 40 shows the results air-oil imbibition tests conducted on the Duvernay CSP samples. The results show that all the samples are almost fully saturated with oil at the end of the tests. Oil saturation ranges from 90% to 98% of total pore volume. Table 22 lists the equilibrium imbibed volume of oil (I_o) for CSP samples.

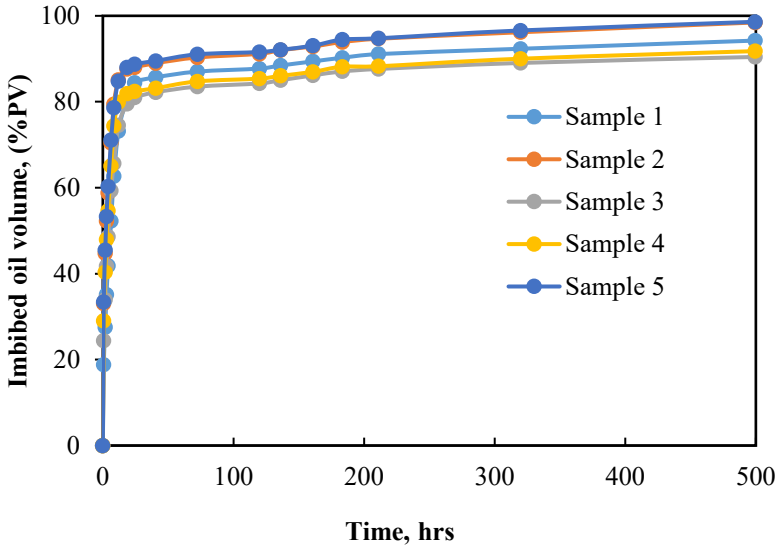

Figure 40: Imbibed volume of oil versus time graph for five packed samples

Table 22: List of Io for CSP samples.

CSP ID	I_o
1	94.23
2	98.45
3	90.43
4	91.78
5	98.60

7.2.2 Soaking test

In this section, we immerse the oil-saturated CSP samples in five soaking fluids listed in Table 21 and record the volume of produced oil accumulated at the top of the Amott cells. Oil RF is calculated by dividing the produced oil volume by the initial oil volume in the CSP. Figure 41 shows the crossplot of oil RF vs. time for all soaking tests. The results of soaking tests in Figure 41 show that the CSP sample immersed in DW+surfactant has the highest oil recovery of 8.1% compared with other soaking fluids. DW shows moderate oil recovery of 2.8% whereas,

produced brine and slickwater shows the minimum oil recovery factor of 0.46% and 0.31%, respectively. CSP sample immersed in DW+clay stabilizer did not show any oil recovery (0%). The results of soaking tests for CSP samples are consistent with that from the core sample (Chapter 6). The results of soaking tests conducted on the core plugs show that DW+surfactant recovers more oil than DW, produced brine, slick water and DW+clay stabilizer (Figure 21). However, in Chapter 6, we observed that oil RF for DW+clay stabilizer was 13.88% which almost near to the oil RF of DW (14.52%). Nevertheless, for the CSP tests, DW+clay stabilizer did not show any oil recovery whereas DW recovered 2.80% of oil as listed in Table 23. Moreover, oil RFs of produced brine and slick water for CSP sample were also very low (Figure 41).

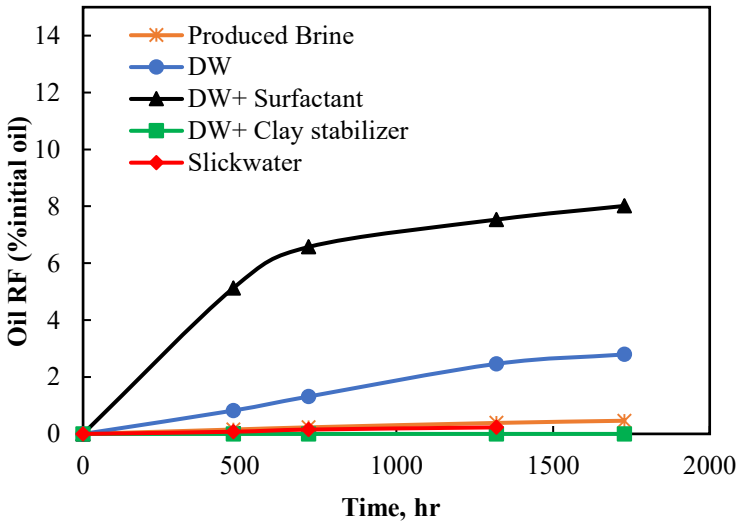

Figure 41: Oil RF for Duvernay CSP samples immersed in different soaking fluids.

Table 23: List of oil recovery factor (%) for CSP samples.

Experiment Set	Oil recovery (%OOIP)
DW+Surfactant	8.01
Slickwater	0.31
DW	2.80
DW+Clay stabilizer	0.00
Produced brine	0.46

7.3 Discussion

In Chapter 6, we investigated the mechanisms controlling oil recovery from core samples by imbibition process. In the CSP, the hydrophobic and hydrophilic pores are artificially mixed together. Comparing I_o of both core sample and CSP sample, I_o is lower in core samples compared with Io in CSP samples. This observation suggests that the CSP samples have more wetting affinity to oil compared with core samples. Similarly, Xu and Dehghanpour (2014) observed that crushed shale packs imbibed more oil than water in gas shales of the Horn River Basin (HRB). They hypothesized that by powdering the shale samples, the poorly-connected hydrophobic pore network of HRB core plugs becomes artificially well-connected. Yassin et al. (2017) found a similar trend in the core and CSP samples from upper part of the Duvernay Formation. They explained this observation with characterizing the TOC content into mobile organic carbon (MOC) and static organic carbon (SOC) (Zhu 2016). It was explained that crushing shale samples increases the surface area of clays which may enhance the accessibility to MOC and SOC, leading to increasing hydrophobicity of CSP samples.

CSPs which are used for this soaking tests are homogeneous and have similar pore networks. We discussed the effect of initial liquid saturations on the results of soaking tests in Chapter 6. However, the pore volume and initial oil saturation (I_o) of CSPs are close to each other and range from 90 to 98 %PV (Table 22). Therefore, initial oil saturation may not affect the results of soaking tests on CSP samples.

The difference between the imbibition of different soaking fluids is attributed to the difference in interfacial tension (IFT) and wettability (contact angle). In Figure 42, we have plotted the oil RF and the IFT of the soaking fluids for CSP tests. Similar to core sample results, we found that soaking fluids with low IFT can displace more volume of oil, leading to higher oil recovery.

Capillary pressure is the main driving force for displacing the oil by soaking fluid. In the soaking test of core samples presented in Chapter 6, we discussed that there is a competition between IFT and wettability that governs the magnitude of capillary pressure. On the one hand, lowering IFT reduces the driving capillary pressure; and on the other hand, the rock has a higher wetting affinity to soaking fluids with lower IFT that increases capillary pressure and consequently spontaneous imbibition of soaking fluid. For both Duvernay core samples and CSPs, stronger water-wetness of soaking fluids with lower IFT can compensate the effect of lower IFT, leading to higher driving capillary pressure and higher oil RF. The repetitive results for both Duvernay core samples and CSPs prove this statement.

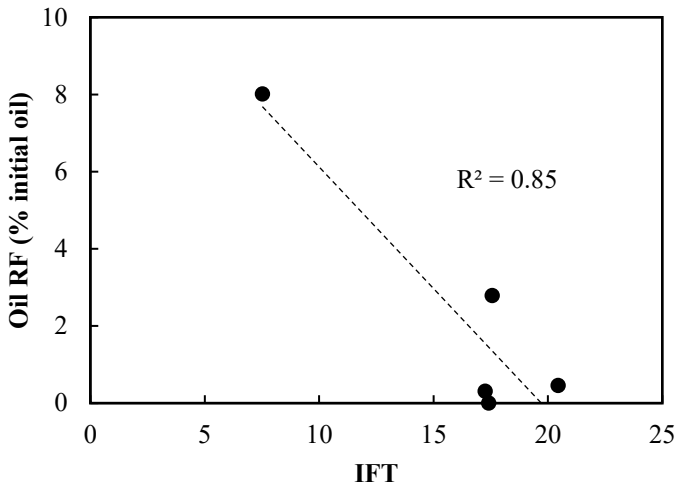

Figure 42: Oil recovery factor vs IFT for soaking tests conducted on the CSP samples

7.4 Conclusions

The main conclusions of this chapter are listed below:

1. The crushed shale pack samples imbibe more oil than core samples, suggesting higher wetting affinity of CSP samples to oil compared with core samples.
2. Oil RF is maximum when oil-saturated CSP samples were immersed into DW+surfactant solution. A similar observation was observed for the soaking tests conducted on the core samples.
3. The oil RF of CSP samples decreases with increasing IFT of soaking fluids. This observation confirms the higher water-wetness of soaking fluids with lower IFT which can compensate the effect of low IFT and results in higher driving capillary pressure and oil RF.

Chapter 8

Conclusions

8.1 Overview

The primary objectives of this research were to investigate the wettability of organic rich Duvernay shale Formation and to inquire into the functional dependence of wettability on the petrophysical properties of the rock. A better understanding of the reservoir characteristics of Upper Duvernay core plugs from laboratory data and microscopic images was essential to obtain the goal of this study. Moreover, mechanisms that control oil recovery was also needed to study to understand the wettability alteration which influences the waterflooding and EOR techniques.

A detailed background of Duvernay geography, depositional environment, position in the stratigraphic column, and the lithology was studied from several previous literature. Determining the source rock characteristics, for example, mineral composition, the presence of organic content such as kerogen, kerogen type, and maturity was the first step towards determining the wettability of the rock. Thus, XRD, TRA, gamma ray log, and rock-eval data were analyzed to explain the rock properties of given core plugs (Chapter-2). Microscopic images from the thin sections and SEM-EDS were also analyzed to examine the rock texture, fabric, pore types and sizes of the samples (Chapter-3).

Air-liquid contact angle and air-liquid spontaneous imbibition tests were conducted for wettability measurements (Chapter-4). Additionally, co-current imbibition of several core plugs also performed to calculate the capillary pressure ratio using Handy's Model and Young-Laplace equation (Chapter-5). After evaluation of wettability, soaking experiments were performed for both oil-saturated core plugs and crush shale packs (CSP). For this experiments, soaking fluids

with different compositions and physical properties were prepared which were characterized by measuring surface tension, interfacial tension (IFT), viscosity, and pH. Liquid-liquid contact angles of soaking fluids were measured on the surface of the oil saturated core plugs. Then, the soaking tests were performed by immersing both the oil-saturated plugs and CSP samples (Chapter-6 and 7 respectively) in soaking fluids. The oil RF due to soaking of core plugs and CSPs were analyzed and compared. Thus, the controlling parameters affecting capillary pressure and imbibition oil recovery factor (RF) were investigated.

8.2 Key Findings

The key findings of this study are summarized as follows:

1-The majority of the Duvernay shale sample pores are hosted by the organic matter or kerogen which indicates that most of the pores are organic pores.

2- Both air-liquid contact angle and air-liquid imbibition tests results of Duvernay plugs show that wetting affinity to oil is stronger than that to brine.

3-The thermal maturity of kerogen also needs to be considered in order to explain the rock wettability. Samples with the high thermal maturity show stronger affinity to oil than the samples with lower thermal maturity. Additionally, due to the hydrophilic behaviour of clay, samples with high clay content imbibe less oil and vice versa.

4- The comparison between the values of capillary pressure ratio calculated by Young-Laplace equation and Handy's model indicates that the capillary pressure is not the only driving force for oil imbibition. The higher oil imbibition may be explained by the adsorption of oil on the surface of the organic matter.

5- Both liquid-liquid contact angle and soaking tests results prove that the wetting affinity of the shales to soaking fluids increases by reducing the IFT of soaking fluids. Thus, the soaking fluids with lower IFT may increase the capillary pressure, leading to higher imbibition in the samples and results in high oil recovery.

6- The presence of surfactant in the soaking fluids may alter wettability of organic pores towards less oil-wet conditions, leading to higher oil recovery. On the other hand, soaking fluids without surfactant can displace only a portion of oil in inorganic hydrophilic pores and can hardly displace the oil out of hydrophobic organic pores, leading to lower oil recovery.

7- Higher initial oil saturation reduces the pore space available for spontaneous imbibition of soaking fluid and reduces the oil recovery. Thus, the results of soaking tests on heated samples show that oil recovery factor is lower in samples with higher initial oil saturation.

8- CSP soaking tests results are also consistent with the soaking tests results of core samples. CSPs also show that soaking fluids with lower IFT increase the capillary pressure, thus, the oil recovery.

8.3 Recommendations for Future Experiments

Further researches can be done to obtain an accurate knowledge regarding the rock-fluid interactions. Some are recommended below-

1. In Chapter 4, it was suggested that the presence of hydrocarbon filled organic pores may reduce the oil imbibition. It can be further studied by determining the initial oil saturation of the well-preserved rock. Correlating imbibed volume with the initial oil saturation of the rock may confirm the effect of hydrocarbon filled organic pores on oil imbibition.

2. The distribution of fluids and the production may affected by the wettability of micro-pore system. Therefore, further SEM images can be taken with the saturated samples to locate the fluid path into the pore system.
3. Hydrocarbon and fracturing fluids interactions with rock may show different behavior at reservoir conditions. A laboratory protocol can be introduced to conduct the imbibition and soaking experiments at high temperature and pressure.

References

Akkutlu, I. Y., & Fathi, E. (2012, December 1). Multiscale Gas Transport in Shales with Local Kerogen Heterogeneities. Society of Petroleum Engineers. doi:10.2118/146422-PA

Alberta Table of Formation (2015): from Alberta Energy Regulator (AER). URL: http://ags.aer.ca/document/Table-of-Formations.pdf

Aplin, A. C. and Larter, S. R., (2005), Fluid flow, pore pressure, wettability, and leakage in mudstone cap rocks, in Evaluating Fault and Cap Rock Seals, edited by P. Boult, and J. Kaldi, pp. 11–19, Am. Assoc. of Petrol. Geol., Tulsa, Okla. doi:10.1306/1060752H23158

Anderson W.O. Wettability literature survey – Part 1: rock/oil/brine interactions and the effects of core handling on wettability. J. Pet. Technol. (1986), pp. 1125-1149

Anderson W.O. Wettability literature survey – Part 2: wettability measurement J. Pet. Technol. (1986), pp. 1246-1262

Anderson W.O. Wettability literature survey – Part 3: the effects of wettability on the electrical properties of porous media J. Pet. Technol. (1986), pp. 1371-1378

Anderson W.O. Wettability literature survey – Part 4: the effects of wettability on capillary pressure J. Pet. Technol. (1987), pp. 1283-1300

Anderson W.O. Wettability literature survey – Part 5: the effects of wettability on relative permeability J. Pet. Technol. (1987), pp. 1453-1468

Anderson W.O. Wettability literature survey – Part 6: the effects of wettability on waterflooding J. Pet. Technol. (1987), pp. 1605-1622

Anovitz, L.M., Littrell, K.C., Cole,D.R., Swift, A.M., Sheets, J., Elston, H.W., Welch, S.A., Chipera, S.J., Mildner, D.F. and Wasbrough, M. (2014) Multiscale (nano to mm) Porosity in the Eagle Ford Shale: Changes as a Function of Maturity. Unconventional Resources Technology Conference, Denver, Colorado, 25-27 August 2014: pp. 1018-1030. https://doi.org/10.15530/urtec-2014-1923519

Anovitz L.M., Cole D.R., Characterisation and Analysis of Porosity and Pore Structures, 2015; doi**:** 10.2138/rmg.2015.80.04

Arogundada, O., Sohrabi, M., 2012. A Review of Recent Development and Challenges in Shale Gas Recovery. Paper SPE 160869-MS presented at SPE Saudi Arabia Section Technical Symposium and Exhibition, Alkhbar, Saudi Arabia, 8-11 April.

Bantignies, J.L., Moulin, C., And Dexpert, H., (1997), Wettability Contrasts in Kaolinite and Illite Clays: Characterization by Infrared and X-Ray Absorption Spectroscopies, Clays and Clay Minerals, Vol. 45, No. 2, 184 193, 1997. http://www.clays.org/journal/archive/volume%2045/45-2-184.pdf

Baskin, D. K. (1997). Atomic H/C Ratio of Kerogen as an Estimate of Thermal. The American Association of Petroleum Geologists, 81(9), 1437-1450.

Bertoncello, A., Wallace, J., Blyton, C., Honarpour, M.M., Kabir, S., (2014). Imbibition and water blockage in unconventional reservoirs: well-management implications during flowback and early production. Soc. Petrol. Eng. http://dx.doi.org/10.2118/167698-PA.

Bobek, J. E., Mattax, C. C., & Denekas, M. O. (1958). Reservoir Rock Wettability - Its Significance and Evaluation. Society of Petroleum Engineers, Vol.213, 155-160. doi: https://www.onepetro.org/general/SPE-895-G

Borysenko, A., Clennell, B., Seved, R., Burgar, I., Ralston, J., Raven, M., Dewhurst, D., Liu, K., 2009, Experimental investigations of the wettability of clays and shales. Journal of Geophysical Research, Vol. 114, B07202, doi:10.1029/2008JB005928, 2009

Boult, P. J., et al. (1997), Capillary seals within the Eromanga basin, AAPG Mem., **67**, 143–167.

Britt, L. K. (1985, January 1). Optimized Oilwell Fracturing of Moderate-Permeability Reservoirs. Society of Petroleum Engineers. doi:10.2118/14371-MS

Brown, R. S., & Fatt, I. (1956). Measurements of Fractional Wettability of Oil Fields' Rocks By The Nuclear Magnetic Relaxation Method. SPE-743-G. Los Angeles, California: Society of Petroleum Engineers. doi: http://dx.doi.org/10.2118/743-G

C. **Clarkson**, N. Solano, R. Bustin, A. Bustin, G. Chalmers, L. He, Y. Melnichenko, A. Radlinski, and T. Blachd. Pore structure characterization of North American shale gas reservoirs using usans/sans, gas adsorption, and mercury intrusion. Fuel, 103:606{616, 2013.

Cao, Q. and Zhou, W. (2015), Characteristic and Controlling Factors of Organic Pores in Continental Shale Gas Reservoir of Chang 7th of Yanchang Formation, Ordos Basin. Acta Geologica Sinica - English Edition, 89: 1–2. doi:10.1111/1755-6724.12302_1

Cassie, A. B. D., & Baxter, S. (1944). Wettability of porous surfaces. Transactions of the Faraday Society, 40, 546-551.

Cheng, Y., (2012). Impact of water dynamics in fractures on the performance of hydraulically fractured wells in gas-shale reservoirs. J. Can. Pet. Technol. 51 (02), 143–151.

Chen, H., Lucas, L., Nogaret, L., Yang, H., & Kenyon, D. (2001). Laboratory Monitoring of Surfactant Imbibition with Computerized Tomography. SPE Reservoir Evaluation & Engineering, 4(01), 16-25. doi:http://dx.doi.org/10.2118/69197-PA

Chenevert, M.E., (1970). Shale alteration by water adsorption. Journal of Petroleum Technology. 22 (09), 1,141–1,148.

Clark, J.B., "A Hydraulic process for increasing the productivity of wells", Petroleum Transactions, AIME, 1949, 1-8.

Curtis, M. E., Ambrose, R. J., Sondergeld, C. H., & Rai, C. S. (2011, January 1). Transmission and Scanning Electron Microscopy Investigation of Pore Connectivity of Gas Shales on the Nanoscale. Society of Petroleum Engineers. doi:10.2118/144391-MS

D. **Zhou**, L. Jia, J. Kamath, and A. Kovscek. Scaling of counter-current imbibition processes in low-permeability porous media. Journal of Petroleum Science and Engineering, 33:61-74, 2002

Dake, L.P., "Fundamentals of Reservoir Engineering", Elsevier Scientific Publishing Company, Amsterdam, 1977.

Dehghanpour, H., Zubair, H. A., Chhabra, A., & Ullah, A. (2012). Liquid Intake of Organic Shales. Energy Fuels, 26 (9), 5750–5758. doi:10.1021/ef3009794

Dehghanpour, H., Lan, Q., Saeed, Y., Fei, H & Qi, Z. 2013. Spontaneous imbibition of brine and oil in gas shale: Effect of water adsorption and resulting micro fractures. Energy & Fuels, (27): 6, 3039-3094

Delshad, M., Bhuyan, D., Pope, G. A., & Lake, L. W. (1986). Effect of Capillary Number on the Residual Saturation of a Three-Phase Micellar Solution. Society of Petroleum Engineers. doi:10.2118/14911-MS.

Donaldson, E. C., Thomas, R. D., & Lorenz, P. B. (1969). Wettability Determination and Its Effect on Recovery Efficiency. Society of Petroleum Engineers Journal, 13-20. http://dx.doi.org/10.2118/2338-PA

Drummond, C., and J. Israelachvili (2004), Fundamental studies of crude oil-surface water interactions and its relationship to reservoir wettability, J. Petrol. Sci. Eng., **45**, 61–81, doi:10.1016/j.petrol.2004.04.007

Dunn, L. A., & Humenjuk, J. (2014). The Duvernay Formation: Integrating Sedimentology, Sequence Stratigraphy and Geophysics to Identify Sweet Spots in a Liquids-Rich Shale Play, Kaybob Alberta. Unconventional Resources Technology Conference. Denver, Colorado, USA: Society of Petroleum Engineers. doi:http://dx.doi.org/10.15530/urtec-2014-1922713

Fothergill, P., Boskovic, D., Schoellkopf, N., Murphy, P., & Mukati, M. (2014). Regional Modelling of the Late Devonian Duvernay Formation, Western Alberta, Canada. Unconventional Resources Technology Conference. Denver, Colorado, USA: Society of Petroleum Engineers. doi:http://dx.doi.org/10.15530/urtec-2014-1923935

Ghanbari, E., Abbasi, M. A., Dehghanpour, H., & Bearinger, D. (2013, November 5). Flowback Volumetric and Chemical Analysis for Evaluating Load Recovery and Its Impact on Early-Time Production. Society of Petroleum Engineers. doi:10.2118/167165-MS

Ghanbari, E., Dehghanpour, H., (2016). The fate of fracturing water: a field and simulation study. Fuel 163, 282–294.

Gonzalez, J., Lewis, R., Hemingway, J., Grau, J., Rylander, E., Pirie, I., (2013). Determination of formation organic carbon content using a new neutron-induced gamma ray spectroscopy service that directly measures carbon. Soc. Petrol. Eng. http://dx.doi.org/10.1190/URTEC2013-112.

Gupta, D. V. S. (2009). Unconventional Fracturing Fluids for Tight Gas Reservoirs. Society of Petroleum Engineers. doi:10.2118/119424-MS

Handwerger, D. A., Willberg, D. M., Pagels, M., Rowland, B., & Keller, J. (2012). Reconciling Retort versus Dean Stark Measurements on Tight Shales. Society of Petroleum Engineers. doi:10.2118/159976-MS

Handy, L.L., 1960. Determination of effective capillary pressures for porous media from imbibition data. Trans. AIME 219, 75–80.

Hensen, E.J.M., Smit, B., (2002). Why clays swell. Journal of Physical Chemistry. B 106 (49), 12664–12667.

Hu, Y., Devegowda, D., & Sigal, R. F. (2014, October 27). Impact of Maturity on Kerogen Pore Wettability: A Modeling Study. Society of Petroleum Engineers. doi:10.2118/170915-MS

Jarvie, D.M., Components and processes affecting producibility and commerciality of shale resource systems. Geological Acta: an international earth science journal 2014. http://www.redalyc.org/html/505/50532719004/

Jeranld, G.R., Rathmell, J.J. (1994) Wettability and relative permeability of Prudhoe Bay: A case study in mixed-wet reservoirs. Proc 3rd Int Symp on Evaluation of Reservoir Wettability and its Effect on Oil Recovery; Laramie, Wyoming. Laramie: Modern Printing. p 1

Jill S. Buckley, Effective wettability of minerals exposed to crude oil, Current Opinion in Colloid & Interface Science, Volume 6, Issue 3, 2001, Pages 191-196, ISSN 1359-0294, http://dx.doi.org/10.1016/S1359-0294(01)00083-8.

Johnson, R. E., and R. H. Dettre. "Wettability and contact angles." Surface and colloid science 2 (1969): 85-153.

Jones, M., Stratton, J., Newton, R., Oekerman, M., Xu, L., & Martin, K. (2016). Case Study: Successful Applications of Weak Emulsifying Surfactants in the Wolfcamp Formation of Reagan County, TX. SPE Liquids-Rich Basins Conference. Midland, Texas, USA: Society of Petroleum Engineers. doi:http://dx.doi.org/10.2118/181771-MS

Kitty L. Milliken, Mark Rudnicki, David N. Awwiller, Tongwei Zhang (2013). Organic matter–hosted pore system, Marcellus Formation (Devonian), Pennsylvania. DOI: https://doi.org/10.1306/07231212048

Krevelen, V. (1950). Graphical-statistical method for the study of structure and reaction processes of coal. Fuel, 29, 269-84.

Lake, L. W. (1989). Enhanced oil recovery.

Lan, Q., Ghanbari, E., Dehghanpour, H., & Hawkes, R. (2014, February 25). Water Loss versus Soaking Time: Spontaneous Imbibition in Tight Rocks. Society of Petroleum Engineers. doi:10.2118/167713-MS

Lan, Q., Yassin, M.R., Habibi, A., Dehghanpour, H., Wood, J., (2015). Relative permeability of unconventional rocks with dual-wettability pore-network. Soc. Petrol. Eng. http://dx.doi.org/10.2118/178549-MS.

Laplace, P. S. (1805). Traité de mécanique céleste/par PS Laplace...; tome premier [-quatrieme] (Vol. 4). de l'Imprimerie de Crapelet.

Law B.E., Curtis, J.B. (2002). Introduction to Unconventional Petroleum Systems AAPG Bulletin, V. 86, No. 11 (November 2002), P. 1851-1852.

http://archives.datapages.com/data/bulletns/2002/11nov/1851/1851.htm?doi=10.1306%2F61EEDDA0-173E-11D7-8645000102C1865D

Mahadevan, J., Le, D., Hoang, H., 2009. Impact of Capillary Suction on Fracture Face Skin Evolution in Water Blocked Wells. Paper SPE presented at SPE Hydraulic Fracturing Technology Conference, The Woodlands, Texas.

Mitchell, A.G., Hazell, L.B., Webb, K.J.,(1990).Wettability determination: pore surface analysis. Soc. Petrol. Eng. http://dx.doi.org/10.2118/20505-MS.

Montgomery, C.T., Smith, M.B., 2010. Hydraulic Fracturing – History of an enduring technology. Journal of Petroleum Technology, 12, 26-32.

Montgomery, C., (2013). Fracturing fluids. Int. Soc. Rock Mech.

Morrow, N. R. (1990). Wettability and Its Effect on Oil Recovery. Journal of Petroleum Technology, 42 (12), 1476-1484. doi:http://dx.doi.org/10.2118/21621-PA

Morrow, N. R., and Masonb, G. Recovery of oil by spontaneous imbibition. Current Opinion in Colloid and Interface Science, 6:321-337, 2001.

Munson, E. O. 2015. Reservoir characterization of the Duvernay Formation, Alberta: a pore-to basin-scale investigation (Doctoral dissertation, University of British Columbia).

Nguyen, D., Wang, D., Oladapo, A., Zhang, J., Sickorez, J., Butler, R., & Mueller, B. (2014). Evaluation of Surfactants for Oil Recovery Potential in Shale Reservoirs. Society of Petroleum Engineers. doi:10.2118/169085-MS

Neog, A., & Schechter, D. S. (2016). Investigation of Surfactant Induced Wettability Alteration in Wolfcamp Shale for Hydraulic Fracturing and EOR Applications. SPE Improved Oil Recovery Conference. Tulsa, Oklahoma, USA: Society of Petroleum Engineers. doi:http://dx.doi.org/10.2118/179600-MS

Nicholas, G., 2000 Sedimentology and Stratigraphy, 2nd Edition. Blackwell Science, Oxford ISBN: 978-1-4051-3592-4

https://raregeologybooks.files.wordpress.com/2014/09/sedimentology-and-stratigraphy-by-gary-nichols.pdf

Odusina, E. O., Sondergeld, C. H., & Rai, C. S. (2011, January 1). NMR Study of Shale Wettability. Society of Petroleum Engineers. doi:10.2118/147371-MS

Qi, Z., Han, M., Fuseni, A., Alsofi, A., Zhang, F., Peng, Y., & Cai, H. (2016). Laboratory Study on Surfactant Induced Spontaneous Imbibition for Carbonate Reservoir. Society of Petroleum Engineers. doi:10.2118/182322-MS

Parra, J. E., Pope, G. A., Mejia, M., & Balhoff, M. T. (2016, September 26). New Approach for Using Surfactants to Enhance Oil Recovery from Naturally Fractured Oil-Wet Carbonate Reservoirs. Society of Petroleum Engineers. doi:10.2118/181713-MS

Passey, Q. R., Bohacs, K., Esch, W. L., Klimentidis, R., & Sinha, S. (2010, January 1). From Oil-Prone Source Rock to Gas-Producing Shale Reservoir - Geologic and Petrophysical Characterization of Unconventional Shale Gas Reservoirs. Society of Petroleum Engineers. doi:10.2118/131350-MS

Peng, S., Zhang, T., Ellis, G.S. Variation of Wettability of Organic-Rich Shales With Thermal Maturity and the Implications for Oil and Gas Distributions. AAPG Annual Convention and Exhibition, Denver, CO. 2015

Penny, G. S., Zelenev, A., Lett, N., Paktinat, J., & O' Neil, B. J. (2012, January 1). Nano Surfactant System Improves Post Frac Oil and Gas Recovery in Hydrocarbon Rich Gas Reservoirs. Society of Petroleum Engineers. doi:10.2118/154308-MS

Raquejo, A. G., Gray, N. R., & Freund, H. (1992). Maturation of Petroleum Source Rocks. 1. Changes in Kerogen Structure and Composition Associated with Hydrocarbon Generation. Energy & Fuels, 6, 203-214. doi:http://pubs.acs.org/doi/pdf/10.1021/ef00032a015

Rezaee, R., 2015. Organic matter rich shale depositional environments. Source: Fundamentals of Gas Shale Reservoirs. Page: 21-45 ; DOI: 10.1002/9781119039228.ch2

Roychaudhuri, B., Tsotsis, T. T., & Jessen, K. (2013). An experimental investigation of spontaneous imbibition in gas shales. Journal of Petroleum Science and Engineering, 111, 87-97.

S. Creaney ., J. Allan., K.S. Cole., M.G. Fowler., P.W. Brooks., K.G. Osadetz., R.W. Macqueen., L.R. Snowdon., CL. Riediger (1994): Petrolum Generation and Migration in the Western Canadian Sedimentary Basin; in Geological Atlas of the Western Canada Sedimentary Basin, G.D. Mossop

and I. Shetsen (comp.), Canadian Society of Petroleum Geologists and Alberta Research Council, URL: http://ags.aer.ca/publications/chapter-31-petroleum-generation-and-migration.htm

Selley, R. C., & Sonnenberg, S. A. (2014). Elements of petroleum geology. Academic Press.

Sheng, J. (2010). Modern chemical enhanced oil recovery: theory and practice. Gulf Professional Publishing.

Standnes, D. C., & Austad, T. (2000). Wettability alteration in chalk: 1. Preparation of core material and oil properties. Journal of Petroleum Science and Engineering, 28(3), 111-121. doi:http://dx.doi.org/10.1016/S0920-4105(00)00083-8

Stoakes, F. (1980). Nature and control of shale basin fill and its effect on reef growth and termination: Upper Devonian Duvernay and Ireton formations of Alberta, Canada. Vol-28, 345-410.

Stark, P., Chew, K., & Jackson, P. (2008, January 1). Importance of Unconventional Oil Resources in Shaping the Far East Energy Future. International Petroleum Technology Conference. doi:10.2523/IPTC-12743-MS

Sulucarnain, I.D., Sondergeld, C.H., Rai, C.S., (2012). An NMR study of shale wettability and effective surface relaxivity. Soc. Petrol. Eng. http://dx.doi.org/10.2118/162236-MS.

Switzer, S., Holland, W., Christie, D., Graf, G., Hedinger, A., McAuley, R., Packard, J. (1994). Devonian Woodbend-Winterburn Strata of the Western Canada Sedimentary Basin. Canadian Society of Petroleum Geologists and the Alberta.

Takahashi, S. and Kovscek, A.R. (2010) Spontaneous countercurrent imbibition and forced displacement characteristics of low-permeability, siliceous shale rocks. Journal of Petroleum Science and Engineering, 71(1), 47-55, 2010.

Tang, X., Jiang, Z., Jiang, S., Wang, P., and Xiang, C., Effect of Organic Matter and Maturity on Pore Size Distribution and Gas Storage Capacity in High-Mature to Post-Mature Shales Energy Fuels, 2016, 30 (11), pp 8985–8996. DOI: 10.1021/acs.energyfuels.6b01499

Tissot, B. P., & Welte, D. H. (1984). Petroleum Formation and Occurrence. New York, Tokyo: Springer-Verlag. Retrieved from. https://raregeologybooks.files.wordpress.com/2014/12/b-p-tissot-and-d-h-welte-petroleum-formation-and-occurence.pdf

W. **Abdullah**, J.S. Buckley, A. Carnegie, J. Edwards, B. Herold, E. Fordham, A. Graue, T. Habashy, N. Seleznev, C. Signer, H. Hussain, B. Montaron, M. Ziauddin: "Fundamentals of Wettability", Schlumberger Oilfield Review, Vol 19, No. 2, pp 44-61, 2007.

Wang, D., Butler, R., Liu, H., & Ahmed, S. (2011). Wettability Survey in Bakken Shale with Surfactant Formulation Imbibition. SPE Annual Technical Conference and Exhibition. doi:http://dx.doi.org/10.2118/145510 MS

Wang, Q., Chen, X., Jha, A.N., et al., (2014). Natural gas from shale formation–the evolution, evidences and challenges of shale gas revolution in United States. Renew. Sust. Energ. Rev. 30, 1–28.

Xiong, X., Devegowda, D., Michel Villazon, G. G., Sigal, R. F., & Civan, F. (2012, January 1). A Fully-Coupled Free and Adsorptive Phase Transport Model for Shale Gas Reservoirs Including Non-Darcy Flow Effects. Society of Petroleum Engineers. doi:10.2118/159758-MS

Xu, M., & Dehghanpour, H. (2014). Advances in understanding wettability of gas shales. Energy & Fuels, 28(7), 4362-4375.

Yarveicy, H., & Haghtalab, A. (2017). Effect of amphoteric surfactant on phase behavior of hydrocarbon-electrolyte-water system-an application in enhanced oil recovery. Journal of Dispersion Science and Technology, (just-accepted).

Yassin, M. R., Begum, M., & Dehghanpour, H. (2017). Organic shale wettability and its relationship to other petrophysical properties: A Duvernay case study, International Journal of Coal Geology, Volume 169, Pages 74-91, http://dx.doi.org/10.1016/j.coal.2016.11.015.

Yassin, M. R., Dehghanpour, H., Wood, J., & Lan, Q. (2016). A Theory for Relative Permeability of Unconventional Rocks with Dual-Wettability Pore Network. Society of Petroleum Engineers. doi:10.2118/178549-PA

Yassin, M. R., Ayatollahi, S., Rostami, B., Hassani, K., & Taghikhani, V. (2015). Micro-emulsion phase behavior of a cationic surfactant at intermediate interfacial tension in sandstone and carbonate rocks. Journal of Energy Resources Technology, 137(1), 012905.

Young, T. (1805). An essay on the cohesion of fluids. Philosophical Transactions of the Royal Society of London, 95, 65-87.

Yue, Z., Fu, Q., Lang, N., & Fan, C. (2014). Liquid Scale Inhibitors for Metallic-Crosslinked Gel Fracturing Systems. SPE International Oilfield Scale Conference and Exhibition. Aberdeen, Scotland: Society of Petroleum Engineers. doi:10.2118/169806-MS